University of Stavanger

FACULTY OF SCIENCE AND TECHNOLOGY

MASTER THESIS

Study program/specializations **Offshore Field Development**	Spring semester, 2023 Open
Author: **Andreas Løkås Halvorsen**	 ..... (Author signature)

Supervisor at UiS: **Professor Yihan Xing**

Co-supervisor: **Ph.D. candidate Yucong Ma**

Master thesis title: **Uncertainty Analysis of a Safety Operating Envelope for a Subsea Shuttle Tanker**

Keywords: **SOE, SST, Jam-to-rise, Jam-to-dive, Gumbel**	Number of pages: 112 appendices/other: 63 Stavanger, 21.06.2023 date/year

Abstract

This thesis investigates the uncertainty of a safety operating envelope (SOE) for a subsea shuttle tanker (SST). The main focus of this work is on the jam-to-rise and jam-to-dive aspects of the accidental cases for the SOE. The SST is investigated using a pitch angle of 10- 15- and 20- degrees for rising and diving. The findings of the free-running simulations, which take into account two current directions and load instances of 0.5 and 1 m/s with 5% and 10% standard variation, while using the Gumbel fitting method, revealed increased recovery depth differences ranging from 0.97% to 21.44% for the jam-to-rise scenario, and 0.42% to 11.26% for the jam-to-dive scenario for the 15-degree pitch angle cases. The cases with 10- and 20-degree pitch angles show similar percent differences. Future studies may look at how differences in recovery depth caused by current directions coming from different angles, such as a 60- and 120-degree angle, might significantly affect the results. To estimate the possible recovery depth and compare it to the Gumbel values in order to get more accurate results, other statistical techniques might be utilized, such as the Average Conditional Exceedance Rate Method

Acknowledgment

I want to sincerely thank and appreciate the following people for their significant assistance and efforts in finishing my master's thesis.

I would like to start by expressing my sincere appreciation to my supervisor, Professor Yihan Xing, for their advice, knowledge, and constant support during the study process. Their astute comments and helpful critique have considerably influenced the growth of my thesis.

Additionally, I would like to express my gratitude to my co-supervisor, Ph.D. candidate Yucong Ma, for their invaluable time, knowledge, and helpful recommendations throughout the thesis. Their suggestions increased the overall quality of this work.

I want to express my sincere gratitude to the University of Stavanger's staff and faculty, especially the Department of Mechanical and Structural Engineering and Materials Science, for offering a vibrant academic atmosphere and the tools required for undertaking research. Access to libraries, databases, and other resources has been essential for compiling the necessary data and performing the required analysis.

Furthermore, I owe a great deal of gratitude to my friends and classmates for their encouragement and support during this difficult path. Their company, inspiration, and openness to discussion have been priceless.

Lastly, I want to thank my family for their unflagging encouragement, tolerance, and empathy throughout the completion of my thesis. Their devotion to me and confidence in my talents have served as a continual source of motivation.

Even though it is not possible to mention everyone that has contributed and helped me in some way or another. I extend my gratitude to all that has supported me during my studies.

Thank you, everyone, for being a part of this journey and for your priceless contributions.

Table of Contents

List of Figures

List of Tables

1 Introduction

Pipelines connect floating production units (FPUs) in the offshore to onshore facilities for the majority of oil and gas production [1]. Since the first pipeline was installed underwater during World War II in the UK, subsea pipeline laying techniques have improved significantly and are now regarded as an established technology [2]. This mode of transportation does, however, have certain drawbacks for both practical and financial reasons. The method's deployment costs are a key drawback since they can be extremely high for remote gas and oil locations with lengthy transmission distances because of the cost increases associated with pipeline lengths. Deep-water pipeline inspections are additionally difficult and expensive. In addition, full or partial line shut-ins are regularly required for pipeline maintenance and repair, which can be economically unfavorable. This indicates that the method is better suited to big fields with high-profit margins and humble step-outs [3], i.e., using underwater pipes to a single remote marginal field is economically undesirable. Shuttle tankers are regularly used in this circumstance [4]. The tanker ship is a very adaptable option that can be quickly deployed to various locations. In addition, deploying a backup tanker in the case of a vessel breakdown is simple. However, because it is a floating structure impacted by significant dynamic load effects from waves and wind, tanker ship operation is very weather-dependent and is not possible in rough seas. Equinor [5] presented a 34,000-tonne baseline design of a Subsea Shuttle Tanker (SST) as a creative workaround to get around the previously mentioned limitations. This design combines the adaptability and economy of the shuttle tanker with the submarine's capacity to operate underwater regardless of the weather conditions.

The concept of employing underwater vehicles for commercial transportation was first put up by Jacobsen [6] and Taylor et al. [7] in the 1970s, who suggested deploying nuclear-powered submarines of different sizes (20,000 to 420,000 DWT) in order to transport Arctic crude oil. A 660,800 DWT nuclear-powered and a 727,400 DWT non-nuclear-powered variant of Jacobsen et al. [8] two enormous underwater Arctic LNG tanker designs were introduced in the 1980s. A 3500 DWT multipurpose submarine for a variety of subsea tasks, including maintenance, repair, installation, and inspection up to water depths of 1500 m in the Arctic, was recently exhibited by Brandt et al. [9]. Ellingsen et al [10] offered a creative solution for shipping freight, proposing a subsea "cargo-train" made up of linked tanks that resembled trains and had autonomous propulsion systems that could be placed at the bow or aft of the ship. A highly efficient immense subsea transport glider was another idea put up by Ellingsen et al [10].

The massive hydrodynamic wings of this underwater glider were intended to house the payload tanks. Xing et al. [11] continued by suggesting a 1500 DWT subsea freight glider with an estimated average power usage of under 10 kW. The previously mentioned works did not move beyond conceptual design suggestions. To fill this knowledge gap, Ma et al. [26] defined a standard SST design that includes thorough global design standards.

Figure 1 - CCS offshore storage process with SST transportation

The main goal of the SST is to autonomously traverse underwater and carry CO2 from offshore or onshore facilities to subsea wells for injection directly. Figure 1 depicts its location relative to offshore carbon capture and storage (CCS) supply chain activities. The baseline SST is intended for use in the Norwegian sector, where Sleipner, Utgard, and Snøhvit are three active CCS projects [12]. In these initiatives, CO2 produced during the extraction of hydrocarbons is caught and reinjected back into the reservoir. Along with these three active initiatives, the Northern Lights project (Equinor ASA [13]), which will go into operation in 2024, will transport CO2 produced by land-based, non-petroleum-related industrial activity to the Troll field for injection in the Utsira formation. Figure 2 depicts the locations of the various CCS projects. These Norwegian fields were chosen because they are currently being used for CCS storage and can meet the mission criteria. The SST may be created to function in many locations throughout the world with various demands. Although CO2 is the intended payload, the SST may also transport other types of cargo, including subsea equipment, hydrocarbons, and electrical power (through batteries). Different strategies exist for the SST to help reduce global warming. It is completely electric-powered and emission-free, ensuring that shipping remains sustainable. Currently, 3.3% of CO2 emissions from fossil fuels are attributed to shipping [14]. On the other hand, it makes it possible to use marginal subsea resources as offshore CO2 storage facilities, helping to fulfill the rising need for CCS in the future. Most of the carbon dioxide emitted by industrial processes may be collected and stored [15]. Any cost-effective approach that may boost the amount of CCS storage available globally is essential to reducing the exaggerated trend in the rise of the global mean temperature. The rising trend in the world's energy consumption, which will result in a doubling of atmospheric carbon dioxide levels in

2100 compared to 1960 levels, is expected to make this situation worse (International Energy Agency (IEA) [16]).

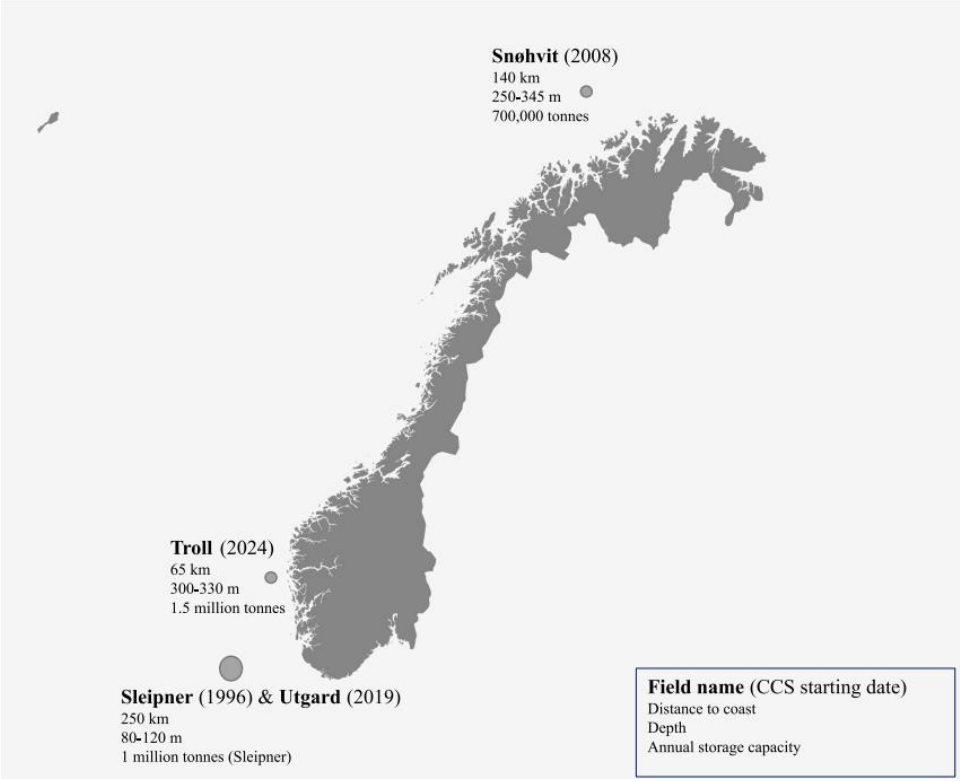

Figure 2 - Current ongoing and planned CCS storage sites in the Norwegian sector [12] [13]

Table 1 - SST main design parameters

Parameter	Value	Unit
Length	164	m
Beam	17	m
Displaced mass	$3.36 * 10^4$	$tonne$
Pitch moment of inertia	$7.6 * 10^{10}$	$kg * m^2$
Centre of gravity	$[0, 0, 5.78]$	m
Safety diving depth (minimum)	40	m
Nominal diving depth	70	m
Collapse diving depth (maximum)	190	m

2 Evolution of the development of the Subsea Shuttle Tanker (SST)

2.1 The safety operating envelope of a Subsea Shuttle Tanker (SST)

SST mishaps can result in several issues, including the loss of the vessel, CO_2 or hydrocarbon leaks, damage to offshore installations, or even injury to third parties. These effects may result in property loss, damage to the environment, and fatalities. Therefore, while designing SST operations, safety comes first and foremost. The Safety Operating Envelope (SOE) is utilized to assure safety. The system's safe operating range is defined by a set of movement restrictions. The SOE's look and maneuverability restrictions differ based on the system. The SOE has been used in several types of vessels, including ships [17], submarines, and airplanes, to assess the operational safety of systems [10].

The SOE for the SST was created based on lessons learned from naval submarines where its use has been utilized for a long time. The most recent standard, the navy submarine code from the Norwegian classification society Det Norske Veritas (DNV), also requires it [19]. To guarantee that submarine operations can survive any plausible breakdown, the SOE sets maneuver restrictions. Marchant and Kimber [20] stated in 2014 that there are two methods to represent the SOE. One is through safe maneuvering envelopes, which show the safety limits on the initial trim conditions, and the other is through maneuvering limitation diagrams, which show the safety limits on the control plane pitch angle.

Research on the emergency recovery of a 150-tonne submarine during surface congestion and floods was carried out in 1966 by Giddings and Louis [21]. The INS Dakar submarine of the Israeli navy suffered 69 casualties [22] in 1968 due to an aft plane blockage that caused it to go deeper than the collapse depth. Burcher and Rydill [23] examined how SOE affected submarine design as well and discovered that it had a substantial influence on the dynamics and control systems of submarines. An analysis of the effects of aft control plane arrangement by the British defense technology company QinetiQ, which discovered that an X aft layout is the most advantageous design, backed this conclusion. Additionally, Park and Kim [24] [25] studied submarine depth excursions and constructed an SOE protection system during an aft control plane jam.

An illustration of a typical submarine SOE is shown in figure 3 as a depth vs velocity diagram. This illustration shows a submarine's capacity to survive believable mishaps like flooding or control plane jams. By ensuring the submarine has sufficient maneuverability in circumstances where these failures occur, the SOE is intended to reduce operational risk. The six separate zones that make up the SST's safety operating envelope are as follows:

- Jam-to-dive avoid zone: When a control plane jam occurs, the SST runs the risk of exceeding the collapse dive depth.
- Jam-to-rise avoid zone: When a control plane jam occurs, the SST runs the danger of breaching the surface or colliding with ships.
- Unrestricted operation zone: This zone is distinguished by low velocity and a wide depth margin. With any pitch angle and any control plane angle, the SST may be simply maneuverer.
- Restricted operation zone: This zone is distinguished by high sailing velocity. Less maneuverability is seen in the SST. As a result, both pitch angle and control plane angle must be limited to specific values.
- Flood avoid zone: There isn't enough lift force to be produced in this zone because of the low velocity. Sailing in this area puts the SST in danger of sinking in the event of floods.
- Collapse diving depth avoid zone: The SST is sailing deeper than the nominal diving depth and therefore is a risk to collapse.

Although SOE analyses are frequently carried out on submarines that are already in operation as a tactic to reduce vessel loss during events, they are also integrated into the design process for new submarines. Design considerations like depth and speed may be affected by the SOE. Additionally, it can spot any possible problems with the design of control systems or hydrodynamics at the last stage of design.

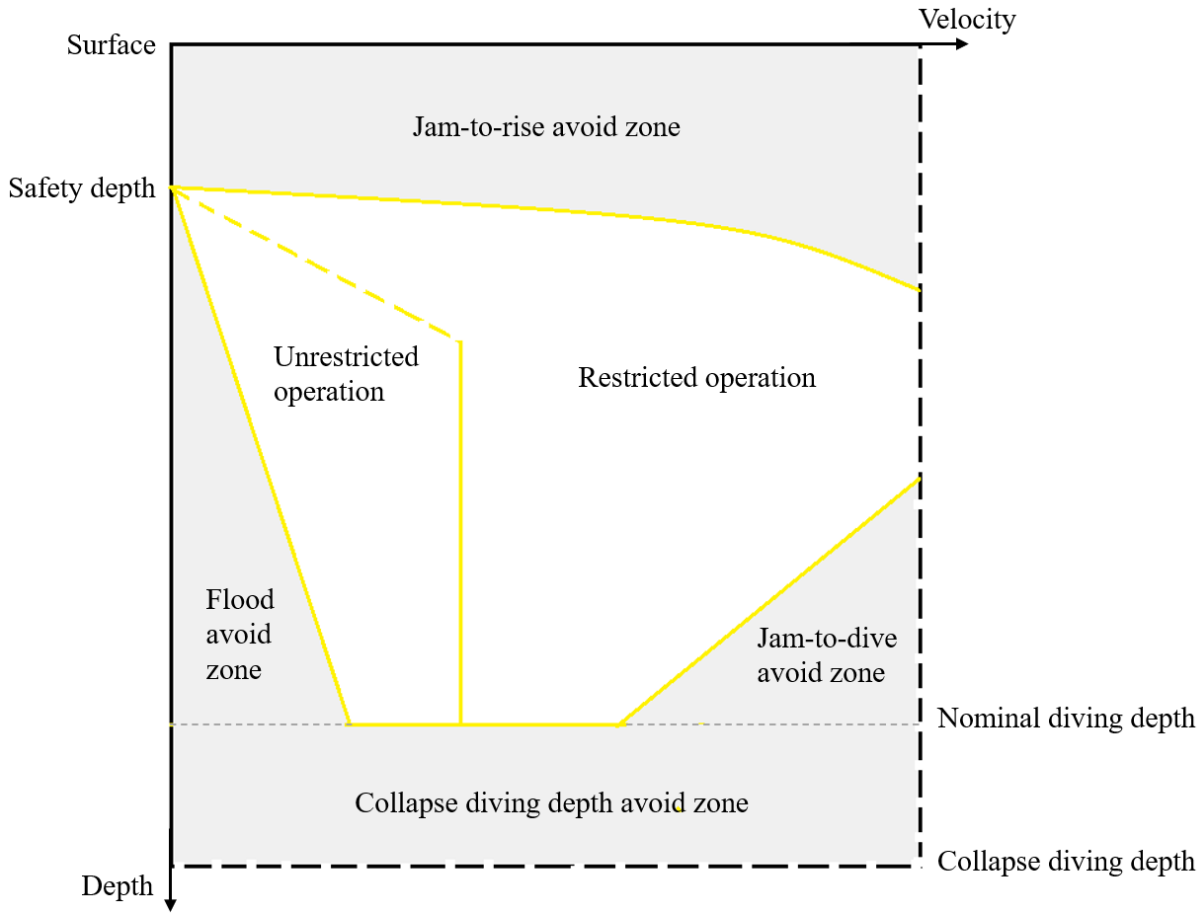

Figure 3 – Safety operating envelope

2.2 Emergency recovery

2.2.1 The hazards

The most significant hazards to a submerged submarine, besides fire, are deep-water flooding and irrational diving. Flooding may appear out of place in the current setting because it is a hydrostatics phenomenon, in contrast to irrational diving which is a dynamic occurrence. However, the way to recovery rests in invoking hydrodynamic forces to overcome threatening hydrostatic forces. Therefore, the current section addresses both the types of safety threats and the steps that can be taken to facilitate emergency recovery. The two parts are intricately linked, and necessary, emergency recovery is a matter of what provision to make in design and what action to take in operation. The operational factors are still quite important, even if we focus on the design aspect in the following. We must only tackle operational factors to the amount necessary to accurately depict the design considerations due to time and space constraints [23].

2.2.2 The flooding incident

Due to the typical modest reserve of buoyancy on the surface and the complete absence of reserve underneath, avoiding accidental flooding has been a concern of submarine designers and submariners since the invention of the submersible. Flooding can result from a variety of events, including [23]:

- Erroneous behavior such as leaving hatches inadequately bound.
- Pipe failure caused by exposure to sea pressure.
- Pressure hull piercing due to collision or hostile activity.
- By improperly constructing the pressure boundary interlocking mechanisms that are meant to stop water from entering accidentally.
- By a lack of quality control for equipment used to carry sea pressure during construction or refitting.

Any such occurrence would be humiliating if the submarine were to be on the surface, but it might be disastrous if it were to take place underwater. The risk increases with the depth of the submarine. At maximum diving depth, a breach as tiny as a few centimeters across may cause flooding to spread quickly and be followed by a blinding spray that might short out any electrical gadgets in its path. The crew would need to be able to escape from the submarine, thus the only course of action would be to bring it up to the surface as rapidly as possible. However, with most modern submarines, the likelihood of this happening is quite low.

Blowing the major ballast tanks or invoking as much buoyancy as could be summoned by releasing water from those tanks, is an essential step in emergency recovery during a flooding catastrophe wherever along the length of the vessel it happened. The majority of submarines can do this by giving the MBTs (main ballast tanks) a full HP (high-pressure) air blow. Even all the air that has been stored would not instantaneously empty the tanks as the sub descended to its maximum diving depth or as it was approaching it. Instead, pockets of air would form that may enlarge as the sub began to ascend to the surface. However, all the air that has been stored would not immediately empty the tanks when the submarine reached or was about to reach full diving depth. Instead, pockets of air would form that may expand once the submarine starts ascending toward the surface. Then, if the submarine could increase its forward speed, the aft and bow hydroplanes could be used to both help drive it upwards and to help counteract the rising negative buoyancy and its moment [51]. This is when hydrodynamics could play a significant role in assisting emergency recovery. The implication is that a submarine operating

such depths cannot afford to move too slowly, and it is crucial to construct the vessel to maintain propulsion even in the event of a catastrophic flooding crisis. Naturally, limiting the amount of internal piping exposed to external sea pressure should be one of the main goals. Any such internal seawater systems ought to include power-operated hull valves that can be quickly closed in order to isolate an internal breakdown and reduce the amount of flooding. As the shutting down of cooling systems may result in an automatic safety shutdown of power generation systems, denying the vessel the ability to drive itself out of trouble due to the flooding, the operational philosophy of such valves needs careful evaluation [23].

2.2.3 The depth excursion incident

Concerns about the possibility of an unintended submarine dive that will be challenging to manage are more recent than concerns about accidental flooding. The hydrodynamic forces can overpower any hydrostatic forces (such as blowing MBTs) that can be swiftly invoked, making it more typical of the high-speed submarine due to both the shorter period in which recovery action can become effective and the hydrodynamic forces' ability to swamp them. A submarine traveling at a speed of for example 30 knots would pass through a 300-meter depth band in less than a minute if its pitch angle was 20 degrees, to illustrate how brief the time scale would be [23].

The occurrence that is regarded as the most dangerous in terms of unintentional dive at high speeds is jammed aft hydroplanes. In contrast to inadvertent flooding, which has happened multiple times during submarine operations, there is limited evidence of aft planes jamming in service, but there have been a few less serious incidents when they have lost contact with their operational equipment. A "maximum credible accident" should thus be considered in the situation of the jammed aft planes [23]. Determining which jam aspect is believable is the challenge.

If the bow planes have not been retracted, an aft plane jam at a high enough speed would cause them to offset but not overcome the aft control moment. Because it emphasizes the relevance of lowering forward speed as much and as fast as feasible, the occurrence has significance as a design hazard. Since time is of the essence, reducing the propulsor's rotations would help the vessel slow down even though it is improbable that the propulsor could be put in reverse in the allotted time, which would have a significant braking impact. An additional contribution could be to put the rudders over which would further add to the braking effect

because of the significant speed drop in turning, but whether or not the submarine was known to have the "stern dipping" tendency would determine the acceptability of that solution. There is a series of steps that could be followed in whichever order and has shown to be practical for emergency recovery from jammed aft planes [51]:

- Blow the MBTs.
- Decrease speed.
- Put rudders hard over.
- Put bow planes hard to rise.

But the main inference to be made from the depth excursion incident is that the issue is primarily caused by high speed, and that speed must be gradually reduced as the submarine dives deeper because it reduces the amount of space between the current depth and full diving depth. Furthermore, the allowable angle should gradually decrease as speed is increased because the aft planes won't jam at a tilt angle greater than when the incident occurs. The previous statement is connected to the presumption of a cruciform stern arrangement, although some restrictions on speed and control surface angles appear reasonable even with different arrangements [23].

2.2.4 Manoeuvring limitations

As would be expected, the existence of risks of the kind mentioned above necessitates the provision of guidance to submarine operators regarding appropriate emergency recovery actions, rules governing how the submarine's speed should be limited in accordance with its operating depth, and related restrictions on the aft plane operating angles that are permitted. However, the restrictions differ based on the kind of incident that needs to be handled: flooding at depth necessitates a minimum speed restriction, whereas jammed aft planes necessitate a maximum speed/plane angle limitation as a function of depth [51].

2.2.5 Impact on design

Conflict exists between some of the relevant issues, as is so common in design. Why then have such big aft planes? In combination with the cruciform stern configurations, the aft planes provide a risk of depth excursion at speed, necessitating a series of reactions that completely extend recovery capabilities. However, switching to an X stern arrangement would be beneficial as well because large aft planes can contribute greatly to the recovery process from

a flooding incident that occurs in the submarine. Therefore, it is only reasonable to consider using alternative methods of adapting in case the aft planes in the cruciform configuration fail to function, like [23]:

- Supplying a high-pressure air cylinder to replace the hydraulic jacks in the event of a failure.
- Adding mechanical brakes that restrict the aft plane angle over a specific speed to ensure the vastness of the maximum jam angle.
- By separating aft planes, of which only half are active at higher speeds.
- Or an assortment of these options.

Another consideration in design is deciding the suitable area of the horizontal stabilizer fins aft; a too large area would result in a slow response when changing depth and unwelcome stabilization to a dive path; a too small area would make it difficult to maintain depth while traveling swiftly, though stability (although not in the sense of "stick fixed" stability) could be built into the autopilot controls. An additional safety concern relates to the region, design, and placement of the bridge fin and its potential to cause snap roll [23].

Although dynamics and control do not play a significant role in determining submarine sizing, they have a significant impact on the handling of the submarine and its inherent safety. The opposite is also true; the shape of the hull and appendages may greatly affect the vessel's natural dynamic behavior and result in various ways to address the control necessities [23].

3 Formulation of “Uncertainty analysis of the safety operating envelope of a Subsea Shuttle Tanker (SST)”

3.1 SOE

The SST can establish its service speed and operational depth from an emergency recovery standpoint by conducting an SOE analysis. For instance, the basic SST is intended to sail at a slow speed of 6 knots while using 90% less energy than a tanker ship [26]. A minimum service speed must be mandated because, as figure 3 illustrates, this slow pace might make the SST unrecoverable after floods. Additionally, the SOE can raise the operating depth of the SST by lowering the safety factor that was given to the structural design. A safety factor of 2.7 is needed for the baseline SST, which has a nominal dive pressure of 7 bar per the DNV naval submarine code [19]. This results in a very high collapse depth of 190 m, or a 19-bar design pressure, necessitating heavy and complicated steel construction. Nevertheless, by comprehending SST recovery behavior during a malfunction, the collapse dive depth may be decreased. Therefore, from the perspective of operational safety, a lower safety factor is suggested. In addition, the qualities of the seafloor and depth have little bearing on the SOE. An SST operation's depth and seabed clearance, however, is decided by the decision-makers with the assistance of the SOE.

Commercial submersibles have no documented examples of SOE studies, in contrast to navy submarines where such analyses have been conducted for decades. Additionally, the SST varies from traditional submarines in several ways since it is a unique mercantile vessel. For instance, while the SST goes far more slowly than a navy submarine, the risks and effects are different. Additionally, for the SST to be economically viable, its payload must be at least 50% of its dry weight, in contrast to a navy submarine, whose structure and equipment make up around 80% of its dry weight [28]. To avoid a heavy-pressure hull, the SST's collapse pressure is far lower than that of a navy submarine.

The identified SST SOE will be substantially different from the SOE for a navy submarine due to these variations. As a result, this work adds contributes to the body of knowledge on SOE analysis for non-military and commercial submersibles. The approach outlined in this study applies to additional novel underwater vessels in development that aim to

support a low-carbon marine industry, such as freight gliders and civilian submersibles [29]. These crafts have a variety of uses, including hovering [30] and depth control [31]. In contrast to Park and Kim's [32] [35] completely connected 6 DoF model, a decoupled 3 degrees of freedom (DoF) planar model is suggested in this study.

This is sufficient to illustrate an emergency recovery action. Ross [33] discovered that a submersible may be broken down into two lateral and longitudinal subsystems that do not communicate. This is particularly relevant to a thin, port-to-starboard symmetric body like a submarine [34]. The coordinate system consists of a body-fixed reference frame positioned at the SST center of buoyancy (CoB) and a North-East-Down (NED) coordinate system with its origin fixed to the Earth's reference point. Figure 5 displays the coordinate system utilized in this research.

3.2 Accidental case and standard operating procedure

An SOE is produced by simulating a large number of simulations tailored to various incidents [35] [36]. Therefore, it is crucial to specify the standard operation procedure (SOP) whenever a failure occurs. The SST should respond to a failure by adhering to a set of SOPs. SOPs for accidental cases are defined in this section. Further on are successful recoveries and loss-of-vessel criteria mentioned.

3.2.1.1 Partial flooding

According to Renilson [36], a submarine can flood through its sea-connected systems, which are generally kept shut. The valves for loading and unloading or loading ballast for the SST may experience this. Flooding is exposed when the SST is moving slowly.

Without displaying a precise arrangement, the graphic of length versus cross section depicts the vessel's volume distribution. The machinery compartments, which are the free-flooding compartments, are susceptible to flooding. This analysis considers an open valve in the aft compartment. To accomplish emergency recovery when flooding occurs in the aft compartment, three steps are done:

1. Increase the speed of the vessel by applying maximum forward rpm.
2. Increase the buoyancy of the vessel by blowing the MBTs.
3. Initiate lift force to pressure the vessel to arise by enforcing maximum bow plane angle.

An unpowered, high-rate ascending maneuver may result in destabilization in the horizontal plane and encourage significant roll motion, according to knowledge gained from naval submarines [38] [39] [40] [41]. Renilson [36] recommended limiting the pitch angle during emergency rising and all of the ballast tanks should be blown simultaneously rather than just the front tank to prevent this issue. The vessel is recovered if it reaches the water's surface during flooding without going beyond:

- The maximum trimming angle.
- The maximum diving depth.
- The seafloor.

The modeling for the flooding rate is as follows:

$$r = \rho A_{fld} \sqrt{2 g h_d(t)} \quad (1)$$

Where:

r	Seawater flood rate
A_{fld}	Area of opening
g	Gravity
$h_d(t)$	Diving depth at the time t

The models' maximum flooded capacity is $600m^3$ because watertight bulkheads also split the free flooding region into smaller compartments, and the area of the opening is set to $0.785m^2$.

3.2.1.2 Control plane jamming

With the SST, each X-plane is independently actuated. Since the remaining three planes can still be able to be utilized for roll control, a single control plane jam is regarded as a failure mode. The SST's control plane jamming failure has two possible outcomes: jam-to-rise or jam-to-dive. For each scenario, the SST should follow a distinct process. The following is the emergency recovery procedure to handle the control plane jamming failure:

3.2.1.3 Jam-to-dive

In order to avoid a jam-to-dive, the submarine performs a rising emergency maneuver. Three stages make up the emergency rising technique. The first stage involves slowing down the propeller revolution to slow down the diving speed. The second step involves increasing the pitch angle through bow-side MBT blowing and bow-plane deflection. After increasing the propeller revolution, stern-side MBT blowing will be employed to accelerate the submarine's ascent if the pitch angle turns positive. For any speed circumstance, the maximum excursion depth or maximum safety depth establishes the SOE jam-to-dive limit. The maximum excursion depths are computed for each speed condition by determining the maximum beginning depth to ensure that the submarine does not go beyond the collapse depth by performing an emergency rising procedure from the jam-to-dive scenario. The jam-to-dive boundary is determined to be the value that is closer to the maximum safety depth than the maximum excursion depth. If the vessel reaches an upward trajectory before colliding with the seafloor or surpasses the collapse depth, it has recovered. The maximum trimming angle ought to not be surpassed either [51].

3.2.1.4 Jam-to-rise

The employment of MBT blowing is inappropriate in this case, thus the crash stop maneuver is used to deal with the jam-to-rise. The submarine slows down and reverses its propeller to come to a stop and then performs a maximum positive bow plane angle to halt the climb. The three free aft control planes maintain the heel angle similarly to jam-to-dive recovery action. The vessel is recovered in a jam-to-rise scenario if it doesn't breach the surface or surpass the pitch limit. Calculating the excursion depth during the crash stop and adding the variance in depth to the minimum safety depth will get the jam-to-rise limit. Based on the above-described process, the emergency rising maneuver and crash stop simulations are carried out to determine the SOE of the submarine [51].

3.2.1.5 Maneuvering limits

When configuring the SOE, a set of maneuvering restrictions is established. These parameters include SST reaction time, control plane response angles, pitch angle restrictions, and depth limits. Table 2 provides a list of the movement restrictions for deploying the SOE. The following definitions are the most important:

- Safety depth: The safety depth is the SST's bare minimum operational depth. The SST runs the danger of colliding with deep-draft ships and other offshore structures if it travels above this depth. The DNV Naval Submarine Code advises against submarine navigation in waters deeper than 30 to 40 meters [19].
- Nominal diving depth: Between this depth and the safety depth, the SST is permitted to operate unrestrictedly. For the SST, this parameter is set to 70 m.
- Collapse diving depth: At collapse dive depth, the hydrostatic pressure equals the 19-bar SST intended pressure. As a result, the structural design of the SST depends heavily on the collapse dive depth.
- Pitch angle restrictions: The SST's maximum pitch angle is not constrained by the human component, or the safety of the crew, because it is autonomous. An excessive pitch inclination, nevertheless, can potentially cause onboard gear and equipment to fail. While operating at high speeds, a large pitch angle can be hazardous because it only takes a minute for the SST to transition from nominal diving depth to collapse diving depth. When the control plane jams, there is not enough time for recovery action. Burcher and Rydill [23] estimated that the greatest pitch angle of submarines, in reality, is around 20 degrees. The pitch limit for a high-speed operation is 5-10 degrees. In this thesis, emergency recoveries are carried out at starting pitch angles of 10, 15, and 20 degrees.
- Reaction time: The response time is the amount of time between a malfunction and a corrective action. Significantly reducing the response time from seconds down to milliseconds is possible with an extremely high degree of autonomy. As a result, when a failure occurs, the SST will respond immediately.

Table 2 - SST manoeuvring limitations

Parameter	Value	Unit
Safety depth	40	m
Nominal diving depth	70	m
Collapse depth	190	m
Pitch angle restriction	$10, 15, 20$	°
Aft control plane jam angle	15	°
Bow control plane reaction angle	20	°
Reaction time	0	s

3.3 Safety margins

You may visualize the safe operating envelope graphically. The operational ranges are depicted in Figure 4 as a succession of "envelopes." Staying within the typical operating range (green zone) is the objective of safe operation. Aside from temporary situations, the SST is not required to run inside the yellow zone that separates the Normal Operating range from the Safe Operating Limit (red zone). This area is known as the "safety margin," and maintaining safety margins is a component of risk management. Operation outside of the design basis is tolerated on the belief that "safety margins can be used to improve production." The financial risk and the safety risk both rise as a result of this [23].

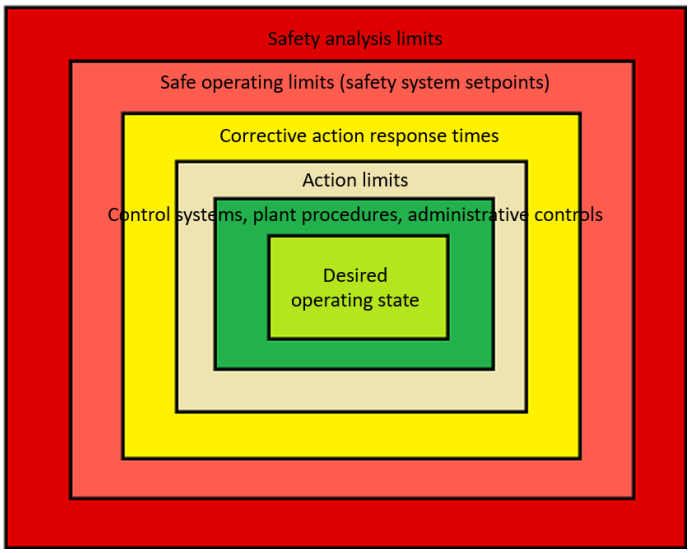

Figure 4 - Graphical representation of the safety operating envelope

4 Dynamics modeling of a Subsea Shuttle Tanker (SST)

4.1 Maneuvering model

This section explains how the SST maneuvering model is set up. The model is created in the block-diagram-based graphical programming environment MATLAB Simulink 2021a [42]. It has been widely employed in the field of subsea drones and is used to graphically build out a real multibody system. The maneuvering model is broad and may be aided with numerous functions to address diverse issues, including depth control [30] and hovering [31]. In contrast to Park and Kim [24], who employed a fully connected 6 DoF model, this work proposes a decoupled 3 DoF planar model [24] [25]. This is sufficient to illustrate an emergency recovery action. A submersible may be broken down into two separate, non-interacting subsystems called the longitudinal and lateral, according to Ross [33]. This is particularly suitable for symmetrical port-starboard thin bodies like submarines [34]. The coordinate system consists of a body-fixed reference frame at the SST center of buoyancy and a North-East-Down (NED) coordinate system with its origin set to the Earth's reference point (CoB). Figure 5 displays the coordinate system utilized in this investigation.

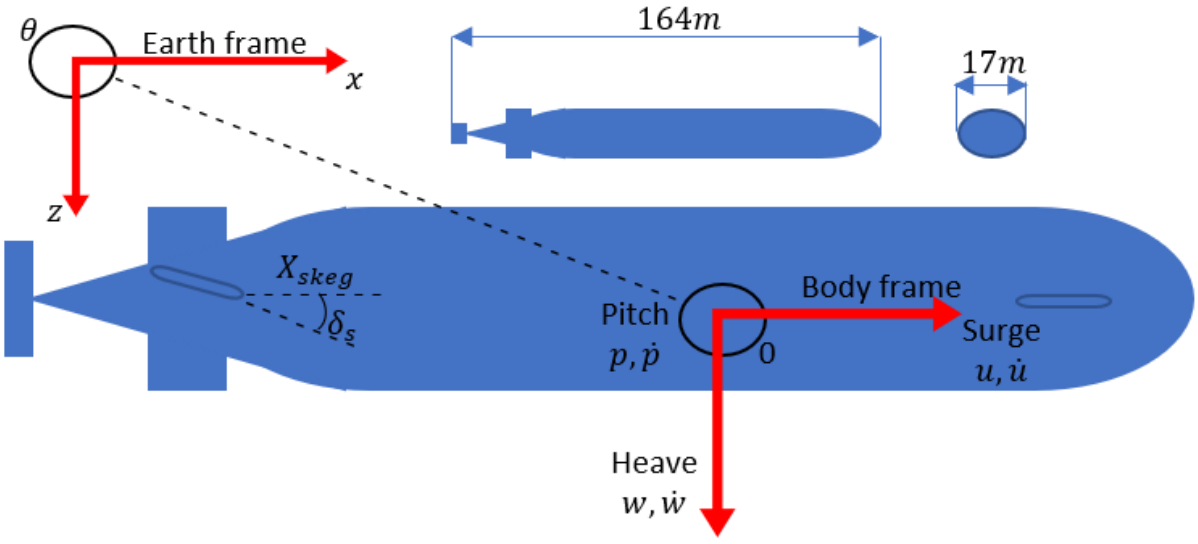

Figure 5 - SST coordinate system

4.1.1 Plant model

Equations (2) and (3) present longitudinal subsystem equations of motion taking surge, heave, and pitch into account and represented in a vectorial manner using Fossen notation [43]:

$$\dot{\eta} = J_\theta(\eta)v \tag{2}$$

$$M\dot{v} + C(v)v + D(v)v + g(\eta) = \tau \tag{3}$$

Where:

$\dot{\eta}$	Vector consisting of NED position and Euler angles
$J_\theta(\eta)$	Euler transformation matrix
v	Linear and angular velocity in the body-fixed system
M	System mass matrix consisting of SST mass and added mass
$C(v)$	Coriolis-centripetal matrix
$D(v)$	Damping matrix
$g(\eta)$	Force vector considering gravitational and buoyancy forces
τ	Control force vector from propellers and hydroplanes acting on the center of gravity

The component form of the kinematic equation (2) is expanded as follows using the Euler angle representation:

$$\underbrace{\begin{bmatrix}\dot{N}\\ \dot{D}\\ \dot{\theta}\end{bmatrix}}_{\dot{\eta}} = \underbrace{\begin{bmatrix}\cos\theta & \sin\theta & 0\\ -\sin\theta & \cos\theta & 0\\ 0 & 0 & 1\end{bmatrix}}_{J_\theta(\eta)}\underbrace{\begin{bmatrix}u\\ w\\ q\end{bmatrix}}_{v} \tag{4}$$

Further on we can write the mass matrix, the Coriolis-centripetal matrix, and the damping matrix. The matrixes are represented in equations (5), (6) and (7) respectfully.

$$M = \begin{bmatrix} m - X_{\dot{u}} & 0 & mz_g \\ 0 & m - Z_{\dot{w}} & -Z_{\dot{q}} \\ mz_g & M_{\dot{w}} & I_{yy} - M_{\dot{q}} \end{bmatrix} \tag{5}$$

$$C(v) = \begin{bmatrix} 0 & 0 & 0 \\ 0 & m - Z_{\dot{w}} & -(m - X_{\dot{u}})u \\ 0 & (Z_{\dot{w}} - X_{\dot{u}}) & 0 \end{bmatrix} \quad (6)$$

$$D(v) = \begin{bmatrix} X_{|u|u}|u| & X_{wq}q & X_{qq}q \\ Z_{uq}q & Z_{|w|w} + Z_{uw}u & Z_{|q|q} \\ M_{uw}W & M_{|w|w} & M_{uq}u + M_{|q|q} \end{bmatrix} \quad (7)$$

Where:

m	Mass
z_g	Centre of gravity in z-coordinate
$X_{\dot{u}}$	Axial added mass
$Z_{\dot{w}}$, $Z_{\dot{q}}$, $M_{\dot{w}}$, $M_{\dot{q}}$	Crossflow added mass terms related to heave and pitch
$Z_{\|w\|w}$, $M_{\|w\|w}$, $Z_{\|q\|q}$, $M_{\|q\|q}$	Crossflow damping terms
X_{wq}, X_{qq}, Z_{uq}, M_{uq}	Cross-term hydrodynamic derivatives
$X_{\|u\|u}\|u\|$	Quadric axial drag derivative
Z_{uw}	Body lift hydrodynamic derivative
M_{uw}	Total cross-term pitch moment hydrodynamic derivative

Table 3 – Hydrodynamic derivatives

Parameter	Value	Unit	Parameter	Value	Unit
$X_{\dot{u}}$	$-5.14 * 10^5$	kg	$Z_{\|q\|q}$	$4.79 * 10^9$	$kg * m$
$Z_{\dot{w}}$	$-3.29 * 10^7$	kg	$M_{\|q\|q}$	$-4.34 * 10^{12}$	$kg * m^2$
$M_{\dot{w}}$	$-4.40 * 10^8$	$kg * m$	X_{wq}	$-3.28 * 10^7$	kg
$Z_{\dot{q}}$	$-4.40 * 10^8$	$kg * m$	X_{qq}	$-4.40 * 10^8$	$kg * m$
$M_{\dot{q}}$	$-6.39 * 10^{10}$	$kg * m^2$	Z_{uq}	$5.14 * 10^5$	kg
$X_{\|u\|u}$	$-1.64 * 10^4$	$kg * m$	M_{uq}	$-4.40 * 10^8$	$kg * m$
$Z_{\|w\|w}$	$-1.42 * 10^6$	$kg * m$	Z_{uw}	$-2.42 * 10^5$	kg/m
$M_{\|w\|w}$	$1.67 * 10^7$	kg	M_{uw}	$-3.99 * 10^7$	kg

Table 3 is a list of the values utilized for each of the hydrodynamic terms. Equations (8) through (26) estimate the hydrodynamic coefficients following Prestero's studies on the REMUS AUV [44].

The empirical formula presented by [45], which estimates the added mass of an ellipsoid, is used for determining the axial added mass of the SST:

$$X_{\dot{u}} = -\frac{4\alpha\pi\rho}{3}\left(\frac{l_{SST}}{2}\right)\left(\frac{d_{SST}}{2}\right)^2 \quad (8)$$

Where:

$X_{\dot{u}}$	Added mass
α	Empirical parameter $= 0.021$
l_{SST}	Length of the SST
d_{SST}	Length of beam

Faltinsen [45] describes the extra mass of a circular slice submerged in water as follows:

$$m_a(x) = \pi\rho R(x)^2 \quad (9)$$

By integrating the added mass of circular slices along the body, the crossflow added mass components relating to heave and pitch are determined. These are stated in equations (10) through (13):

$$Z_{\dot{w}} = -\int_{x_{tail}}^{x_{bow}} m_a(x)dx \quad (10)$$

$$M_{\dot{w}} = \int_{x_{tail}}^{x_{bow}} x m_a(x)dx \quad (11)$$

$$Z_{\dot{q}} = M_{\dot{w}} \quad (12)$$

$$M_{\dot{q}} = -\int_{x_{tail}}^{x_{bow}} x^2 m_a(x)dx \quad (13)$$

Where:

x_{bow} Location of bow $= 88.7\ m$

x_{tail} Location of tail $= 75.3\ m$

It is possible to determine the quadratic axial drag derivative as:

$$X_{|u|u} = -0.5\rho c_d A_f \quad (14)$$

Where:

c_d Axial drag coefficient $= 0.145$

A_f The frontal projected area of the SST $= 227.0\ m^2$

Equations (15) through (18) express the crossflow damping terms:

$$Z_{|w|w} = -0.5\rho c_{dc} \int_{x_{tail}}^{x_{bow}} 2R(x)dx \quad (15)$$

$$M_{|w|w} = 0.5\rho c_{dc} \int_{x_{tail}}^{x_{bow}} 2xR(x)dx \quad (16)$$

$$Z_{|q|q} = 0.5\rho c_{dc} \int_{x_{tail}}^{x_{bow}} 2x|x|R(x)dx \quad (17)$$

$$M_{|q|q} = -0.5\rho c_{dc} \int_{x_{tail}}^{x_{bow}} 2x^3R(x)dx \quad (18)$$

Where:

c_{dc} Crossflow drag coefficient = 1.1 [47]

The following (19) through (23) is how cross-term hydrodynamic derivatives are obtained:

$$X_{wq} = Z_{\dot{w}} \quad (19)$$

$$X_{qq} = Z_{\dot{q}} \quad (20)$$

$$Z_{uq} = -X_{\dot{u}} \quad (21)$$

$$M_{uq} = -Z_{\dot{q}} \quad (22)$$

$$M_{uw_a} = -(Z_{\dot{w}} - X_{\dot{u}}) \quad (23)$$

SST body lift is represented as (24) and lift-induced pitch moment as (25).

$$Z_{uw} = -0.5\rho d^2 c_{yd\beta} \quad (24)$$

$$M_{uw_l} = -0.5\rho d^2 c_{yd\beta} x_{cp} \quad (25)$$

Where:

$c_{yd\beta}$ Lift slope coefficient $= 0.003$ [44]

x_{cp} Viscous force centre $= -31.6\ m$ [47]

Finally, the added mass contribution and body lift contribution are summed to describe the total cross-term pitch moment hydrodynamic derivative:

$$M_{uw} = M_{uw_a} + M_{uw_l} \quad (26)$$

4.1.2 Actuation Model

The components of the SST actuation system which are related to jam-to-rise and jam-to-dive are the propeller, the control planes, and the compensation tanks blowing.

4.1.2.1 Propeller

A Wageningen B4-70 propeller powers the SST. Table 4 is a list of the propeller's design specifications. It has a pitch ratio of 1.0. The open-water thrust coefficient K_T is extrapolated using an 8th-order polynomial function of advance number J from the open-water test result in Smogeli [48]. The formula for the fitted polynomial function is (27):

$$K_T = -2.157J^8 + 5.006J^7 - 1.399J^6 - 4.309J^5 + 2.999J^4 + 0.564J^3 - 0.998J^2 - 0.133J^2 + 0.444 \quad (27)$$

The calculation for the advance number J is as follows:

$$J = \frac{1 - w_T}{nD} u \quad (28)$$

Where:

w_T	Wake fraction
n	Propeller's rotational speed
D	Propeller diameter
u	Surge velocity

The propeller is managed using a Proportional-Integral-Derivative (PID) controller. The PID controller uses the target propeller rpm and the actual propeller rpm error to determine the required motor output. A saturation block then symbolizes the motor torque's highest level. The shaft's and the propeller's rotational inertia is represented by a second-order transfer function. It can mimic reaction lag brought on by the dynamics of the motor and shaft. This often occurs whenever there is a sudden change in the thrust reference. Lastly, the SST surge velocity and propeller revolution speed are used to determine the propeller's real-time thrust [51].

Table 4 - Propeller parameters

Parameter	Value	Unit
Type	Wageningen B4-70	–
Blade number	4	–
Diameter	7	m
Expanded blade ratio	0.7	–
Pitch ratio	1	–
Wake fraction	0.47	–
Rotational inertia	$4.5 * 10^5$	$kg * m^2$
Maximum engine torque	$2.5 * 10^5$	$N * m$

4.1.2.2 Control plane

A linear lift rate coefficient is used to describe the contribution of the control planes to the forces and moments acting on the SST. The control plane generates the following forces: Drag force, lift force, and pitch moment, the forces can be calculated using equations (29) though (31) respectfully.

$$X_{\delta c} = -0.5\rho V^2 A_c C_{D\delta} \quad (29)$$

$$Z_{\delta c} = 0.5\rho V^2 A_c C_{L\delta} \quad (30)$$

$$M_{\delta c} = 0.5\rho V^2 A_c x_c C_{L\delta} \quad (31)$$

Where:

$X_{\delta c}$	Control plane drag
$Z_{\delta c}$	Control plane lift
$M_{\delta c}$	Control plane pitch moment
V	Relative velocity
$C_{D\delta}$	Drag rate coefficient
$C_{L\delta}$	Lift rate coefficient

Table 5 is a list of the bow and aft control plane configurations.

Table 5 - Control plane parameters

Parameter	Symbol	Value	Unit
Bow plane position	x_{bow}	30	m
Bow plane area	A_{bow}	50	m^2
Bow plane drag rate coefficient	$C_{DB\delta}$	2.1	$-$
Bow plane lift rate coefficient	$C_{LB\delta}$	0.01	$-$
Bow plane angle rate limit	$-$	± 5	$°/s$
Aft plane position	x_{aft}	-70	m

Aft plane area	A_{aft}	40	m^2
Aft plane drag rate coefficient	$C_{LA\delta}$	6.1	$-$
Aft plane lift rate coefficient	$C_{DA\delta}$	0.01	$-$
Aft plane angle rate limit	$-$	± 5	$°/s$

4.1.2.3 Compensation tanks blowing

The SST has two compensating tanks that are placed in the free flooding compartments at the bow and aft. Throughout the normal operation, these tanks are stocked with ballast. To guarantee neutral buoyancy, or that the SST's weight is equal to buoyancy, the ballast contents within compensating tanks are dependent on the cargo tank condition. The compensating tank blowing is done during the emergency rising maneuver. The mechanism of the SST's tank blowing is identical to that of a crewed navy submarine and has been well-documented [37] [40] [55] [56]. The compensating tank blowing during emergency recovery is schematically shown in Figure 6.

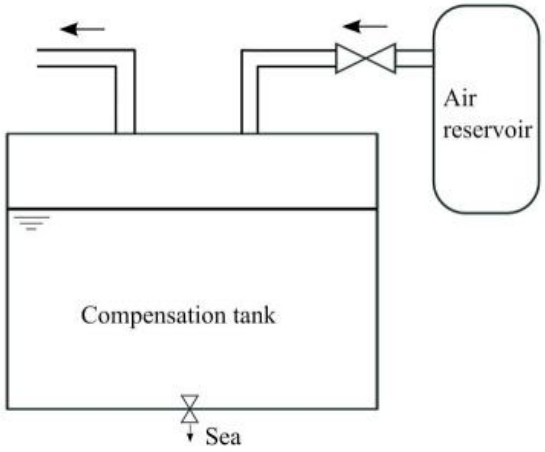

Figure 6 - Schematic of compensation tank blowing [51]

There are three phases to this procedure:

- First, compressed air from the air reservoir is injected into the tank via the high-pressure air system. As a result, the compensation tank's pressure quickly rises and surpasses the hydrostatic pressure outside.
- Second, the compensating tank's air volume expands, expelling the ballast water's bottom.

- Last, when the buoyancy force finally exceeds the SST weight, the SST is compelled to ascend.

This procedure is referred to as an air-volume ratio in the compensating tank [37]. This mathematical description of the SST is given as:

$$\frac{V_a}{V_t} = A_1 + \sqrt{A_1^2 + A_2^2} \quad (32)$$

$$A_1 = \frac{-p_a - \rho g(Z_0 - x_t sin\theta - 0.45 D_t cos\theta)}{1.8 \rho g D_t cos\theta} \quad (33)$$

$$A_2 = \frac{m_{a0} C_g T(1 - e^{-tC_b})}{0.9 \rho g D_t n_t V_t cos\theta} \quad (34)$$

Where:

V_a	The volume of air inside the compensation tank
V_t	The volume of a compensation tank
p_a	Atmospheric pressure
z_0	Diving depth
x_t	Position of the compensation tank along the x-axis
D_t	Tank diameter
m_{a0}	The initial mass of compressed air inside the reservoir
C_g	Gas constant
T	The temperature inside the compensation tank
t	Time since the emergency recovery action started
C_b	Tank blowing constant
n_t	Total number of compensation tanks

Table 6 lists the variables related to compensating tank blowing.

Table 6 - Compensation tank blowing parameters

Parameter	Symbol	Value	Unit
Compensation tank volume	V_t	800	m^3
Atmospheric pressure	p_a	$1 * 10^5$	Bar
Compensation tank position	x_t	$67.8, -67.8$	M
Compensation tank diameter	D_t	8	M
Reservoir air mass	m_{a0}	13,000	Kg
Gas constant	C_g	8.31	$Kg * m^2 * s^{-2} * K^{-1} * mol^{-1}$
Tank temperature	T	283.15	K
Tank blowing constant	C_b	-0.03	$-$

4.2 Current

A current model is presented and is based on the work of Fossen [43] and Sørensen [49]. Both the current speed V_c and the inflow angle θ_c may be described by a first-order Gauss-Markov process:

$$\omega_1 = \dot{V}_c + \mu_1 V_c \quad (35)$$

$$\omega_2 = \dot{\theta}_c + \mu_2 \theta_c \quad (36)$$

Where μ_1, μ_2 are constants linked to the time constant of the Gauss-Markov process, and they should both be positive; As greater values might lengthen the rising time until a steady state current is obtained, it was decided to set both μ_1, μ_2 values to low $(= 1)$ values. ω_1, ω_2 are Gaussian white noise [43]. Two values are chosen for the inflow angle cc, 0 (following current) and π (heading current).

This model examines mean current velocity at 0.5 m/s and 1 m/s with STD variation equal to 5% and 10% where:

$$STD_{variation}(CV) = \frac{\sigma}{V_c} \quad (37)$$

Where:

σ	Standard deviation
V_c	Mean current velocity

Figuring out how to describe the current velocity in the global frame was the first step in this paradigm, see figure 5. Next, the current velocity is converted into the SST body-fixed frame and added to the SST velocity to obtain the relative velocity. The hydrodynamic forces are then computed:

$$\begin{bmatrix} u_c \\ \omega_c \end{bmatrix} = \underbrace{\begin{bmatrix} \cos\theta & \sin\theta \\ -\sin\theta & \cos\theta \end{bmatrix}}_{Transformation\ matrix} \begin{bmatrix} \dot{x}_c \\ \dot{z}_c \end{bmatrix} \quad (38)$$

$$\dot{x}_c = V_c \cos\theta_c \quad (39)$$

$$\dot{z}_c = V_c \sin\theta_c \quad (40)$$

Where:

$\left.\begin{matrix} u_c \\ \omega_c \end{matrix}\right\}$	Current components in the SST body-fixed frame
θ	Pitch angle
$\left.\begin{matrix} \dot{x}_c \\ \dot{z}_c \end{matrix}\right\}$	Global frame's current velocity components

4.3 Simulink model

The Simulink model shown in figure 7 is constructed using the authors' earlier work [50] [51] [52]. The model is divided into 4 parts, which are:

- Command blocks
- Actuation model
- Current: for the stochastic current to be simulated
- Plant model

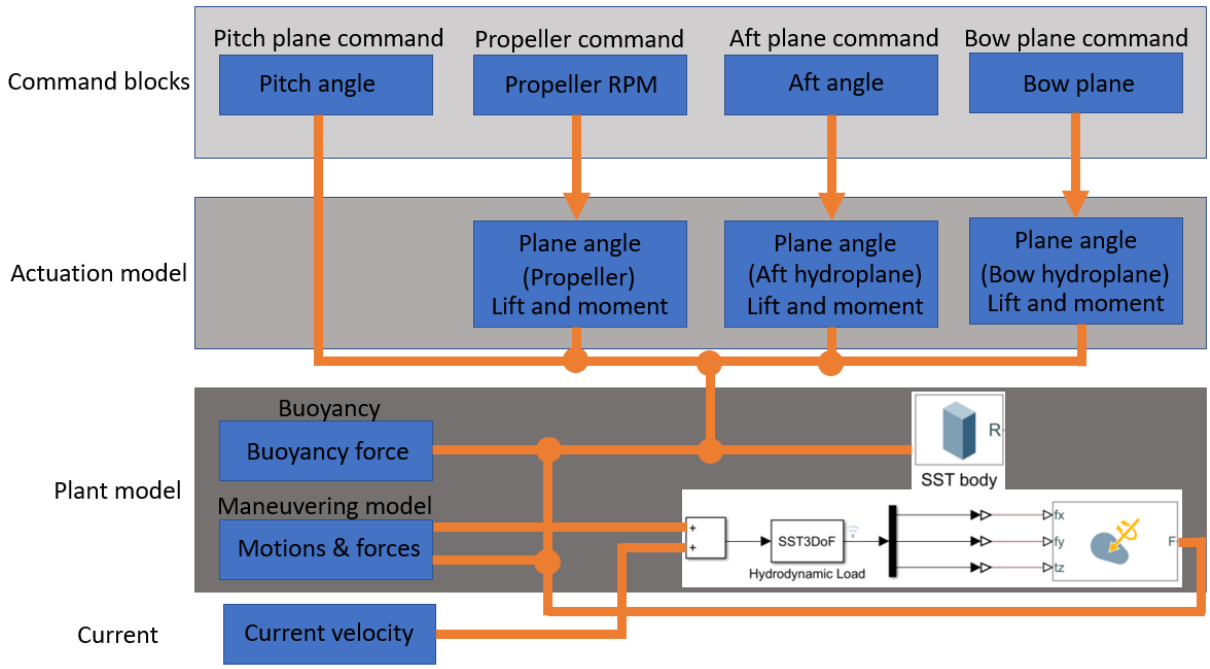

Figure 7 - Simulink model

4.4 Extreme value prediction and Gumbel distribution

4.4.1 Extreme value prediction

The biggest maximum derived from a realization (X_e) is referred to as the extreme value in any stochastic process $X(t)$ taken over a time period (t), such as 1000 seconds. The multiple maxima are thus independently and identically distributed throughout the common distribution function $F_{X_m}(x)$ in a common realization based on this supposition.

As a result, the distribution of X_e is identified as follows from the equation below:

$$F_{X_e}(x) = Prob\{X_e \leq x\} = [F_{X_m}(x)]^n \quad (41)$$

An extreme value distribution has been approximated using a variety of statistical techniques. In this study, the extreme recovery depth values for the SST in the event of jam-to-rise and jam-to-dive will be predicted using the Gumbel distribution.

4.4.2 Gumbel fitting method

Several times it has been shown that if the sample size (n) is high enough, equation (38) will converge to the Gumbel, Fréchet, or Weibull distribution. These distributions are a family of cumulative distribution probability that incorporates the generalized extreme value (GEV) distribution and are hence also known as the type I, II, and III extreme value distributions, respectively.

$$F_{X_e}(x) = exp\,(-1 + \gamma\left(\frac{x-\mu}{\sigma}\right)^{-\frac{1}{\gamma}}) \quad (42)$$

Where:

γ	Shape parameter
μ	Location parameter
σ	Scale parameter

For modeling maritime structures, limiting $\gamma \to 0$ enables the approximation to fit the Gumbel distribution [53].

$$F_{X_e}(x) = exp(-exp(-\alpha\,(x-\mu))) \quad (43)$$

Where:

α	Scale parameter
μ	Location parameter

Equation (43) may be recast as a linear function by applying a logarithm to the equation.

$$-ln\left[-ln\left(F_{X_e}(x)\right)\right] = \alpha\,(x-\mu) \quad (44)$$

The least-square fitting approach from the cumulative distribution probability, which is a straight line on a probability paper, may be used to approximate the parameters α and μ from the original data [54]. To find the extreme values for a given return time, we must first estimate the exceedance probability q, which may be found from the Poisson distribution. The Poisson distribution calculates the likelihood that an event will happen a certain number of times within a given period of time.

$$P(X=k) = \frac{\lambda^k e^{-\lambda}}{K!} \quad (45)$$

Where:

k	Number of events in an interval
λ	The average number of occurrences per interval

That allows us to write:

$$P(X=0) = e^{-\lambda} \quad (46)$$

And then the exceedance probability will be:

$$q = 1 - e^{-\lambda} \quad (47)$$

5 Motion simulation of a Subsea Shuttle Tanker (SST)

This study examines the uncertainty band for the aft control plane jam-to-dive and jam-to-rise cases in the presence of stochastic currents. 960 free running simulations have been run for each case with three inceptive pitch angles and four inceptive velocities for that goal. To dampen out the early transient period and achieve the steady-state phase the time for each simulation is set to 1000 seconds. Additionally, this simulation duration is sufficient to record the greatest and lowest depth excursion for each simulation. The post-processing step is when the time period between the occurrence and the success of the emergency recovery activity is chosen. This section presents the SST behavior during emergency recovery when jam-to-rise and jam-to-dive occur through an in-depth discussion of simulation outcomes. In addition, 24 further free-running simulations were done for each case for each initial pitch angle for the deterministic current scenario. Figures 8 and 11 show these to compare to later in this work.

5.1 Jam-to-rise

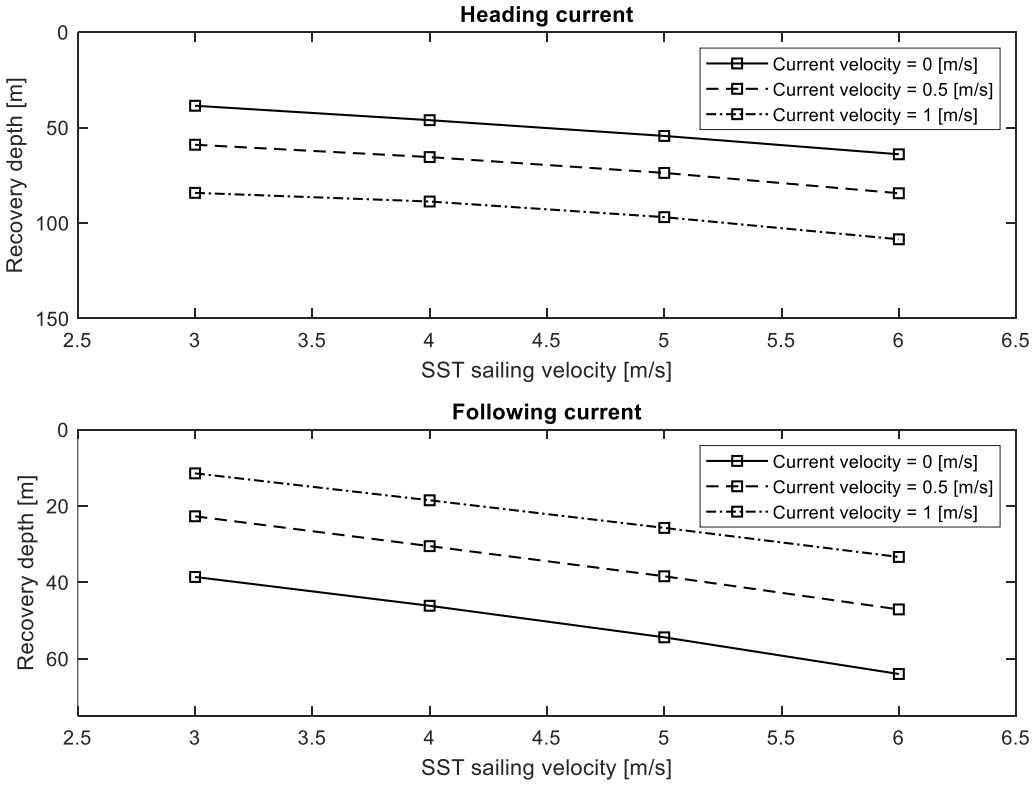

Figure 8 - Jam-to-rise recovery depth curve for different steady current cases for a 15-degree pitch angle.

Figure 8 supports the findings of earlier research [51]and demonstrates how the SST responds differently to following and heading currents. When up against the heading current, the recovery depth rises as the current speed does as well. According to the findings, a heading current causes the SST to rise, hence an increase in current velocity is going to increase the depth of recovery. However, when the SST is exposed to a following current, the recovery depth reduces as the current speed increases. In this case, the SST's rising motion is resisted by the following current. All SST sailing velocities exhibit these patterns. Additionally, Figure 8 shows that when the SST's speed increases, the gradient of the six lines increases. The percentage variation in recovery depth measured versus steady-current recovery depth is thus shown to decrease as the SST's speed is increased for both the following and heading current. These tendencies can also be seen in the cases with pitch angles of 10- and 20-degree (added in appendix). This is because the influence of the present velocity (following or heading) gets smaller as the SST travels at a faster rate.

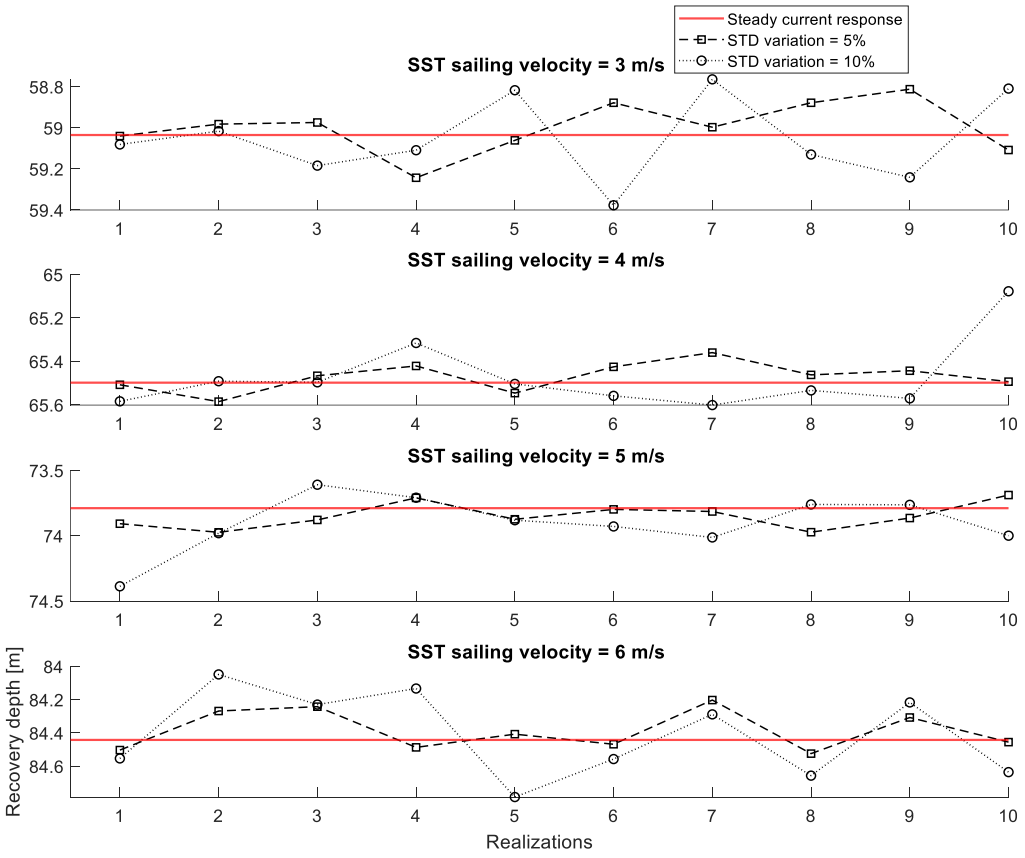

Figure 9 - Simulated SST responses during emergency recovery from jam-to-rise at different sailing velocities and heading current velocity = 0.5 m/s

Figure 9 displays the 10x2 realizations estimated based on a simulation time of 1000 seconds with an SST sailing speed of 3-6 m/s and a heading current velocity of 0.5 m/s.

Figure 10 displays the Gumbel fit for four recovery depth samples with SST velocity equal to 3 m/s, in heading current direction, and with varying velocities and STD fluctuations. On the graph, the extreme values for the 6-month, 1-year, and 5-year return periods are also shown. A 6-month recovery depth of 60.272m and 61.148m, respectively, were obtained from Figure 10 (top left, top right, respectively) for the two distinct STD variations with the current speed of 0.5 m/s. Even with little variations, these results are noteworthy, especially given that the other confidence interval and the two separate values do not overlap. For both the 1- and 5-year return periods, the data reveal comparable trends. A 6-month recovery depth of 87.486m and 87.812m, respectively, was obtained by increasing the current speed to 1 m/s and maintaining the other condition constant, as shown in Figure 10 (bottom left, bottom right, respectively). Similar to the justification provided before, the results revealed notable variations.

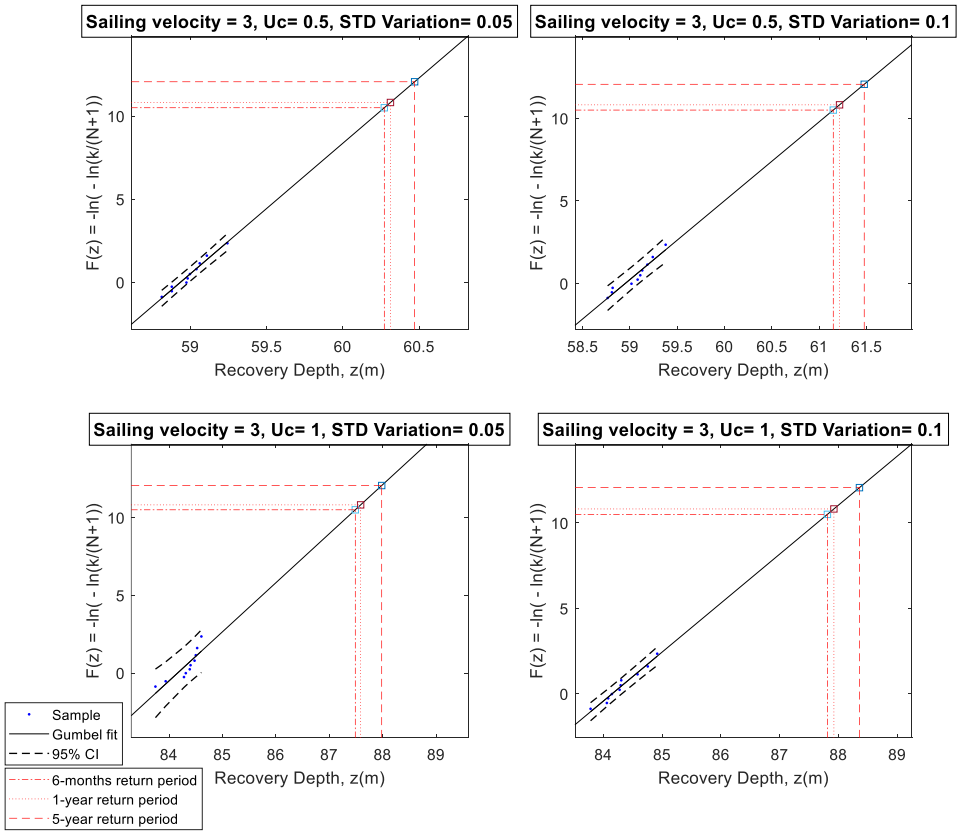

Figure 10 - Probability paper for Gumbel distribution for recovery depth corresponding to SST's velocity if 3 m/s, in heading current direction

With varied SST's sailing velocities, current speed, direction, and return times when compared with the two distinct STD variation values, a similar pattern, and conclusion may be reached using Tables 7 and 8. The difference in recovery depth for stochastic current under all SST's speeds, current speeds, directions, and return periods are shown in Table 9 when employing the two distinct STD variants. The results acquired from the simulations and the values received from the deterministic current case simulations are compared in this table. As an example, it is shown that an SST traveling at 3 m/s with a heading current of 0.5 m/s and exhibiting 5% STD variation throughout a 6-month return time resulted in a 2.1% increase in recovery depth compared to its equivalent deterministic value. Like how the 5-year return term produced a 2.43% rise in recovery depth under identical circumstances, this result was expected because lengthening the return periods will only raise the probable extreme recovery depth. Another example shows that a 5-year return time with a heading current of 1 m/s and 5% STD variation and an SST speed of 3 m/s increased recovery depth by 4.44% in comparison to its comparable deterministic value. The recovery depth rises to 4.89% for the identical scenario with a 10% STD variance. In a similar vein, given that rising STD differences alter recovery depth, this behavior is also predicted. However, the relative changes shown in Table 9 might differ by a percent of 0.97 to 21.44 %. By changing the SST's velocity from 3 to 6 m/s in a 1 m/s following speed direction and 10% STD variation during a 5-year return period, it is possible to examine how these return values behave, with the recovery depth values decreasing from 21.44% to 5.51%, respectively. This pattern also fits the predicted knowledge of the system, as it enables the SST to respond to changes more forcefully and quickly with a reduced recovery depth when the following current speed is maintained while the SST's speed is increased. As a result, it is clear from all of the figures and tables that the SST was designed with the forecasts of the extreme recovery depths in mind. By including improved control systems, backup recovery methods, or materials, these metrics can enhance the SST's design and make it more resilient to unforeseen changes.

Table 7 - Recovery depth predictions for several return periods for following current

SST sailing velocity [m/s]	$V_c = 0.5\ m/s$ $CV = 0\%$	$V_c = 0.5\ m/s$ $CV = 5\%$	$V_c = 0.5\ m/s$ $CV = 10\%$	$V_c = 1\ m/s$ $CV = 0\%$	$V_c = 1\ m/s$ $CV = 5\%$	$V_c = 1\ m/s$ $CV = 10\%$
			6 months return period			
3	22.729	(23.687)	(24.438)	11.480	(12.863)	(13.620)
		(23.633, 23.732)	(24.324, 24.550)		(12.775, 12.949)	(13.470, 13.758)
4	30.542	(31.272)	(33.200)	18.534	(19.938)	(21.243)
		(31.231, 31.313)	(33.091, 33.312)		(19.830, 20.041)	(21.057, 21.432)
5	38.435	(39.414)	(39.597)	25.763	(27.392)	(28.338)
		(39.364, 39.465)	(39.533, 39.661)		(27.258, 27.522)	(28.216, 28.461)
6	47.113	(48.185)	(49.460)	33.381	(35.206)	(34.979)

		(48.114, 48.257)	(49.367, 49.553)		(35.121, 35.293)	(34.859, 35.097)
			1-year return period			
3	22.729	(23.717)	(24.481)	11.480	(12.906)	(13.685)
		(23.663, 23.772)	(24.378, 24.603)		(12.818, 12.992)	(13.538, 13.820)
4	30.542	(31.296)	(33.284)	18.534	(19.982)	(21.326)
		(31.255, 31.337)	(33.174, 33.396)		(19.875, 20.085)	(21.140, 21.515)
5	38.435	(39.445)	(39.634)	25.763	(27.445)	(28.422)
		(39.394, 39.497)	(39.570, 39.698)		(27.312, 27.575)	(28.300, 28.547)
6	47.113	(48.221)	(49.535)	33.381	(35.260)	(35.028)
		(48.149, 48.293)	(49.442, 49.628)		(35.174, 35.348)	(34.908, 35.145)
			5-year return period			
3	22.729	(23.835)	(24.700)	11.480	(13.075)	(13.941)
		(23.780, 23.891)	(24.588, 24.811)		(12.989, 13.158)	(13.805, 14.064)
4	30.542	(31.389)	(33.615)	18.534	(20.156)	(21.653)
		(31.348, 31.431)	(33.502, 33.729)		(20.052, 20.255)	(21.464, 21.844)
5	38.435	(39.568)	(39.779)	25.763	(27.654)	(28.756)
		(39.516, 39.621)	(39.715, 39.844)		(27.524, 27.781)	(28.631, 28.883)
6	47.113	(48.359)	(49.830)	33.381	(35.472)	(35.219)
		(48.287, 48.431)	(49.737, 49.924)		(35.383, 35.563)	(35.102, 35.335)

Table 8 - Recovery depth predictions for several return periods for heading current

SST sailing velocity [m/s]	$V_c = 0.5\ m/s$ $CV = 0\%$	$V_c = 0.5\ m/s$ $CV = 5\%$	$V_c = 0.5\ m/s$ $CV = 10\%$	$V_c = 1\ m/s$ $CV = 0\%$	$V_c = 1\ m/s$ $CV = 5\%$	$V_c = 1\ m/s$ $CV = 10\%$
			6 months return period			
3	59.035	(60.272)	(61.148)	84.237	(87.486)	(87.812)
		(60.205, 60.340)	(61.007, 61.288)		(87.277, 87.666)	(87.614, 88.011)
4	65.498	(66.133)	(67.549)	88.773	(91.094)	(92.086)
		(66.103, 66.163)	(67.505, 67.582)		(90.949, 91.239)	(91.862, 92.313)
5	73.789	(74.871)	(76.159)	96.953	(99.470)	(100.424)
		(74.798, 74.943)	(75.949, 76.381)		(99.340, 99.601)	(100.129, 100.710)
6	84.442	(85.682)	(87.068)	108.550	(110.369)	(114.951)
		(85.571, 85.790)	(86.871, 87.266)		(110.257, 110.481)	(114.359, 115.491)
			1-year return period			
3	59.035	(60.312)	(61.214)	84.237	(87.587)	(87.921)
		(60.245, 60.380)	(61.074, 61.354)		(87.386, 87.760)	(87.723, 88.122)
4	65.498	(66.154)	(67.615)	88.773	(91.165)	(92.192)
		(66.124, 66.184)	(67.582, 67.639)		(91.020, 91.310)	(91.968, 92.421)
5	73.789	(74.904)	(76.231)	96.953	(99.546)	(100.534)
		(74.831, 74.975)	(76.018, 76.455)		(99.416, 99.678)	(100.241, 100.818)
6	84.442	(85.723)	(87.152)	108.550	(110.429)	(115.160)
		(85.613, 85.830)	(86.955, 87.350)		(110.317, 110.542)	(114.577, 115.690)
			5-year return period			
3	59.035	(60.471)	(61.475)	84.237	(87.981)	(88.356)
		(60.403, 60.540)	(61.335, 61.614)		(87.812, 88.127)	(88.155, 88.560)
4	65.498	(66.236)	(67.873)	88.773	(91.444)	(92.612)
		(66.206, 66.267)	(67.887, 67.863)		(91.298, 91.590)	(92.384, 92.844)
5	73.789	(75.031)	(76.512)	96.953	(99.847)	(100.967)
		(74.960, 75.101)	(76.292, 76.743)		(99.715, 99.982)	(100.680, 101.244)
6	84.442	(85.885)	(87.483)	108.550	(110.669)	(115.980)
		(85.777, 85.989)	(87.285, 87.681)		(110.556, 110.783)	(115.438, 116.473)

Table 9 - Percentage change in recovery depth compared to the deterministic current case

	Following current				**Heading current**			
SST sailing velocity [m/s]	$V_c = 0.5$ $CV = 5\%$	$V_c = 0.5$ $CV = 10\%$	$V_c = 1$ $CV = 5\%$	$V_c = 1$ $CV = 10\%$	$V_c = 0.5$ $CV = 5\%$	$V_c = 0.5$ $CV = 10\%$	$V_c = 1$ $CV = 5\%$	$V_c = 1$ $CV = 10\%$
	6-months return period							
3	4.22	7.52	12.05	18.64	2.10	3.58	3.86	4.24
4	2.39	8.70	7.58	14.62	0.97	3.13	2.62	3.73
5	2.55	3.02	6.32	10.00	1.47	3.21	2.60	3.58
6	2.28	4.98	5.47	4.79	1.47	3.11	1.68	5.90
	1-year return period							
3	4.35	7.71	12.42	19.21	2.16	3.69	3.98	4.37
4	2.47	8.98	7.81	15.06	1.00	3.23	2.70	3.85
5	2.63	3.12	6.53	10.32	1.51	3.31	2.68	3.69
6	2.35	5.14	5.63	4.94	1.52	3.21	1.73	6.09
	5-year return period							
3	4.87	8.67	13.89	21.44	2.43	4.13	4.44	4.89
4	2.77	10.06	8.75	16.83	1.13	3.63	3.01	4.33
5	2.95	3.50	7.34	11.62	1.68	3.69	2.99	4.14
6	2.65	5.77	6.26	5.51	1.71	3.60	1.95	6.85

5.2 Jam-to-dive

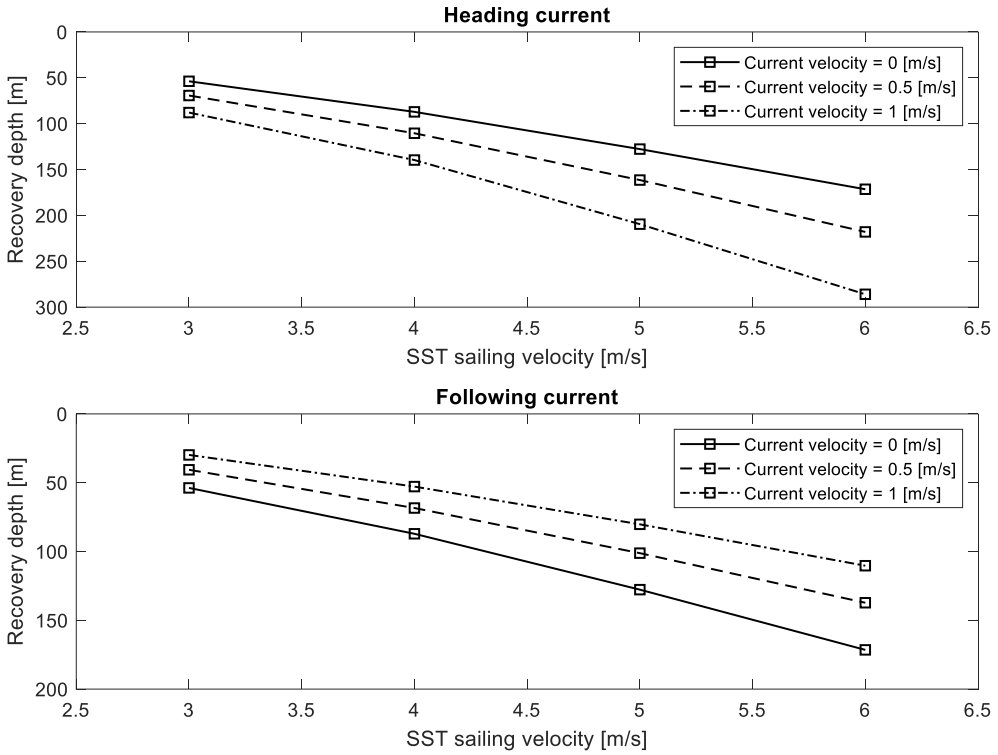

Figure 11 - Jam-to-dive curve for different steady current cases

Figure 11 supports the findings of earlier research [51] and demonstrates how the SST responds differently to following and heading currents. Recovery depth increases as current speed increases when going against the heading current. The results show that a heading current causes the SST to dive; as a result, an increase in current velocity will increase the depth of recovery. The recovery depth, however, decreases as the current speed increases when the SST gets exposed to a following current. The following current is here preventing the SST from diving. These trends may be seen in all SST sailing velocities. Figure 11 demonstrates how the gradient of the six lines grows as the SST's speed rises. As the SST's speed is raised for both the following and heading current, it is thus demonstrated that the percentage variance in recovery depth observed vs steady-current recovery depth decreases. The instances with 10- and 20-degree pitch angles (included in the appendix) exhibit the same patterns. This is because when the SST moves more quickly, the impact of the current velocity (following or heading) diminishes.

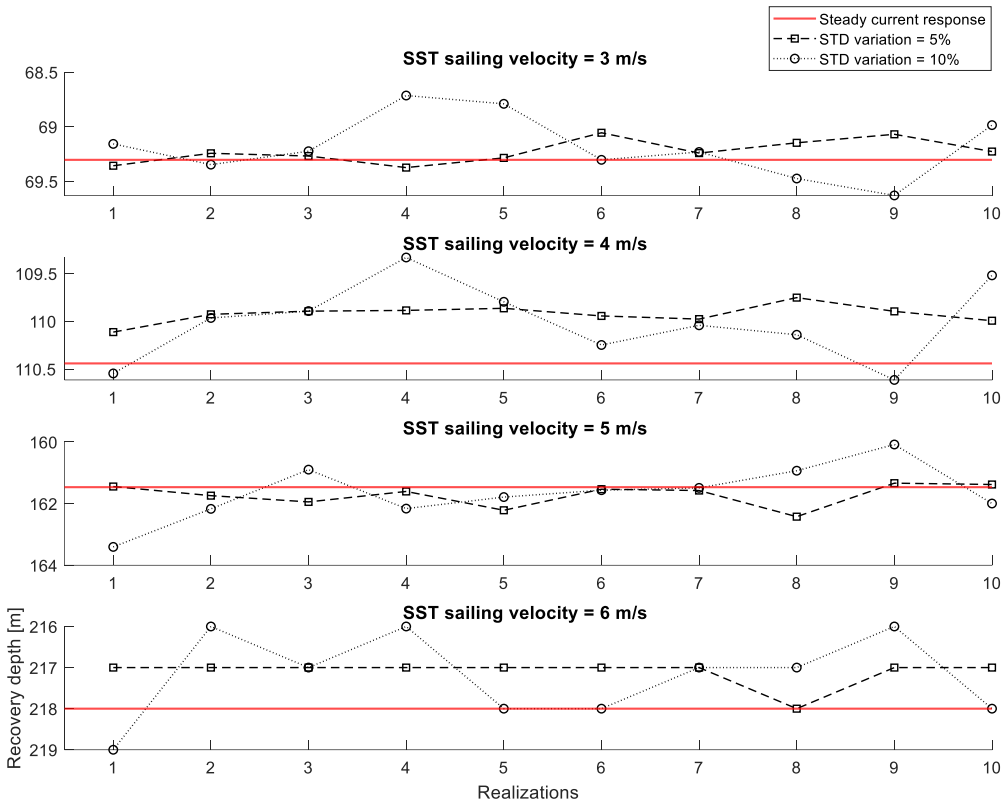

Figure 12 - Simulated SST responses during emergency recovery from jam-to-dive at different sailing velocities and heading current velocity = 0.5 m/s

According to a simulation time of 1000 seconds, an SST sailing speed of 3-6 m/s, and a heading current velocity of 0.5 m/s, Figure 12 shows the anticipated 10x2 realizations.

The Gumbel fit for four recovery depth samples with an SST velocity of 3 m/s, in the direction of the current, and with varied velocities and STD variations is shown in Figure 13. The graph also displays the maximum and minimum values for the 6-month, 1-year, and 5-year return periods. With the present speed of 0.5 m/s, Figure 13 showed that the 6-month recovery depths for the two different STD variations were 70.366 m and 72.169 m, respectively. These results are significant even with minor alterations, especially because the other confidence interval and the two distinct values do not overlap. Similar trends can be seen in the data for both the 1- and 5-year return periods. By raising the current speed to 1 m/s and keeping the other condition constant, a 6-month recovery depth of 91.604 m and 95.429 m, respectively, was attained, as shown in Figure 13. The findings showed significant variability, which is consistent with the earlier reasoning.

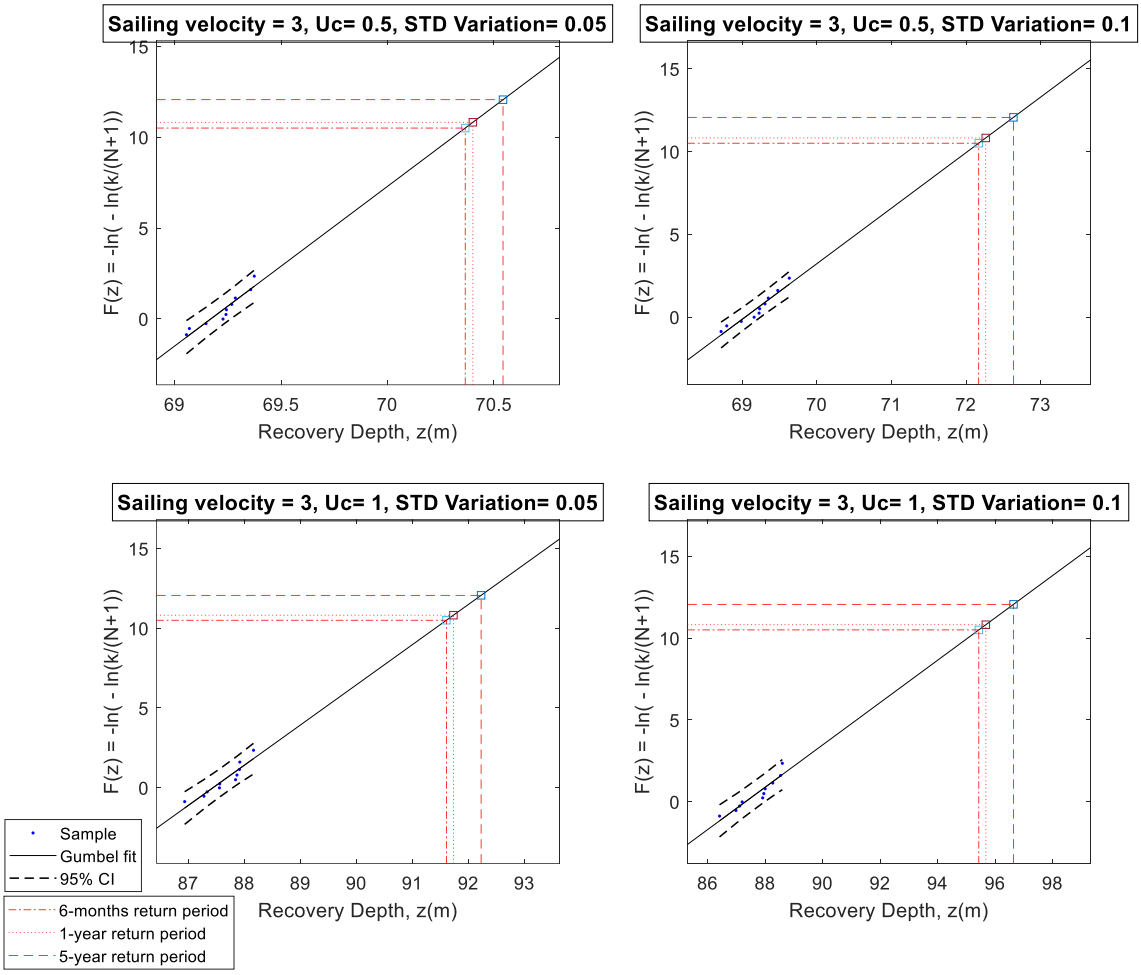

Figure 13 - Probability paper for Gumbel distribution for recovery depth corresponding to SST's velocity if 3 m/s, in heading current direction

Using Tables 10 and 11, a similar pattern and conclusion can be drawn with different SST sailing velocities, current speed, direction, and return durations when compared with the two different STD variation values. When using the two different STD versions, Table 12 illustrates the difference in recovery depth for stochastic current for all SST's speeds, current speeds, directions, and return periods. This table compares the values obtained from the deterministic current case simulations with the results obtained from the simulations. As an illustration, it is demonstrated that an SST facing a heading current velocity of 0.5 m/s with a 6-month return period, a 3 m/s speed, and 5% STD variance had a 1.53% greater recovery depth than its comparable deterministic value. This result was anticipated because prolonging the return durations will only increase the likely extreme recovery depth. Under identical conditions, the 5-year return term yielded a 1.79% rise in recovery depth. Another example demonstrates how recovery depth increased by 4.92% in contrast to its equivalent deterministic value for a 5-year return period with 5% STD variation, 1 m/s current velocity, and 3 m/s SST

speed. For the same case with a 10% STD variation, the recovery depth increases to 9.94%. In a similar vein, this behavior is also expected given that increasing STD variations change recovery depth. The relative changes depicted in Table 12 might, however, vary from 0.42 to 11.26%. It is feasible to study how these return values behave by varying the SST's velocity from 3 to 6 m/s in a 1 m/s following speed direction and 10% STD variation throughout a 5-year return period, with the recovery depth values dropping from 10.49% to 5.83%, respectively. The SST may react to changes more strongly and swiftly with a smaller recovery depth when the following current speed is maintained while the SST's speed is increased according to this pattern, which also fits the system's projected knowledge. These measurements can improve the SST's design and increase its resistance to unanticipated changes by including better control systems, backup recovery techniques, or materials.

Table 10 - Recovery depth predictions for several return periods for following current

SST sailing velocity [m/s]	$V_c = 0.5\ m/s$ $CV = 0\%$	$V_c = 0.5\ m/s$ $CV = 5\%$	$V_c = 0.5\ m/s$ $CV = 10\%$	$V_c = 1\ m/s$ $CV = 0\%$	$V_c = 1\ m/s$ $CV = 5\%$	$V_c = 1\ m/s$ $CV = 10\%$
			6 months return period			
3	40.621	(42.535)	(42.388)	29.807	(31.225)	(32.534)
		(42.406, 42.659)	(42.328, 42.449)		(31.118, 31.335)	(32.385, 32.683)
4	68.403	(69.264)	(71.183)	52.831	(55.343)	(56.501)
		(69.172, 69.358)	(70.973, 71.384)		(55.126, 55.534)	(56.363, 56.641)
5	101.200	(103.614)	(104.174)	80.250	(83.662)	(83.939)
		(103.523, 103.706)	(104.017, 104.332)		(83.376, 83.934)	(83.776, 84.105)
6	137.238	(139.553)	(143.326)	110.334	(114.854)	(115.888)
		(139.392, 139.696)	(142.868, 143.774)		(114.167, 115.644)	(115.457, 116.293)
			1-year return period			
3	40.621	(42.595)	(42.443)	29.807	(31.275)	(32.615)
		(42.467, 42.717)	(42.382, 42.504)		(31.167, 31.385)	(32.764)
4	68.403	(69.301)	(71.278)	52.831	(55.431)	(56.624)
		(69.208, 69.394)	(71.071, 71.478)		(55.220, 55.617)	(56.484, 56.764)
5	101.200	(103.680)	(104.260)	80.250	(83.774)	(84.063)
		(103.589, 103.772)	(104.102, 104.418)		(83.490, 84.043)	(83.899, 84.230)
6	137.238	(139.630)	(143.520)	110.334	(114.993)	(116.065)
		(139.473, 139.769)	(143.064, 143.965)		(114.297, 115.792)	(115.640, 116.465)
			5-year return period			
3	40.621	(42.830)	(42.596)	29.807	(31.469)	(32.933)
		(42.708, 42.947)	(42.596, 42.720)		(31.359, 31.580)	(32.784, 33.082)
4	68.403	(69.445)	(71.654)	52.831	(55.776)	(57.105)
		(69.352, 69.539)	(71.454, 71.846)		(55.588, 55.943)	(56.964, 57.247)
5	101.200	(103.938)	(104.598)	80.250	(84.212)	(84.551)
		(103.845, 104.031)	(104.440, 104.031)		(83.940, 84.470)	(84.384, 84.721)
6	137.238	(139.932)	(144.281)	110.334	(115.536)	(116.763)
		(139.795, 140.054)	(143.834, 144.718)		(114.805, 116.376)	(116.360, 117.141)

Table 11 - Recovery depth predictions for several return periods for heading current

SST sailing velocity [m/s]	$V_c = 0.5\ m/s$ $CV = 0\%$	$V_c = 0.5\ m/s$ $CV = 5\%$	$V_c = 0.5\ m/s$ $CV = 10\%$	$V_c = 1\ m/s$ $CV = 0\%$	$V_c = 1\ m/s$ $CV = 5\%$	$V_c = 1\ m/s$ $CV = 10\%$
			6 months return period			
3	69.303	(70.366) (70.283, 70.446)	(72.169) (71.979, 72.356)	87.902	(91.604) (91.311, 91.887)	(95.429) (94.845, 95.996)
4	110.441	(110.906) (110.827, 110.986)	(114.177) (113.942, 114.411)	139.650	(143.330) (143.040, 143.608)	(147.137) (146.579, 147.700)
5	161.466	(165.443) (165.178, 165.717)	(170.999) (170.297, 171.710)	209.544	(216.467) (215.363, 217.726)	(218.706) (217.708, 219.762)
6	218,000	(221.955) (220.024, 225.742)	(227.966) (227.079, 228.867)	286.000	(294.307) (293.084, 295.661)	(313.840) (312.269, 315.404)
			1-year return period			
3	69.303	(70.402) (70.319, 70.482)	(72.264) (72.075, 72.450)	87.902	(91.730) (91.439, 92.010)	(95.674) (95.093, 96.237)
4	110.441	(110.937) (110.858, 111.017)	(114.309) (114.074, 114.543)	139.650	(143.444) (143.156, 143.720)	(147.382) (146.824, 147.947)
5	161.466	(165.560) (165.294, 165.837)	(171.296) (170.591, 172.007)	209.544	(216.696) (215.578, 217.971)	(219.017) (218.011, 220.082)
6	218,000	(222.109) (220.140, 225.970)	(228.307) (227.417, 229.230)	286.000	(294.553) (293.319, 295.923)	(314.724) (313.155, 316.285)
			5-year return period			
3	69.303	(70.544) (70.463, 70.623)	(72.635) (72.449, 72.818)	87.902	(92.224) (91.943, 92.495)	(96.636) (96.071, 97.186)
4	110.441	(111.059) (110.980, 111.140)	(114.828) (114.594, 115.060)	139.650	(143.891) (143.613, 144.158)	(148.348) (147.784, 148.917)
5	161.466	(166.024) (165.749, 166.310)	(172.460) (171.750, 173.177)	209.544	(217.596) (216.423, 218.935)	(220.240) (219.200, 221.342)
6	218,000	(222.713) (220.596, 226.864)	(229.646) (228.747, 230.560)	286.000	(295.525) (294.243, 296.946)	(318.201) (316.641, 319.754)

Table 12 - Percentage change in recovery depth compared to the deterministic current case

	Following current				**Heading current**			
SST sailing velocity [m/s]	$V_c = 0.5$ $CV = 5\%$	$V_c = 0.5$ $CV = 10\%$	$V_c = 1$ $CV = 5\%$	$V_c = 1$ $CV = 10\%$	$V_c = 0.5$ $CV = 5\%$	$V_c = 0.5$ $CV = 10\%$	$V_c = 1$ $CV = 5\%$	$V_c = 1$ $CV = 10\%$
				6-months return period				
3	4.71	4.35	4.76	9.15	1.53	4.14	4.21	8.56
4	1.26	4.06	4.75	6.95	0.42	3.38	2.64	5.36
5	2.39	2.94	4.25	4.60	2.46	5.90	3.30	4.37
6	1.69	4.44	4.10	5.03	1.81	4.57	2.90	9.73
				1-year return period				
3	4.86	4.49	4.93	9.42	1.59	4.27	4.35	8.84
4	1.31	4.20	4.92	7.18	0.45	3.50	2.72	5.54
5	2.45	3.02	4.39	4.75	2.54	6.09	3.41	4.52
6	1.74	4.58	4.22	5.19	1.88	4.73	2.99	10.04
				5-year return period				
3	5.44	4.86	5.58	10.49	1.79	4.81	4.92	9.94
4	1.52	4.75	5.57	8.09	0.56	3.97	3.04	6.23
5	2.71	3.36	4.94	5.36	2.82	6.81	3.84	5.10
6	1.96	5.13	4.71	5.83	2.16	5.34	3.33	11.26

6 Conclusion

The SST must be designed using the SOE analysis to guarantee that it is ready to handle any circumstances that might lead to failure. There have been a lot of recent studies on the SST to make sure that all the various components are appropriately taken into account to achieve proper prototype levels. Therefore, appropriate designing would include considering numerous modifications for each of the various SST operating situations and monitoring how the SST responds to them. Even though they may seem tedious at first, a thorough analysis of such metrics will ultimately improve the project's design, cost-effectiveness, and viability. Additionally, every failure has a big impact on how long the SST can survive. As previously mentioned, this paper has expanded the investigation of the SOE zones and has discovered that adding a stochastic current to the SST computation results in considerable variations. In this study, the Gumbel distribution was utilized to forecast an SST's recovery depth following a jam-to-dive and jam-to-rise failure for various return periods. The recovery depth values at the two current speeds and directions with 5% and 10% standard deviations in altering SST's speed and pitch angle have confirmed that the uncertainties in the SOE can be substantial under stochastic current loads. The findings of the free-running simulations, which take into account two current directions and load instances of 0.5 and 1 m/s with 5% and 10% standard variation, revealed enhanced recovery depth differences ranging from 0.97% to 21.44% for the jam-to-rise scenario, and 0.42% to 11.26% for the jam-to-dive scenario for the cases with an initial pitch angle of 15 degrees. The cases with 10- and 20-degree pitch angles show similar percent differences, but the recovery depth will be less with a lower pitch angle because the SST is traveling more horizontally. The recovery depth percent changes are less in the jam-to-dive cases compared to the jam-to-rise cases. A contributing factor for this is that the recovery depth is greater in the first place for the jam-to-dive cases compared to the jam-to-rise cases with the same initial values for SST velocity, current direction and velocity, and STD variation.

Future studies may look at how differences in recovery depth caused by current directions coming from different angles, such as a 60- and 120-degree angle, might significantly affect the results. To estimate the possible recovery depth and compare it to the Gumbel values in order to get more accurate results, other statistical techniques might be utilized, such as the Average Conditional Exceedance Rate Method [54].

7 Literature

1. Fullenbaum, R., Fallon, J., Flanagan, B., 2013. Oil & Natural Gas Transportation & Storage Infrastructure: Status, Trends, & Economic Benefits. Technical report. IHS Global Inc. https://www.circleofblue.org/wp-content/uploads/2014/12/API-Infrastructure-Investment-Study.pdf.
2. Palmer, A., King, R., 2008. Subsea Pipeline Engineering, second ed. PennWell Corp, Oklahoma, USA.
3. Wilson, J., 2008. Shuttle tankers vs pipelines in the GOM frontier. World Oil 229 (4), 149–151.
4. Vestereng, C., 2019. Shuttle Tankers in Brazil assessed Sep 2020 from. https://www.dnv. com/expert-story/maritime-impact/shuttle-tankers-Brazil.html.
5. Equinor Energy AS, 2019. RD662093 Subsea Shuttle System.
6. Jacobsen, L.R., 1971. Subsea Transport of Arctic Oil - A Technical and Economic Evaluation. Offshore Technology Conference, OTC-1425-MS, Houston, TX, USA, 2 May 1971. https://doi.org/10.4043/1425-MS.
7. Taylor, P., Montgomery, J., 1977. Arctic Submarine Tanker System. Offshore Technology Conference, OTC-2998, Houston, TX, USA, 2 May 1977. https://doi.org/10.404 3/2998-MS.
8. Jacobsen, L., Lawrence, K., Hall, K., Canning, P., Gardner, E., 1983. Transportation of LNG from the Arctic by commercial submarine. Marine Technology and SNAME News 20 (4), 377–384. https://doi.org/10.5957/mt1.1983.20.4.377.
9. Brandt, H., Fruhling, C., Hollung, A., Schiemann, M., Vob, T., 2015. A Multipurpose Submarine Concept for Arctic Offshore Operations, OTC Arctic Technology Conference. OTC-25501-MS, Copenhagen, Denmark. March 2015. https://doi. org/10.4043/25501-MS.
10. Ellingsen, K.E., Ravndal, O., Reinas, R., Hansen, J.H., Marra, F., Myhre, E., Dupuy, P.M., Sveberg, K. (2020). RD677082 Subsea Shuttle System.
11. Xing, Y., Ong, M.C., Hemmingsen, T., Ellingsen, K.E., Reinas, L., 2021. Design considerations of a subsea shuttle tanker system for liquid carbon dioxide transportation. J. Offshore Mech. Arctic Eng. 143 (4), 045001 https://doi.org/ 10.1115/1.4048926.
12. Norwegian Petroleum Directorate (NPD), 2020. Carbon Capture and Storage assessed Aug 2020 from. http://www.norskpetroleum.no/en/environment-and-technology/carbon-capture-and-storage/.
13. Equinor ASA, 2020. Northern Lights CCS assessed Sep 2020 from. https://www.equinor. com/en/what-we-do/northern-lights.html.
14. Papanikolaou, A., 2014. Ship Design: Methodologies of Preliminary Design. Springer, Dordrecht Heidelberg New York London.
15. Carbon Capture and Storage Association (CCSA), 2020. What Is CCS?, assessed Sep 2020 from. http://www.ccsassociation.org/what-is-ccs/.
16. International Energy Agency (IEA), 2010. Energy Technology Perspectives 2010: Scenarios and Strategies to 2050. OECD Publishing, Paris, France.

17. Kery, S.M., Eaton, M., Henry, S.C., Vasilakos, J., Kery, S.M., 2018. On the Creation of a Safe Operating Envelope for Ships. SNAME Maritime Convention, Rhode Island, USA.
18. Lombaerts, T.J.J., Schuet, S.R., Wheeler, K.R., Acosta, D., Kaneshige, J.T., 2013. Safe maneuvering envelope estimation based on a physical approach. In: AIAA Guidance, Navigation, and Control Conference 2013, Boston, MA.
19. DNV, 2018. Rules for Classification, Naval Vessels, Part 4 Sub-surface Ships (Chapter 1) Submarines.
20. Marchant, P., Kimber, N., 2014. Assuring the Safe Operation of Submarines with Operator Guideline. Underwater Defence Technology, Liverpool, UK.
21. Giddings, A.J., Louis, W.L., 1966. Overcoming submarine control surface jams and flooding casualties. Navel Engineerings Journal 78 (6), 1055–1067. https://doi.org/10.1111/j.1559-3584.1966.tb04132.x.
22. Tingle, C., 2009. Submarine accidents a 60-year statistical assessment. Professional Safety 54 (9).
23. Burcher, R., Rydill, L., 1994. Concepts in Submarine Design. Cambridge University Press, Cambridge.
24. Park, J.-Y., Kim, N., 2017. Design of a safety operational envelope protection system for the pitch angle of a submarine. Proceedings of the Institution of Mechanical Engineers, Part M: Journal of Engineering for the Maritime Environment 231 (2), 441–451. https://doi.org/10.1177/1475090216644281.
25. Park, J.-Y., Kim, N., 2018. Design of a safety operational envelope protection system for a submarine. Ocean Engineering 148, 602–611. https://doi.org/10.1016/j.oceaneng.2017.11.016.
26. Ma, Y., Xing, Y., Ong, M.C., Hemmingsen, T.H., 2021b. Baseline design of a subsea shuttle tanker system for liquid carbon dioxide transportation. Ocean Engineering 240. https://doi.org/10.1016/j.oceaneng.2021.109891.
27. DNV, 2018. Rules for Classification, Naval Vessels, Part 4 Sub-surface Ships (Chapter 1) Submarines.
28. Xing, Y., Ong, M.C., Hemmingsen, T., Ellingsen, K.E., Reinås, L., 2021a. Design considerations of a subsea shuttle tanker system for liquid carbon dioxide transportation. Journal of Offshore Mechanics and Arctic Engineering 143 (4). https://doi.org/10.1115/1.4048926.
29. Xing, Y., 2021. A conceptual large autonomous subsea freight-glider for liquid CO2 transportation. In: ASME 2021 40th International Conference on Ocean, Offshore and Arctic Engineering, Virtual. https://doi.org/10.1115/omae2021-61924. Online.
30. Ma, Y., Sui, D., Xing, Y., Ong, M.C., Hemmingsen, T.H., 2020. Depth control modeling and analysis of a subsea shuttle tanker ASME 2021 40th international conference on ocean, offshore and arctic engineering. Virtual. https://doi.org/10.1115/ OMAE2021-61827. Online.
31. Ma, Y., Xing, Y., Sui, D., 2022. Trajectory envelope of a subsea shuttle tanker hovering in stochastic ocean current - model development and tuning. Journal of Offshore Mechanics and Arctic Engineering. https://doi.org/10.1115/1.4055282.

32. Park, J.-Y., Kim, N., 2017. Design of a safety operational envelope protection system for the pitch angle of a submarine. Proceedings of the Institution of Mechanical Engineers, Part M: Journal of Engineering for the Maritime Environment 231 (2), 441–451. https://doi.org/10.1177/1475090216644281.
33. Ross, A., Fossen, T.I., Johansen, T.A., 2004. Identification of underwater vehicle hydrodynamic coefficients using free decay tests. In: IFAC Conference on Computer Applications in Marine Systems. Elsevier BV, Ancona, Italy, pp. 363–368. https://doi.org/10.1016/s1474-6670(17)31759-7.
34. Tinker, S.J., 1982. Identification of submarine dynamics from free-model test. In: Admiralty Marine Technology Establishment, UK, Proceedings of the DRG Seminar on Advanced Hydrodynamic Testing Facilities, Session 3, Paper 16, The Netherlands. Paper: P1982-1.
35. Park, J.-Y., Kim, N., 2018. Design of a safety operational envelope protection system for a submarine. Ocean Engineering 148, 602–611. https://doi.org/10.1016/j.oceaneng.2017.11.016.
36. Renilson, M., 2018. Submarine Hydrodynamics. Springer International Publishing AG, Cham, Switzerland.
37. Bettle, M.C., Gerber, A.G., Watt, G.D., 2009. Unsteady analysis of the six DOF motion of a buoyantly rising submarine. Computers & Fluids 38 (9), 1833–1849. https://doi.org/10.1016/j.compfluid.2009.04.003.
38. Chen, Q., Li, H., Zhang, S., Wang, J., Pang, Y., Wang, Q., 2020. Effect of waves on the behavior of emergent buoyantly rising submarines using CFD. Applied Sciences 10 (23), 8403. https://doi.org/10.3390/app10238403.
39. Watt, G.D., 2001. A Quasi-Steady Evaluation of Submarine Rising Stability: the Stability Limit, NATO Research and Technology Organisation Applied Vehicle Technology Panel Symposium, Leon, Norway.
40. Watt, G.D., 2007. Modeling and Simulating Unsteady Six Degrees-Of-Freedom Submarine Rising Maneuvers. Defence Research and Development Canada-Atlantic. Canada, Dartmouth.
41. Zhang, S., Li, H., Zhang, T., Pang, Y., Chen, Q., 2019. Numerical simulation study on the effects of course-keeping on the roll stability of submarine emergency rising. Applied Sciences 9 (16), 3285. https://doi.org/10.3390/app9163285.
42. MathWorks, 2022. Simulink User's Guide. The MathWorks, Inc., MA, USA.
43. Fossen, T.I., 2011. Handbook of Marine Craft Hydrodynamics and Motion Control. John Willey & Sons, Ltd, West Sussex, UK.
44. Prestero, T., 2001. Verification of a Six-Degree of Freedom Simulation Model for the REMUS Autonomous Underwater Vehicle. Massachusetts Institute of Technology & Woods Hole Oceanographic Institution. https://doi.org/10.1575/1912/3040.
45. Blevins, R.D., 1979. Formulas for Natural Frequency and Mode Shape. Van Nostrand Reinhold Co., New York.
46. Faltinsen, O., 1993. Sea Loads on Ships and Offshore Structures. Cambridge University Press, Cambridge.
47. Hoerner, S.F., 1965. Fluid-dynamic Drag: Practical Information on Aerodynamic Drag and Hydrodynamic Resistance. Published by the author, California, USA.

48. Smogeli, Ø.N., 2006. Control of Marine Propellers-From Normal to Extreme Conditions. Department of Marine Technology. Norwegian University of Science and Technology, Trondheim.
49. Sørensen, A. J., 2018, "Marine Cybernetics, Towards Autonomous Marine Operations and Systems," Department of Marine Technology, NTNU, Trondheim
50. Ma, Y., Xing, Y., and Sui, D., " Trajectory Envelope of a Subsea Shuttle Tanker Hovering in Stochastic Ocean Current - Model Development and Tuning," Journal of Offshore Mechanics and Arctic Engineering, 145(3): 030901. DOI: 10.1115/1.4055282
51. Ma, Y., and Xing, Y., 2022, "Identification of the Safety Operating Envelope of a Novel Subsea Shuttle Tanker," Ocean Engineering, 266, p. 112750. DOI: 10.1016/j.oceaneng.2022.112750
52. Ma, Y., Xing, Y., Sui, D., Ong, M. C., and Hemmingsen, T., 2022, "2D planar modeling of the depth control of a subsea shuttle tanker," Journal of Offshore Mechanics and Arctic Engineering. DOI: 10.1115/1.4056418
53. Naess, A., and Moan, T., 2013, Stochastic dynamics of marine structures, Cambridge University Press. [22] Fu, P., Leira, B. J., and Myrhaug, D., 2017, "Reliability analysis of wake-induced collision of flexible risers," Applied Ocean Research, 62, pp. 49 -56
54. Naess, A., Gaidai, O., and Karpa, O., 2013, "Estimation of extreme values by the average conditional exceedance rate method," Journal of Probability and Statistics, 2013
55. Font, R., García-Pelaez, ´ J., 2013. On a submarine hovering system based on blowing and venting of ballast tanks. Ocean Engineering 72, 441–447. https://doi.org/10.1016/j.oceaneng.2013.07.021.
56. Font, R., García, J., Ovalle, D., 2010. Modeling and Simulating Ballast Tank Blowing and Venting Operations in Manned Submarines, 8th IFAC Conference on Control Applications in Marine Systems. Rostock-Warnemude, Germany. https://doi.org/10.3182/20100915-3-de-3008.00029.

8 Appendices

8.1 Appendix A – Jam-to-rise with 10-degree pitch angle

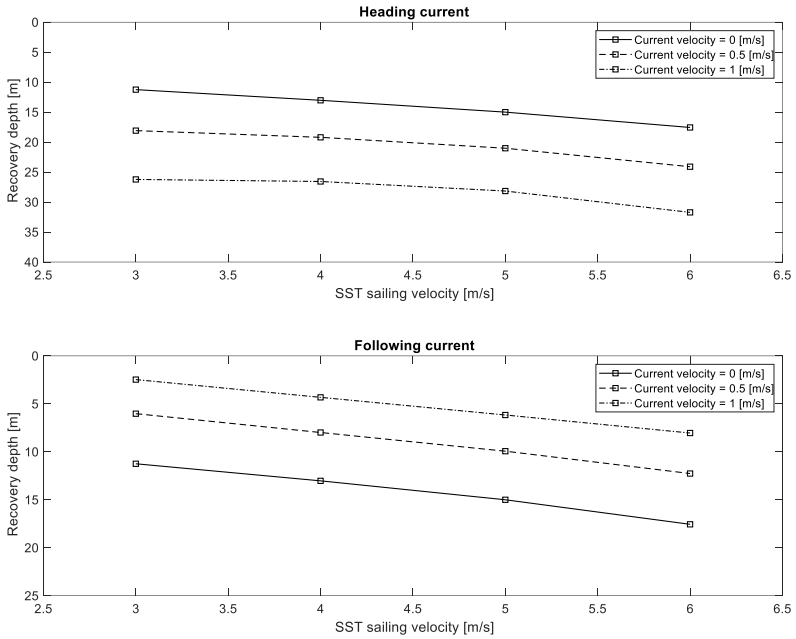

Figure 14 – Jam-to-rise curve for different steady current cases

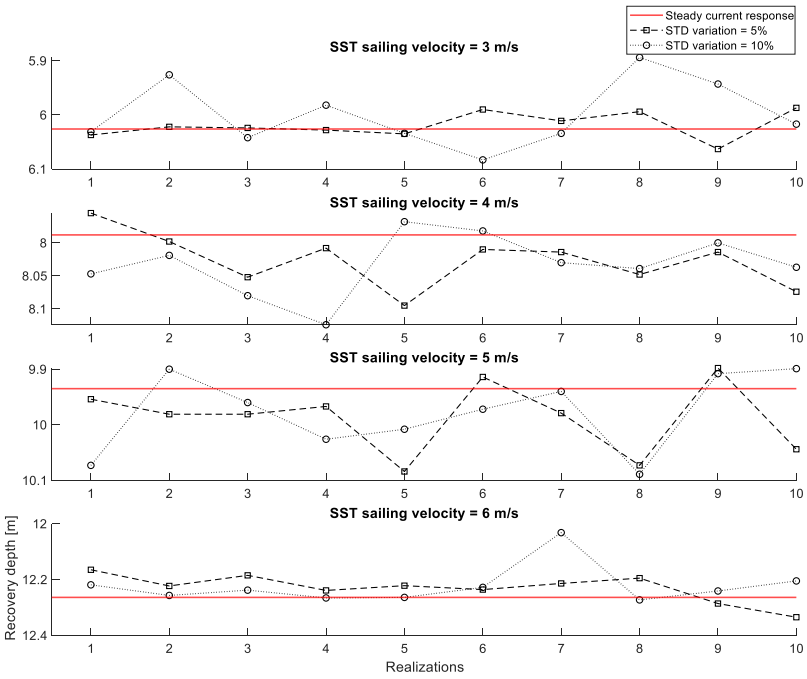

Figure 15 - Simulated SST responses during emergency recovery from jam-to-rise at different sailing velocities and following current velocity = 0.5 [m/s]

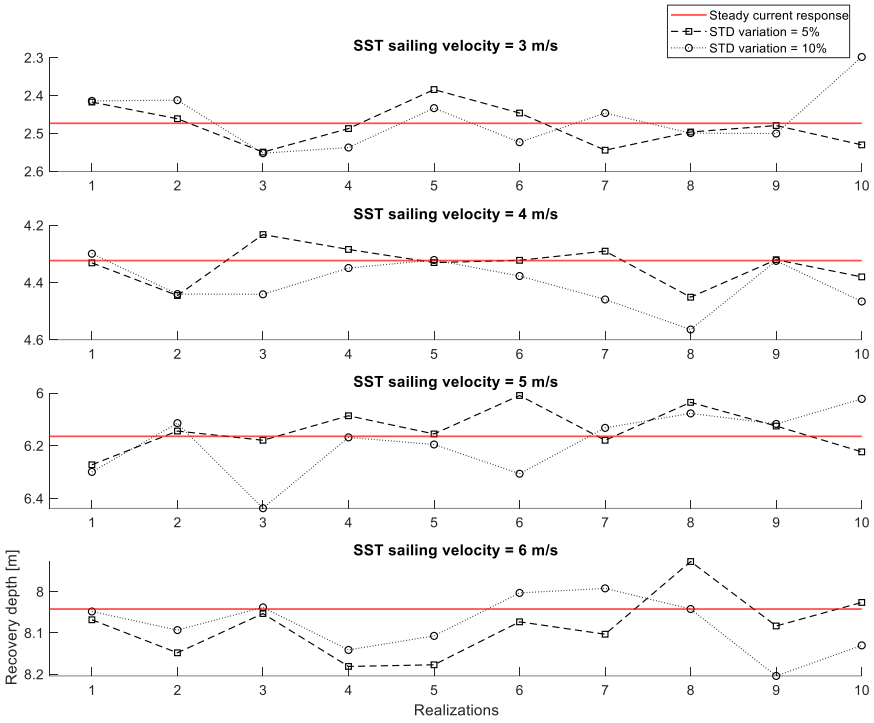

Figure 16 - Simulated SST responses during emergency recovery from jam-to-rise at different sailing velocities and following current velocity = 1 [m/s]

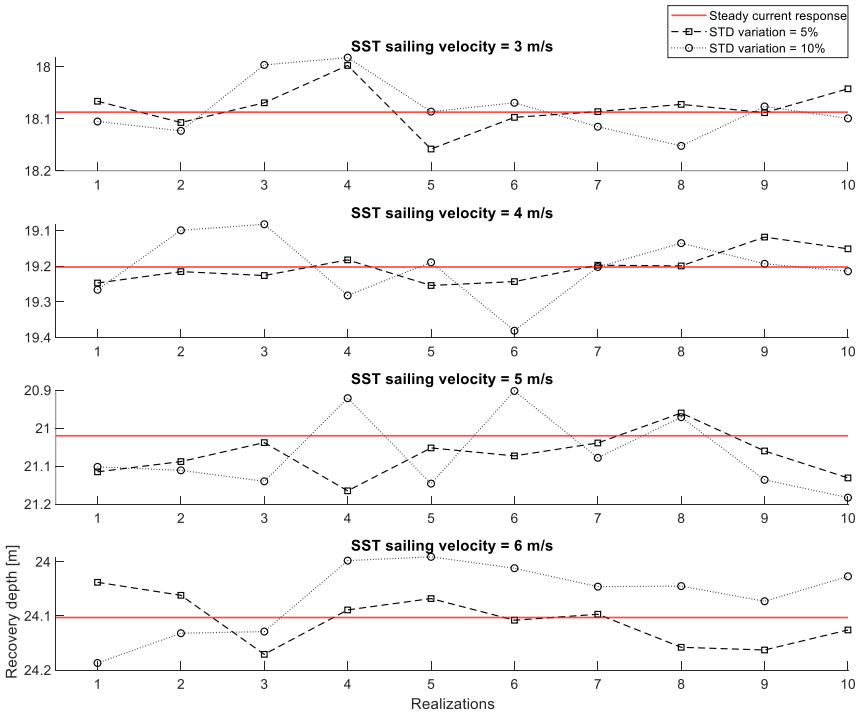

Figure 17 - Simulated SST responses during emergency recovery from jam-to-rise at different sailing velocities and heading current velocity = 0.5 [m/s]

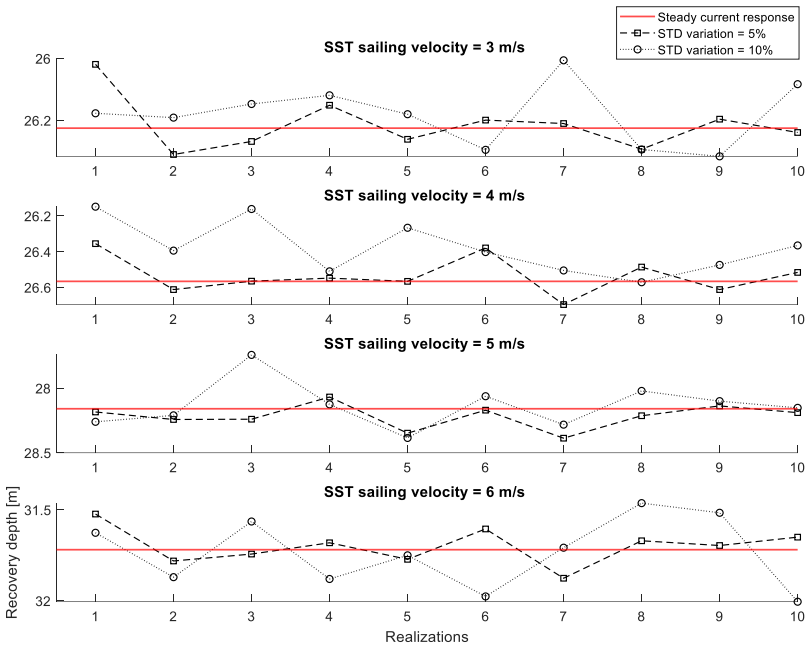

Figure 18 - Simulated SST responses during emergency recovery from jam-to-rise at different sailing velocities and heading current velocity = 1 [m/s]

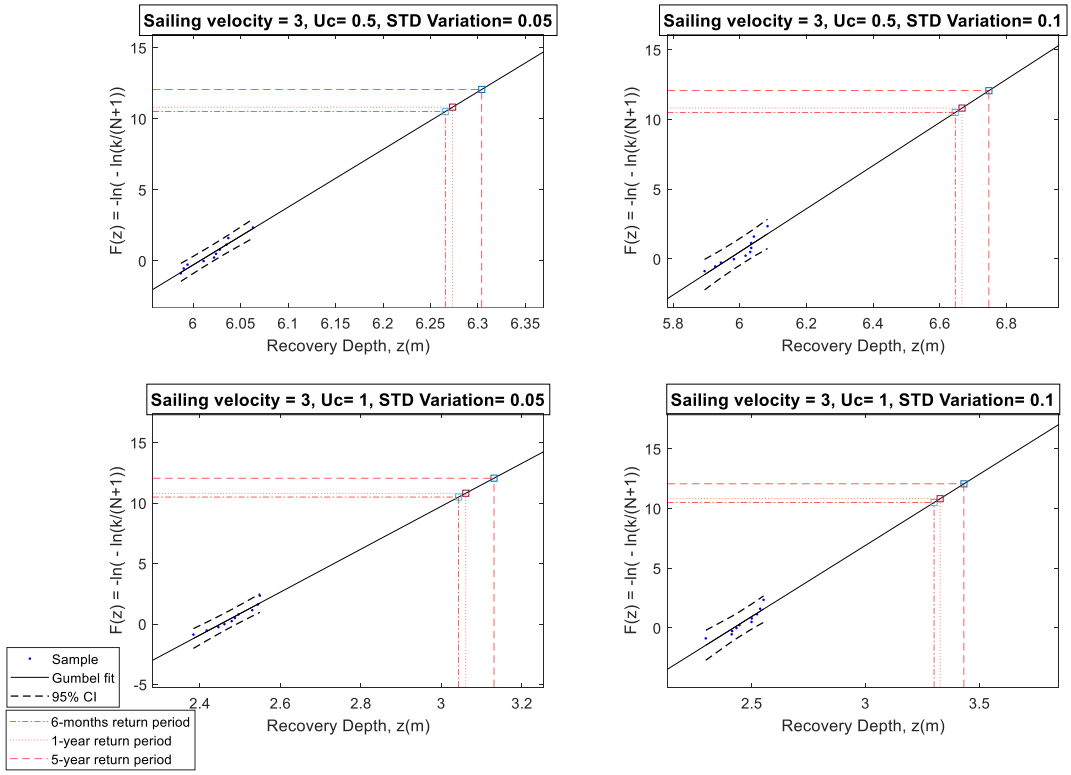

Figure 19 - Probability paper for Gumbel distribution for recovery depth corresponding to SST's velocity of 3 m/s, following current direction

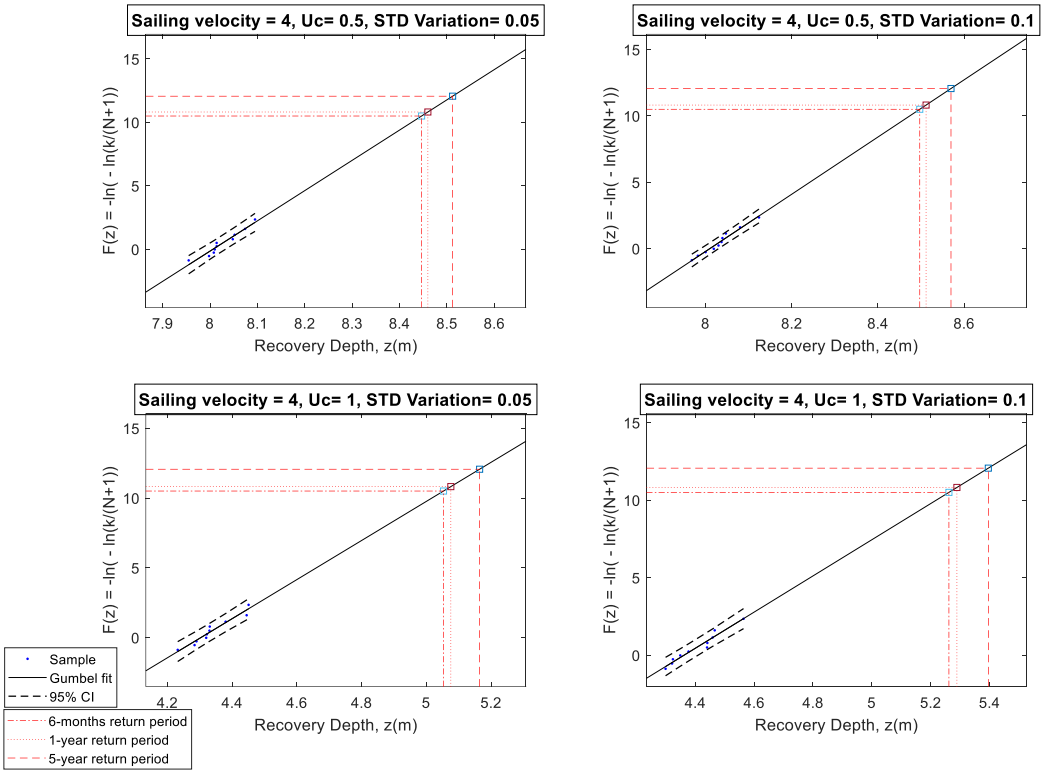

Figure 20 - Probability paper for Gumbel distribution for recovery depth corresponding to SST's velocity of 4 m/s, following current direction

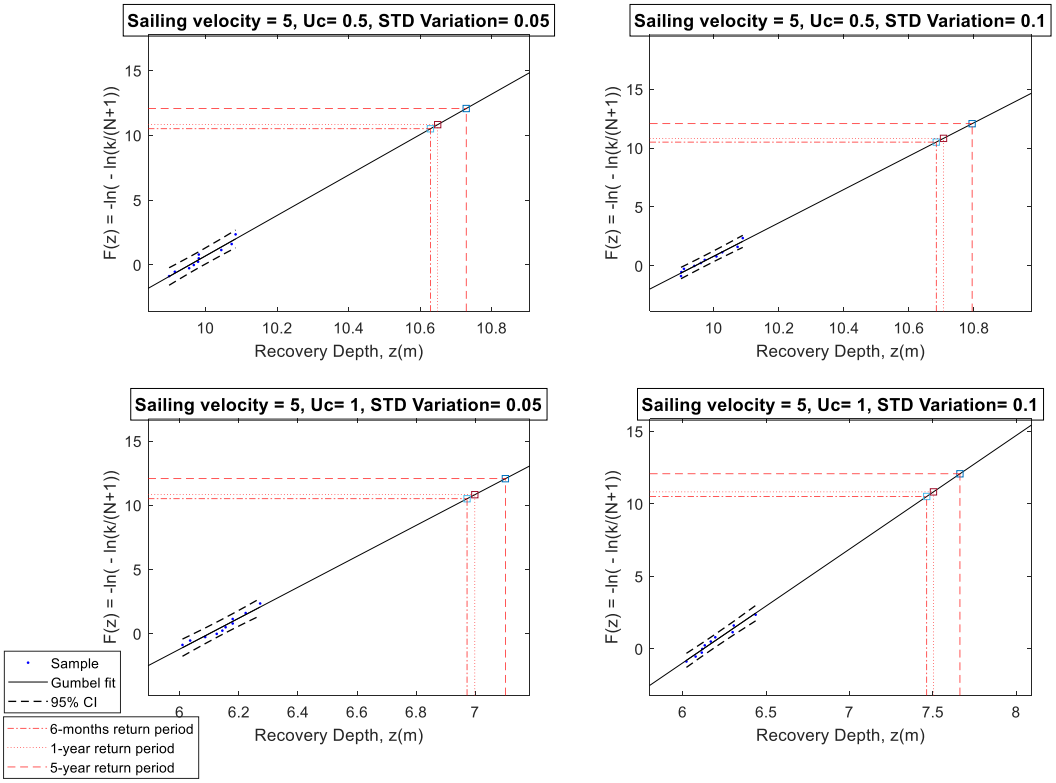

Figure 21 - Probability paper for Gumbel distribution for recovery depth corresponding to SST's velocity of 5 m/s, following current direction

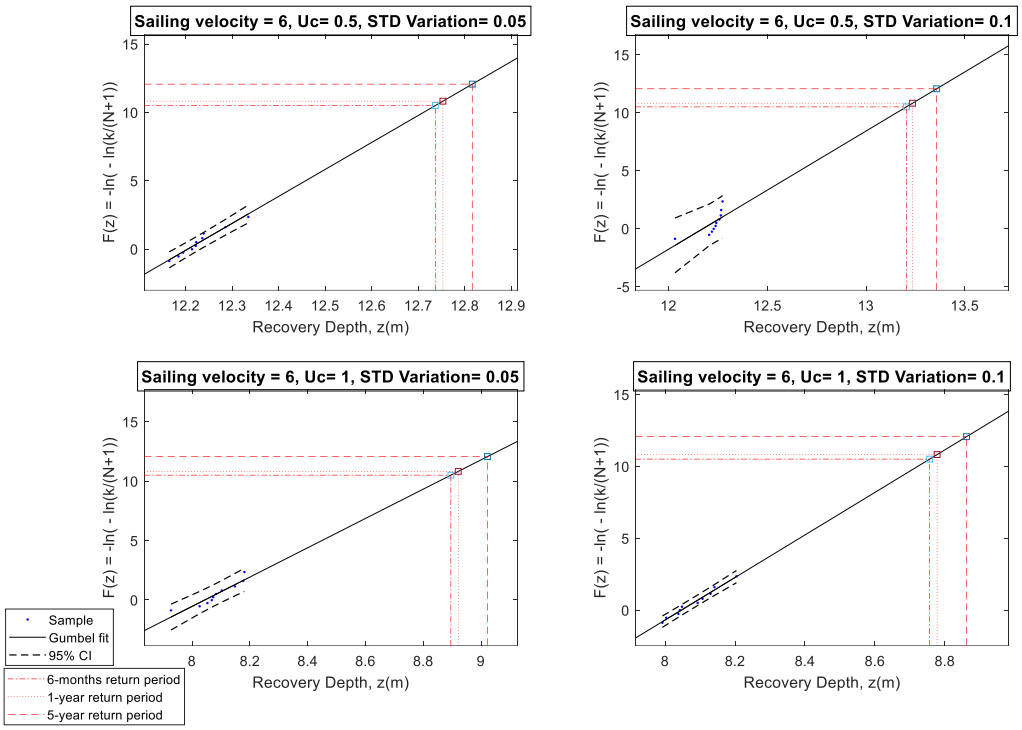

Figure 22 - Probability paper for Gumbel distribution for recovery depth corresponding to SST's velocity of 6 m/s, following current direction

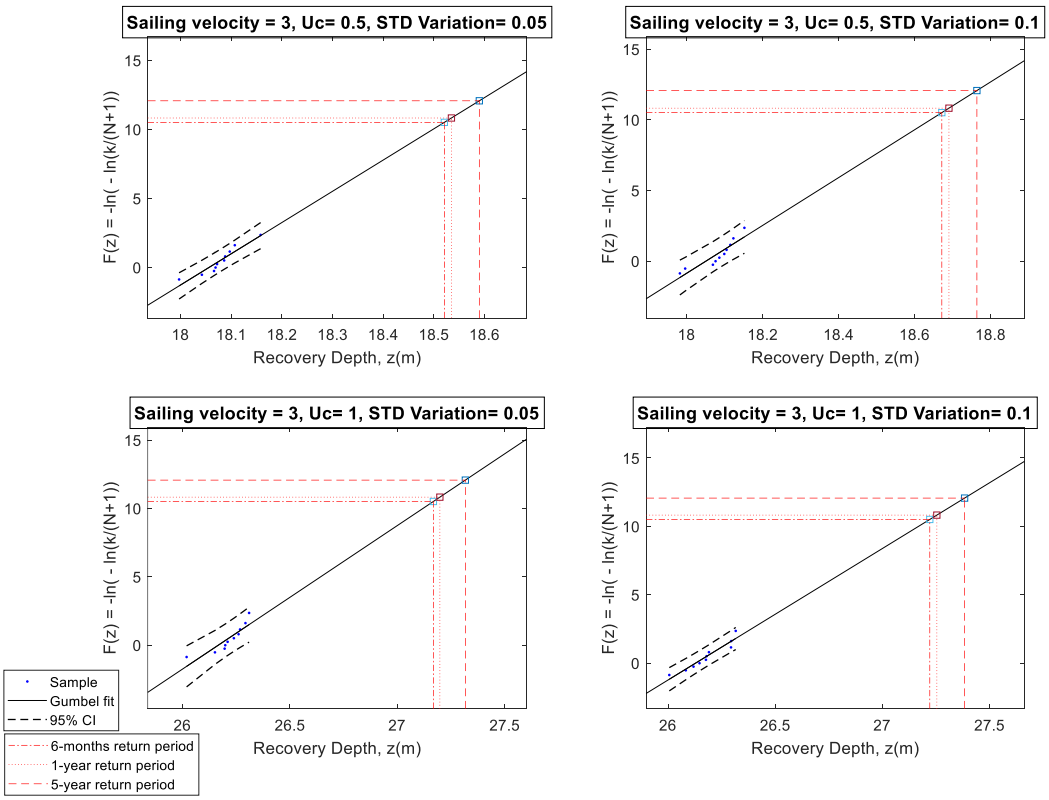

Figure 23 - Probability paper for Gumbel distribution for recovery depth corresponding to SST's velocity of 3 m/s, heading current direction

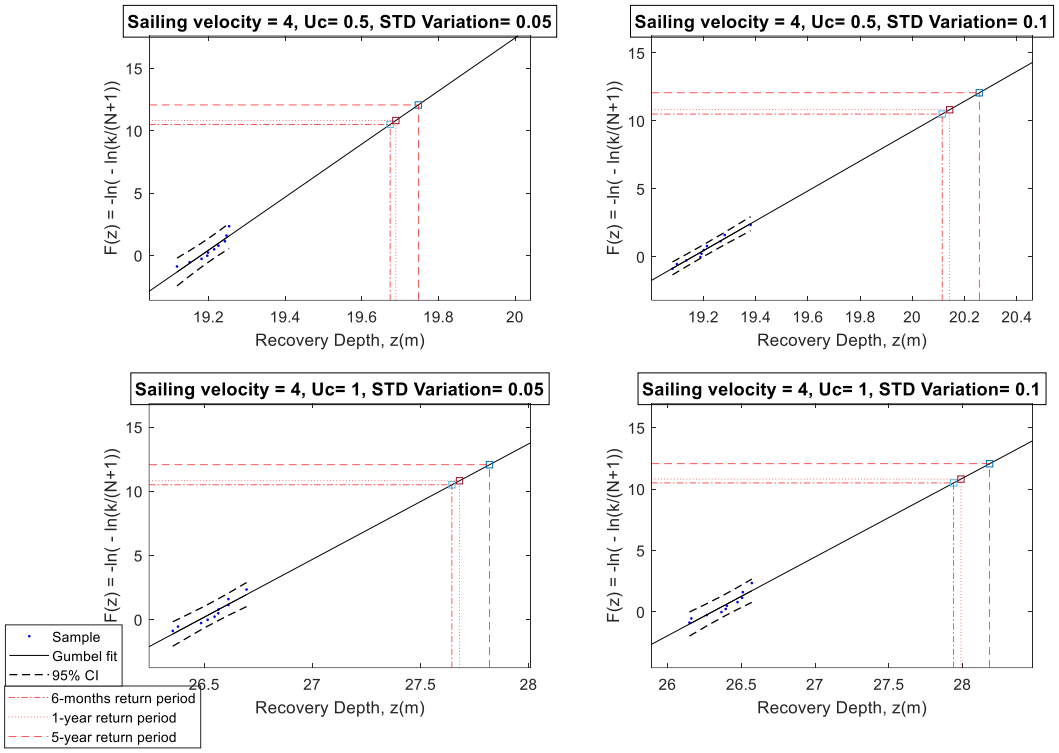

Figure 24 - Probability paper for Gumbel distribution for recovery depth corresponding to SST's velocity of 4 m/s, heading current direction

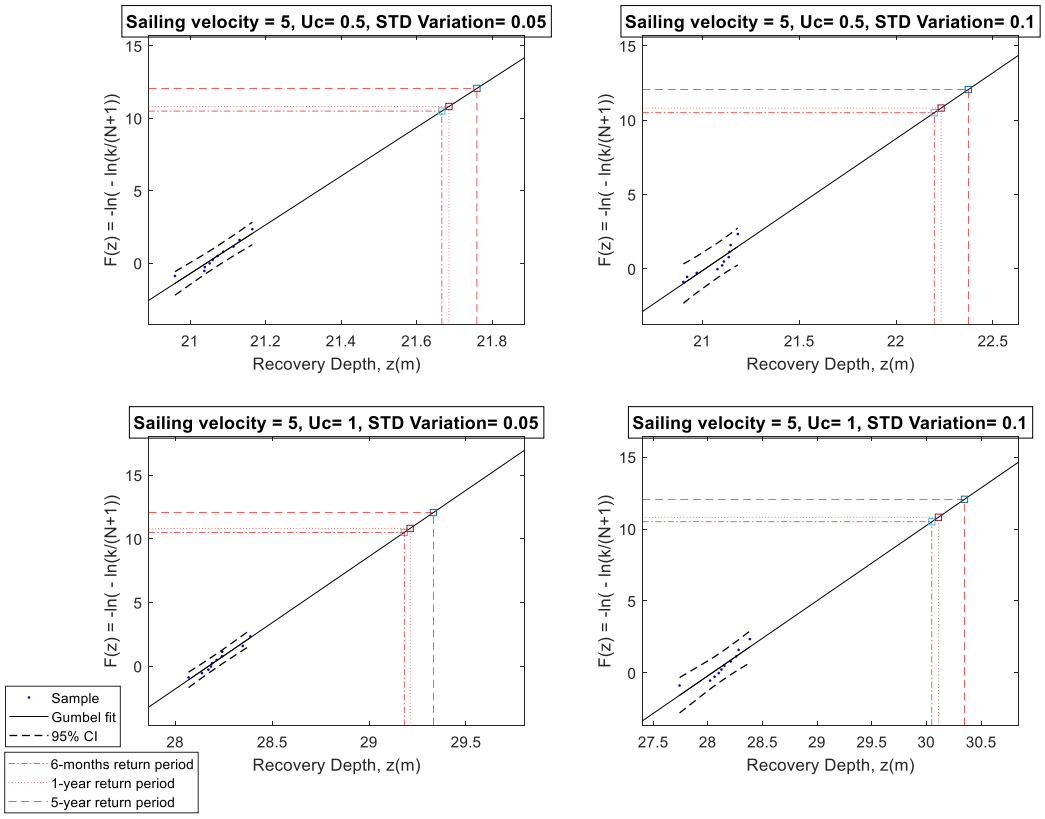

Figure 25 - Probability paper for Gumbel distribution for recovery depth corresponding to SST's velocity of 5 m/s, heading current direction

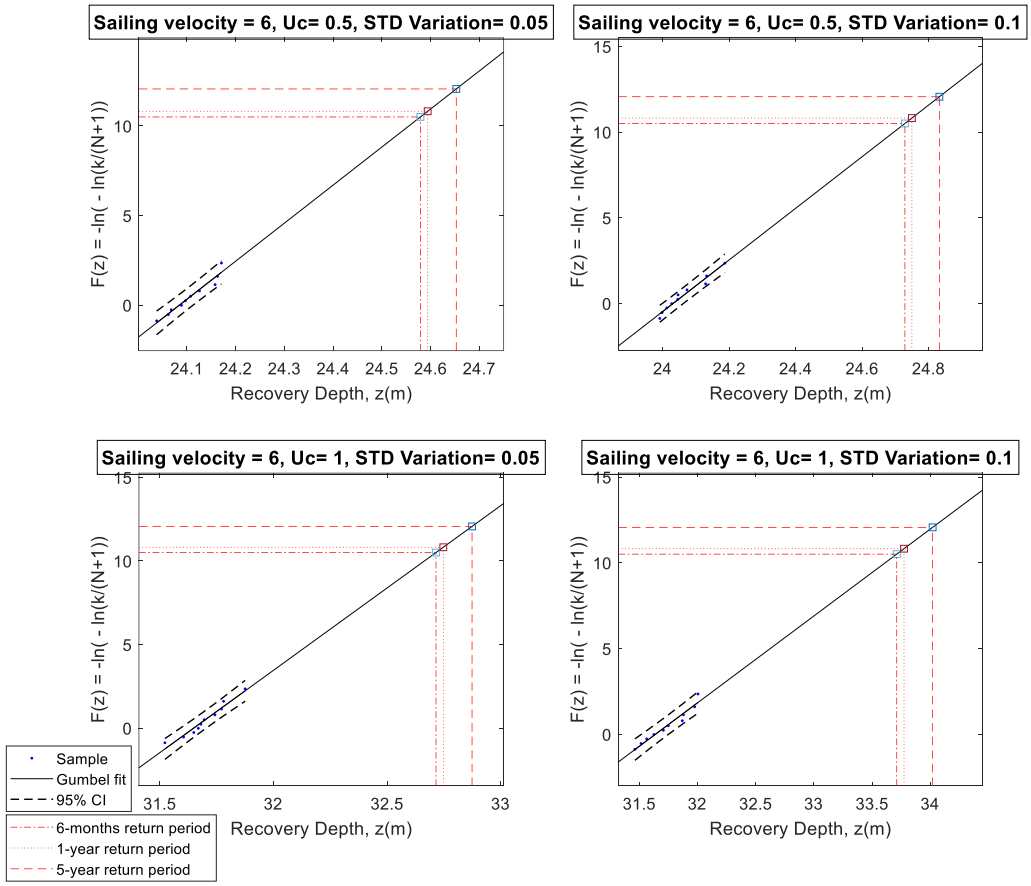

Figure 26 - Probability paper for Gumbel distribution for recovery depth corresponding to SST's velocity of 6 m/s, heading current direction

Table 13 - Recovery depth predictions for several return periods for following current

SST sailing velocity [m/s]	$V_c = 0.5\ m/s$ $CV = 0\%$	$V_c = 0.5\ m/s$ $CV = 5\%$	$V_c = 0.5\ m/s$ $CV = 10\%$	$V_c = 1\ m/s$ $CV = 0\%$	$V_c = 1\ m/s$ $CV = 5\%$	$V_c = 1\ m/s$ $CV = 10\%$
			6 months return period			
3	6.026	(6.266) (6.250, 6.282)	(6.646) (6.595, 6.695)	2.473	(3.043) (3.006, 3.079)	(3.301) (3.240, 3.357)
4	7.988	(8.447) (8.418, 8.475)	(8.497) (8.472, 8.523)	4.323	(5.053) (4.997, 5.111)	(5.262) (5.204, 5.321)
5	9.935	(10.629) (10.584, 10.675)	(10.685) (10.646, 10.724)	6.164	(6.972) (6.924, 7.020)	(7.463) (7.387, 7.542)
6	12.264	(12.737) (12.699, 12.777)	(13.205) (13.173, 13.255)	8.042	(8.896) (8.836, 8.953)	(8.757) (8.727, 8.787)
			1-year return period			
3	6.026	(6.273) (6.257, 6.289)	(6.666) (6.615, 6.715)	2.473	(3.061) (3.024, 3.097)	(3.327) (3.267, 3.383)
4	7.988	(8.460) (8.432, 8.488)	(8.512) (8.486, 8.538)	4.323	(5.076) (5.020, 5.134)	(5.289) (5.231, 5.348)
5	9.935	(10.649) (10.604, 10.696)	(10.707) (10.668, 10.746)	6.164	(6.951) (6.951, 7.046)	(7.427) (7.427, 7.583)
6	12.264	(12.753) (12.715, 12.794)	(13.236) (13.198, 13.295)	8.042	(8.921) (8.862, 8.978)	(8.778) (8.748, 8.808)
			5-year return period			
3	6.026	(6.304)	(6.747)	2.473	(3.131)	(3.432)

		(6.288, 6.320)	(6.698, 6.794)		(3.095, 3.166)	(3.376, 3.483)
4	7.988	(8.512)	(8.570)	4.323	(5.165)	(5.396)
		(8.484, 8.541)	(8.543, 8.597)		(5.108, 5.224)	(5.337, 5.456)
5	9.935	(10.729)	(10.795)	6.164	(7.102)	(7.662)
		(10.683, 10.776)	(10.755, 10.835)		(7.055, 7.150)	(7.583, 7.744)
6	12.264	(12.816)	(13.358)	8.042	(9.022)	(8.862)
		(12.776, 12.858)	(13.298, 13.453)		(9.177, 8.965)	(8.893, 8.832)

Table 14 - Recovery depth predictions for several return periods for heading current

SST sailing velocity [m/s]	$V_c = 0.5\ m/s$ $CV = 0\%$	$V_c = 0.5\ m/s$ $CV = 5\%$	$V_c = 0.5\ m/s$ $CV = 10\%$	$V_c = 1\ m/s$ $CV = 0\%$	$V_c = 1\ m/s$ $CV = 5\%$	$V_c = 1\ m/s$ $CV = 10\%$
			6 months return period			
3	18.087	(18.521)	(18.672)	26.225	(27.168)	(27.222)
		(18.485, 18.557)	(18.628, 18.712)		(27.110, 27.219)	(27.145, 27.298)
4	13.027	(19.674)	(20.114)	26.566	(27.645)	(27.940)
		(19.640, 19.706)	(20.065, 20.164)		(27.565, 27.723)	(27.824, 28.051)
5	21.020	(21.667)	(22.197)	28.159	(29.182)	(30.049)
		(21.628, 21.705)	(22.103, 22.284)		(29.118, 29.246)	(29.919, 30.169)
6	24.103	(24.579)	(24.729)	31.719	(32.715)	(33.712)
		(24.549, 24.609)	(24.688, 24.771)		(32.658, 32.773)	(33.593, 33.831)
			1-year return period			
3	18.087	(18.535)	(18.691)	26.225	(27.198)	(27.255)
		(18.499, 18.571)	(18.648, 18.730)		(27.142, 27.247)	(27.178, 27.330)
4	13.027	(19.689)	(20.143)	26.566	(27.680)	(27.989)
		(19.656, 19.720)	(20.094, 20.193)		(27.601, 27.757)	(27.875, 28.099)
5	21.020	(21.686)	(22.233)	28.159	(29.212)	(30.110)
		(21.647, 21.724)	(22.140, 22.318)		(29.148, 29.277)	(29.982, 30.228)
6	24.103	(25.594)	(24.750)	31.719	(32.747)	(33.775)
		(24.564, 24.624)	(24.709, 24.792)		(32.690, 32.805)	(33.656, 33.894)
			5-year return period			
3	18.087	(18.590)	(18.725)	26.225	(27.270)	(27.308)
		(18.554, 18.626)	(18.725, 18.801)		(27.270, 27.358)	(27.308, 27.459)
4	13.027	(19.748)	(20.256)	26.566	(27.819)	(28.183)
		(19.716, 19.777)	(20.206, 20.308)		(27.741, 27.893)	(28.073, 28.290)
5	21.020	(21.760)	(22.373)	28.159	(29.332)	(30.230)
		(21.722, 21.798)	(22.286, 22.453)		(29.267, 29.398)	(30.230, 23.457)
6	24.103	(24.653)	(24.833)	31.719	(32.874)	(34.021)
		(24.623, 24.683)	(24.791, 24.876)		(32.817, 32.931)	(33.902, 34.140)

Table 15 - Percentage change in recovery depth compared to the deterministic current case

	Following current				Heading current			
SST sailing velocity [m/s]	$V_c = 0.5$ $CV = 5\%$	$V_c = 0.5$ $CV = 10\%$	$V_c = 1$ $CV = 5\%$	$V_c = 1$ $CV = 10\%$	$V_c = 0.5$ $CV = 5\%$	$V_c = 0.5$ $CV = 10\%$	$V_c = 1$ $CV = 5\%$	$V_c = 1$ $CV = 10\%$
	6-months return period							
3	3.98	10.29	23.05	33.48	2.40	3.23	3.60	3.80
4	5.75	6.37	16.89	21.72	51.02	54.40	4.06	5.17
5	6.99	7.55	13.11	21.07	3.08	5.60	3.63	6.71
6	3.86	7.67	10.62	8.89	1.97	2.60	3.14	6.28
	1-year return period							
3	4.10	10.62	23.78	34.53	2.48	3.34	3.71	3.93
4	5.91	6.56	17.42	22.35	51.14	54.63	4.19	5.36
5	7.19	7.77	12.77	20.49	3.17	5.77	3.74	6.93
6	3.99	7.93	10.93	9.15	6.19	2.68	3.24	6.48
	5-year return period							
3	4.61	11.96	26.61	38.78	2.78	3.53	3.98	4.13
4	6.56	7.29	19.48	24.82	51.59	55.49	4.72	6.09
5	7.99	8.66	15.22	24.30	3.52	6.44	4.17	7.35
6	4.50	8.92	12.19	10.20	2.28	3.03	3.64	7.26

8.2 Appendix B – Jam-to-rise with 15-degree pitch angle

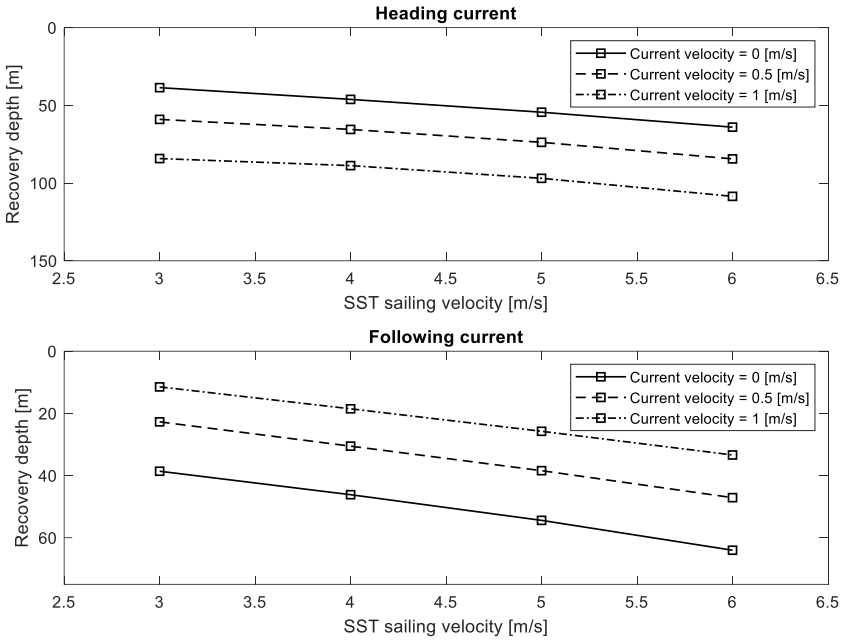

Figure 27 - Jam-to-rise curve for different steady current cases

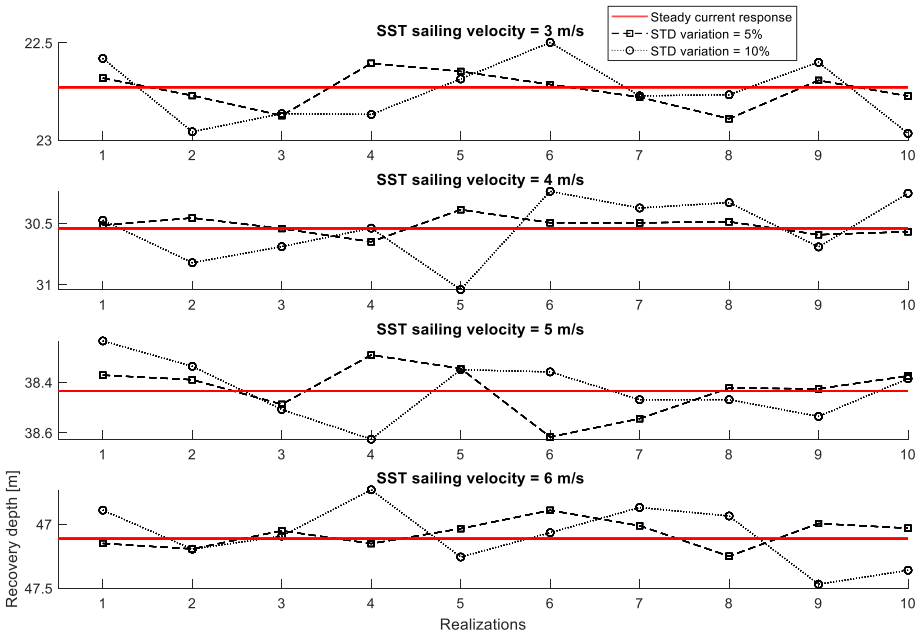

Figure 28 - Simulated SST responses during emergency recovery from jam-to-rise at different sailing velocities and following current velocity = 0.5 [m/s]

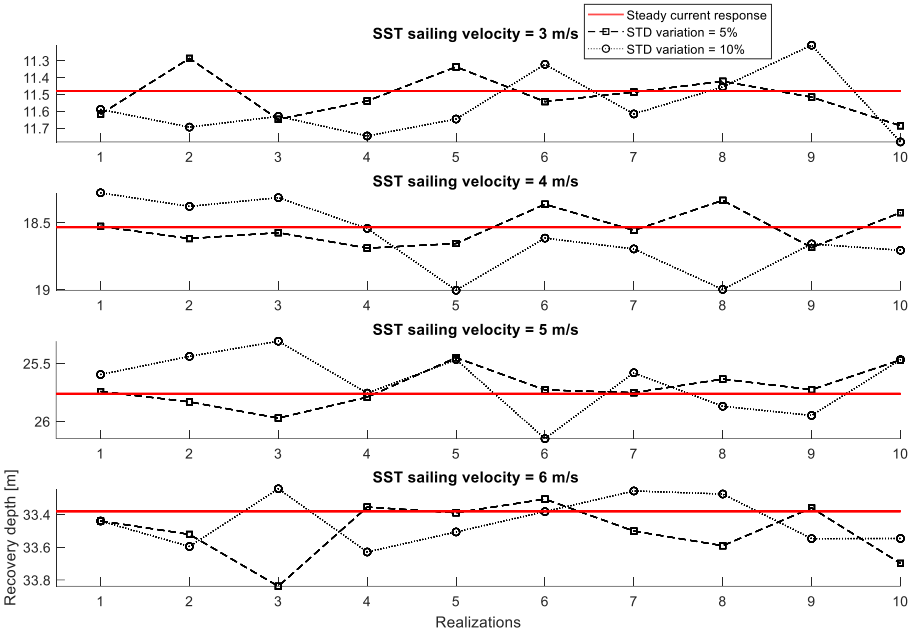

Figure 29 - Simulated SST responses during emergency recovery from jam-to-rise at different sailing velocities and following current velocity = 1 [m/s]

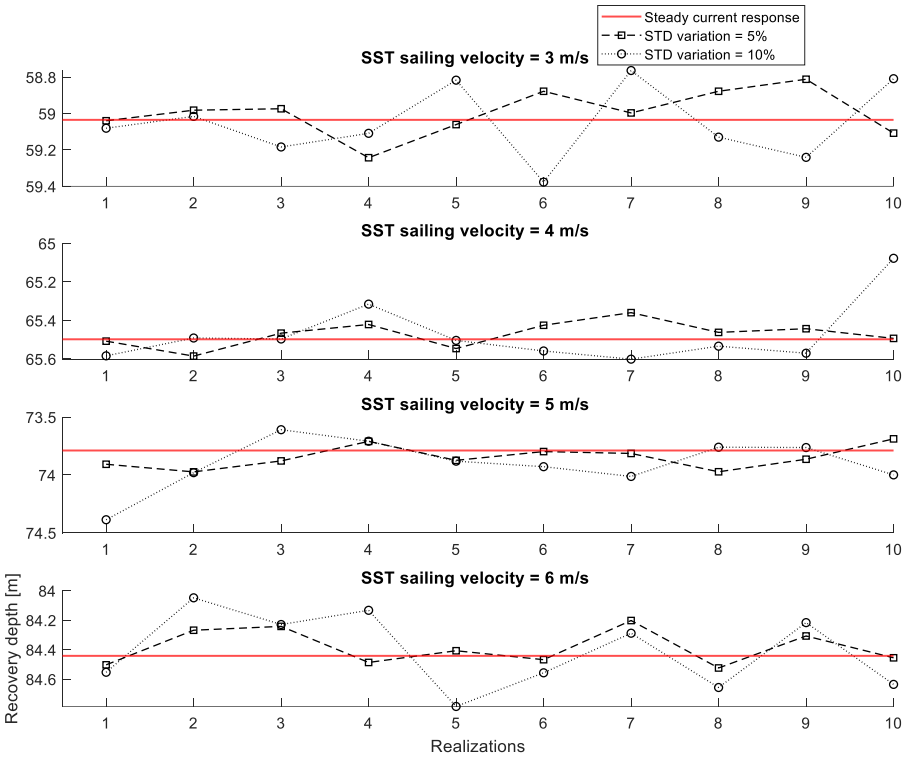

Figure 30 - Simulated SST responses during emergency recovery from jam-to-rise at different sailing velocities and heading current velocity = 0.5 [m/s]

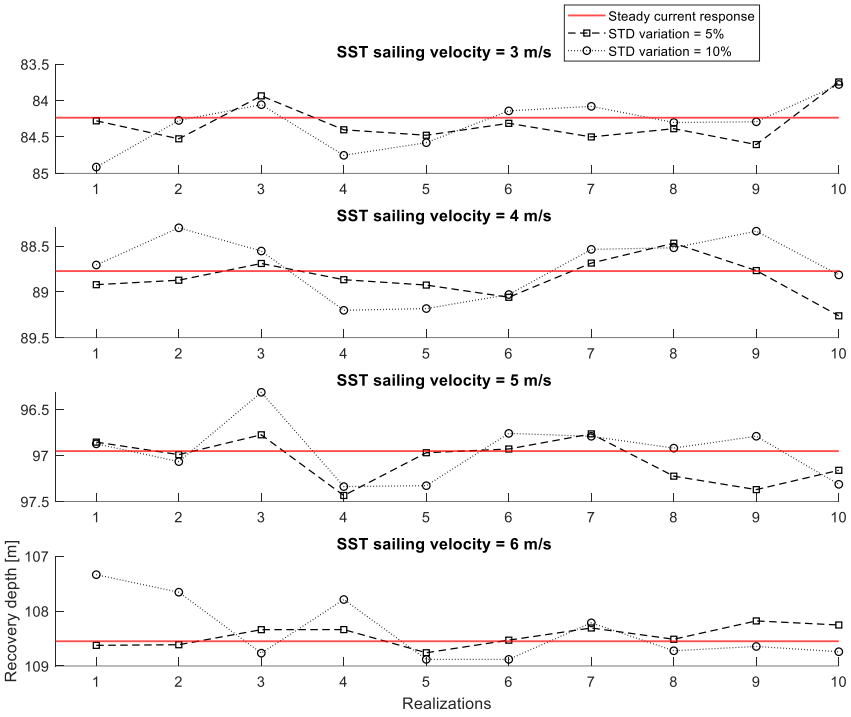

Figure 31 - Simulated SST responses during emergency recovery from jam-to-rise at different sailing velocities and heading current velocity = 1 [m/s]

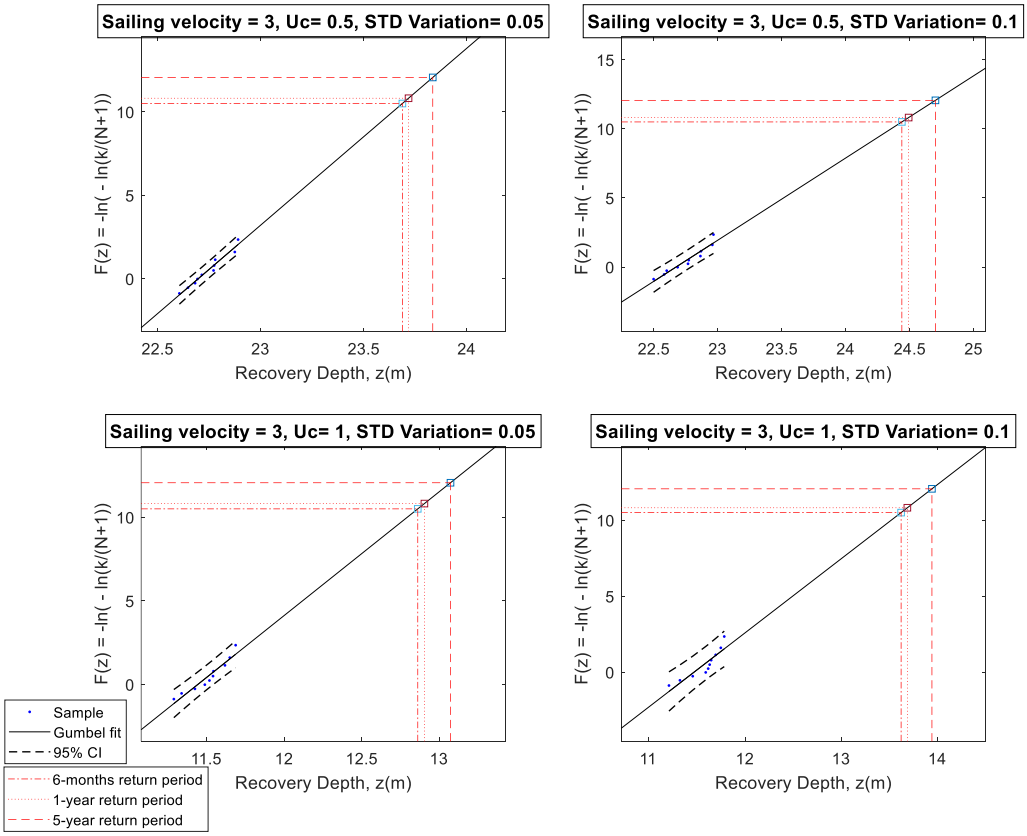

Figure 32 - Probability paper for Gumbel distribution for recovery depth corresponding to SST's velocity of 3 m/s, following current direction

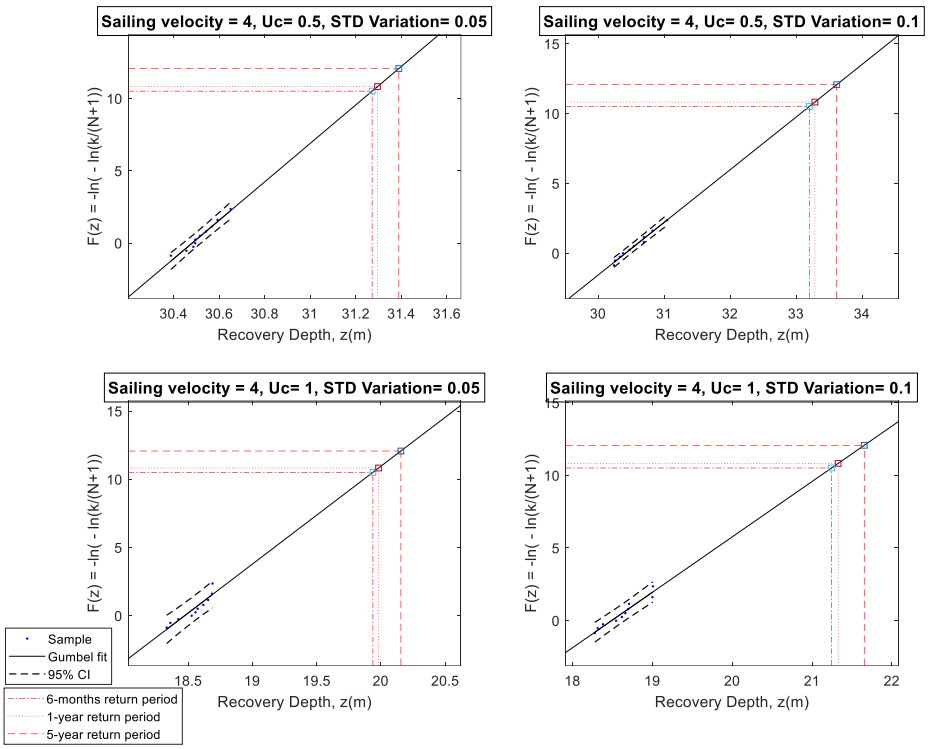

Figure 33 - Probability paper for Gumbel distribution for recovery depth corresponding to SST's velocity of 4 m/s, following current direction

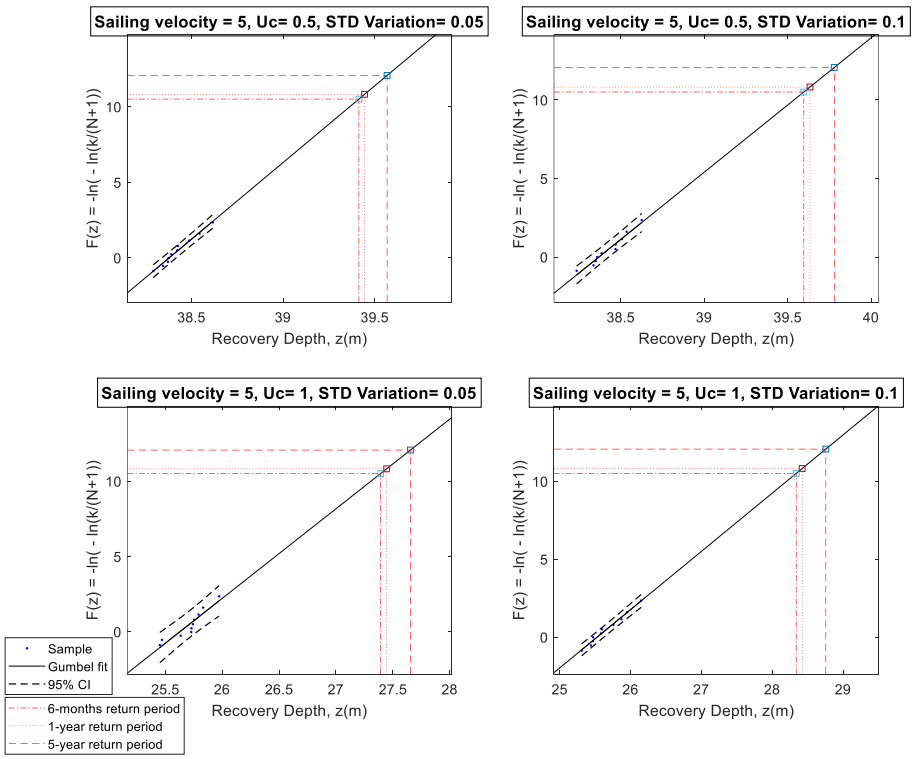

Figure 34 - Probability paper for Gumbel distribution for recovery depth corresponding to SST's velocity of 5 m/s, following current direction

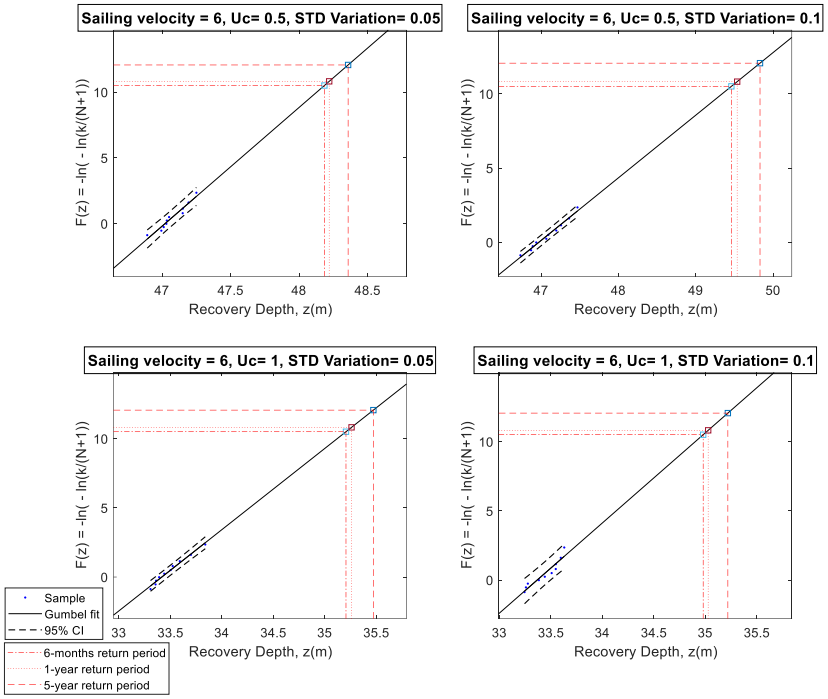

Figure 35 - Probability paper for Gumbel distribution for recovery depth corresponding to SST's velocity of 6 m/s, following current direction

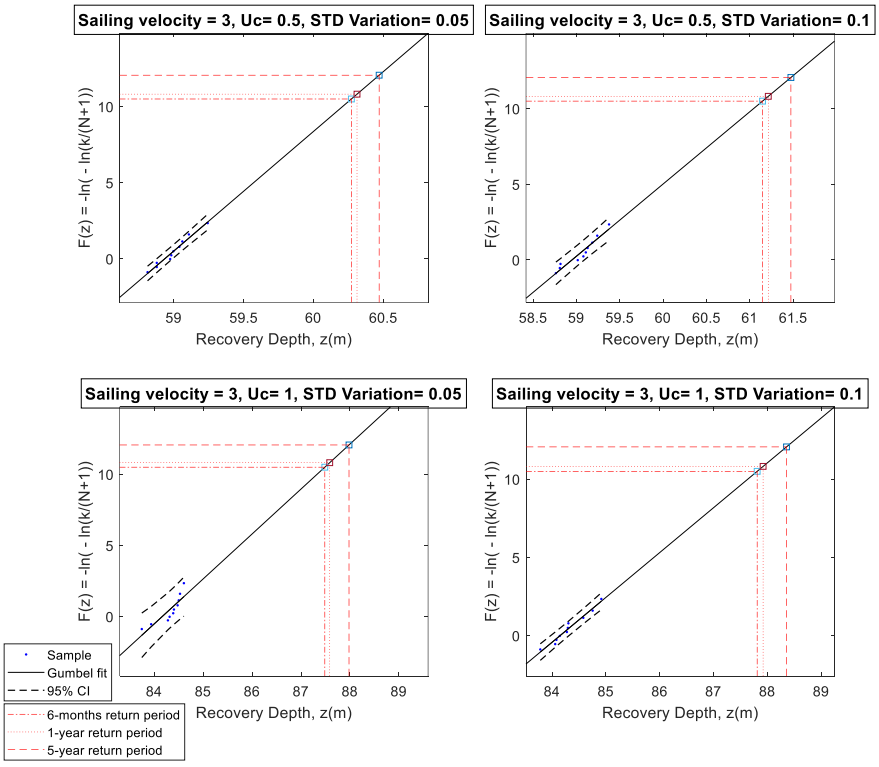

Figure 36 - Probability paper for Gumbel distribution for recovery depth corresponding to SST's velocity of 3 m/s, heading current direction

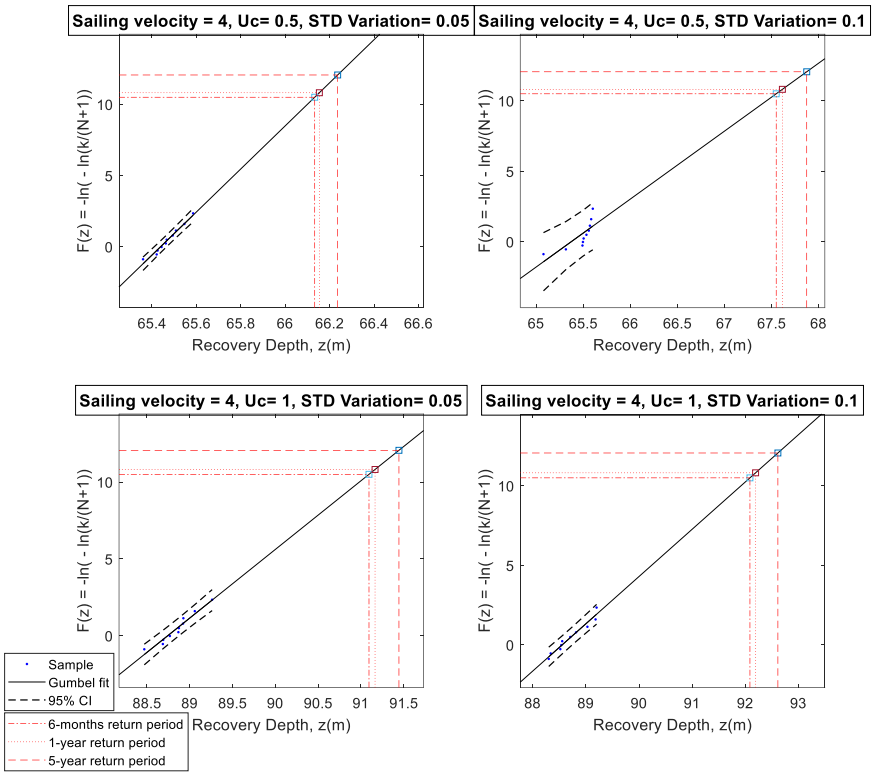

Figure 37- Probability paper for Gumbel distribution for recovery depth corresponding to SST's velocity of 4 m/s, heading current direction

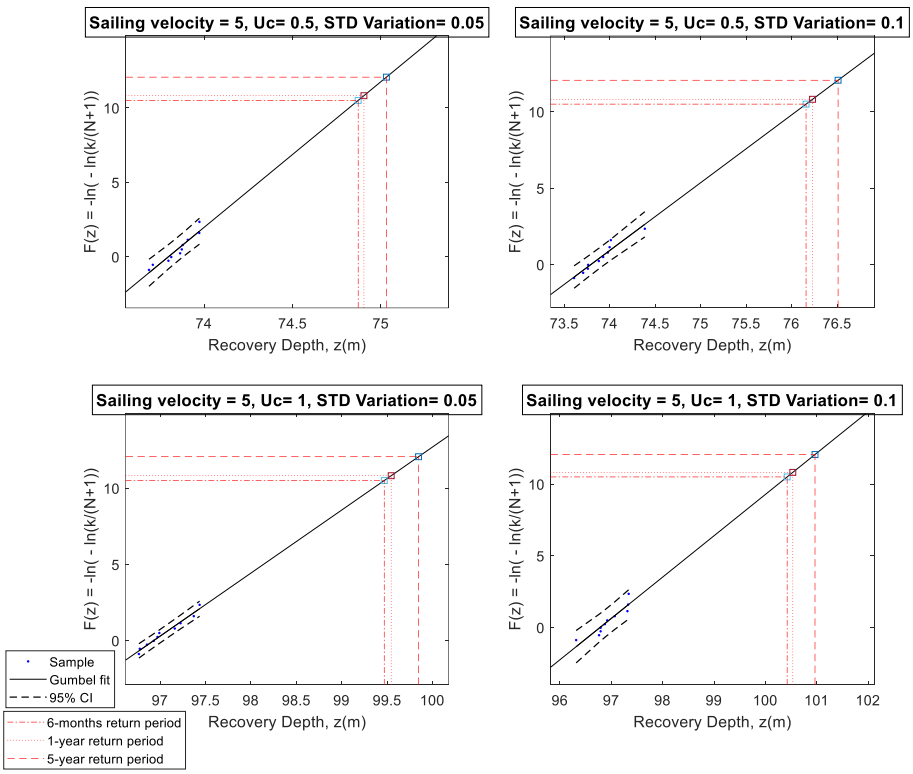

Figure 38 - Probability paper for Gumbel distribution for recovery depth corresponding to SST's velocity of 5 m/s, heading current direction

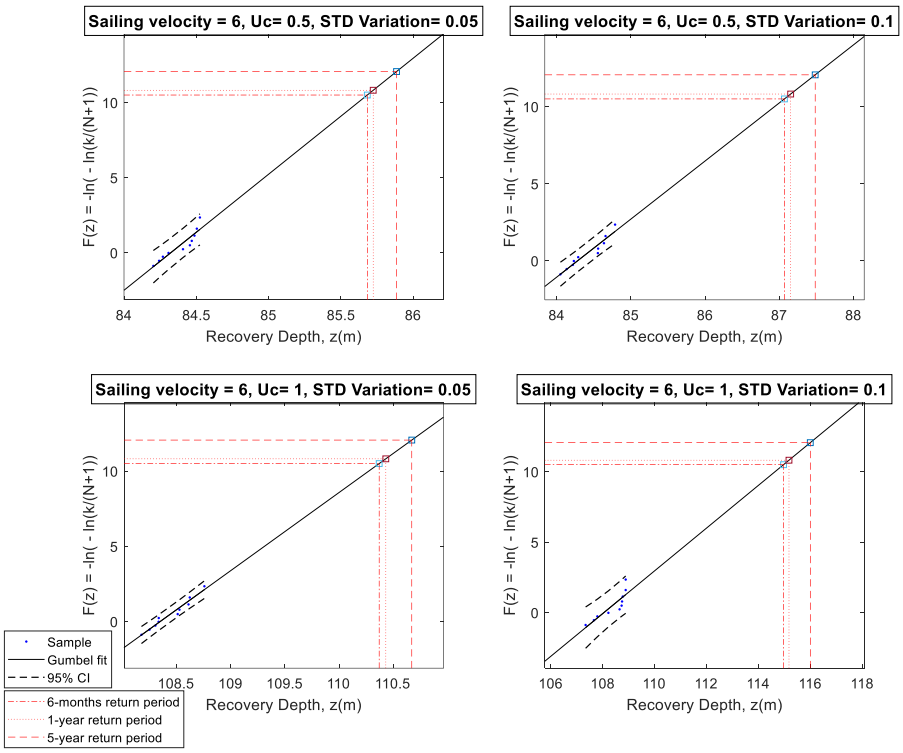

Figure 39 - Probability paper for Gumbel distribution for recovery depth corresponding to SST's velocity of 6 m/s, heading current direction

Table 16 - Recovery depth predictions for several return periods for following current

SST sailing velocity [m/s]	$V_c = 0.5\ m/s$ $CV = 0\%$	$V_c = 0.5\ m/s$ $CV = 5\%$	$V_c = 0.5\ m/s$ $CV = 10\%$	$V_c = 1\ m/s$ $CV = 0\%$	$V_c = 1\ m/s$ $CV = 5\%$	$V_c = 1\ m/s$ $CV = 10\%$
			6 months return period			
3	22.729	(23.687) (23.633, 23.732)	(24.438) (24.324, 24.550)	11.480	(12.863) (12.775, 12.949)	(13.620) (13.470, 13.758)
4	30.542	(31.272) (31.231, 31.313)	(33.200) (33.091, 33.312)	18.534	(19.938) (19.830, 20.041)	(21.243) (21.057, 21.432)
5	38.435	(39.414) (39.364, 39.465)	(39.597) (39.533, 39.661)	25.763	(27.392) (27.258, 27.522)	(28.338) (28.216, 28.461)
6	47.113	(48.185) (48.114, 48.257)	(49.460) (49.367, 49.553)	33.381	(35.206) (35.121, 35.293)	(34.979) (34.859, 35.097)
			1-year return period			
3	22.729	(23.717) (23.663, 23.772)	(24.481) (24.378, 24.603)	11.480	(12.906) (12.818, 12.992)	(13.685) (13.538, 13.820)
4	30.542	(31.296) (31.255, 31.337)	(33.284) (33.174, 33.396)	18.534	(19.982) (19.875, 20.085)	(21.326) (21.140, 21.515)
5	38.435	(39.445) (39.394, 39.497)	(39.634) (39.570, 39.698)	25.763	(27.445) (27.312, 27.575)	(28.422) (28.300, 28.547)
6	47.113	(48.221) (48.149, 48.293)	(49.535) (49.442, 49.628)	33.381	(35.260) (35.174, 35.348)	(35.028) (34.908, 35.145)
			5-year return period			
3	22.729	(23.835) (23.780, 23.891)	(24.700) (24.588, 24.811)	11.480	(13.075) (12.989, 13.158)	(13.941) (13.805, 14.064)
4	30.542	(31.389) (31.348, 31.431)	(33.615) (33.502, 33.729)	18.534	(20.156) (20.052, 20.255)	(21.653) (21.464, 21.844)
5	38.435	(39.568)	(39.779)	25.763	(27.654)	(28.756)

6	47.113	(39.516, 39.621) (48.359) (48.287, 48.431)	(39.715, 39.844) (49.830) (49.737, 49.924)	33.381	(27.524, 27.781) (35.472) (35.383, 35.563)	(28.631, 28.883) (35.219) (35.102, 35.335)

Table 17 - Recovery depth predictions for several return periods for heading current

SST sailing velocity [m/s]	$V_c = 0.5\ m/s$ $CV = 0\%$	$V_c = 0.5\ m/s$ $CV = 5\%$	$V_c = 0.5\ m/s$ $CV = 10\%$	$V_c = 1\ m/s$ $CV = 0\%$	$V_c = 1\ m/s$ $CV = 5\%$	$V_c = 1\ m/s$ $CV = 10\%$
			6 months return period			
3	59.035	(60.272) (60.205, 60.340)	(61.148) (61.007, 61.288)	84.237	(87.486) (87.277, 87.666)	(87.812) (87.614, 88.011)
4	65.498	(66.133) (66.103, 66.163)	(67.549) (67.505, 67.582)	88.773	(91.094) (90.949, 91.239)	(92.086) (91.862, 92.313)
5	73.789	(74.871) (74.798, 74.943)	(76.159) (75.949, 76.381)	96.953	(99.470) (99.340, 99.601)	(100.424) (100.129, 100.710)
6	84.442	(85.682) (85.571, 85.790)	(87.068) (86.871, 87.266)	108.550	(110.369) (110.257, 110.481)	(114.951) (114.359, 115.491)
			1-year return period			
3	59.035	(60.312) (60.245, 60.380)	(61.214) (61.074, 61.354)	84.237	(87.587) (87.386, 87.760)	(87.921) (87.723, 88.122)
4	65.498	(66.154) (66.124, 66.184)	(67.615) (67.582, 67.639)	88.773	(91.165) (91.020, 91.310)	(92.192) (91.968, 92.421)
5	73.789	(74.904) (74.831, 74.975)	(76.231) (76.018, 76.455)	96.953	(99.546) (99.416, 99.678)	(100.534) (100.241, 100.818)
6	84.442	(85.723) (85.613, 85.830)	(87.152) (86.955, 87.350)	108.550	(110.429) (110.317, 110.542)	(115.160) (114.577, 115.690)
			5-year return period			
3	59.035	(60.471) (60.403, 60.540)	(61.475) (61.335, 61.614)	84.237	(87.981) (87.812, 88.127)	(88.356) (88.155, 88.560)
4	65.498	(66.236) (66.206, 66.267)	(67.873) (67.887, 67.863)	88.773	(91.444) (91.298, 91.590)	(92.612) (92.384, 92.844)
5	73.789	(75.031) (74.960, 75.101)	(76.512) (76.292, 76.743)	96.953	(99.847) (99.715, 99.982)	(100.967) (100.680, 101.244)
6	84.442	(85.885) (85.777, 85.989)	(87.483) (87.285, 87.681)	108.550	(110.669) (110.556, 110.783)	(115.980) (115.438, 116.473)

Table 18 - Percentage change in recovery depth compared to the deterministic current case

	Following current				Heading current			
SST sailing velocity [m/s]	$V_c = 0.5$ $CV = 5\%$	$V_c = 0.5$ $CV = 10\%$	$V_c = 1$ $CV = 5\%$	$V_c = 1$ $CV = 10\%$	$V_c = 0.5$ $CV = 5\%$	$V_c = 0.5$ $CV = 10\%$	$V_c = 1$ $CV = 5\%$	$V_c = 1$ $CV = 10\%$
	6-months return period							
3	4.22	7.52	12.05	18.64	2.10	3.58	3.86	4.24
4	2.39	8.70	7.58	14.62	0.97	3.13	2.62	3.73
5	2.55	3.02	6.32	10.00	1.47	3.21	2.60	3.58
6	2.28	4.98	5.47	4.79	1.47	3.11	1.68	5.90
	1-year return period							
3	4.35	7.71	12.42	19.21	2.16	3.69	3.98	4.37
4	2.47	8.98	7.81	15.06	1.00	3.23	2.70	3.85
5	2.63	3.12	6.53	10.32	1.51	3.31	2.68	3.69
6	2.35	5.14	5.63	4.94	1.52	3.21	1.73	6.09
	5-year return period							
3	4.87	8.67	13.89	21.44	2.43	4.13	4.44	4.89
4	2.77	10.06	8.75	16.83	1.13	3.63	3.01	4.33
5	2.95	3.50	7.34	11.62	1.68	3.69	2.99	4.14
6	2.65	5.77	6.26	5.51	1.71	3.60	1.95	6.85

8.3 Appendix C – Jam-to-rise with 20-degree pitch angle

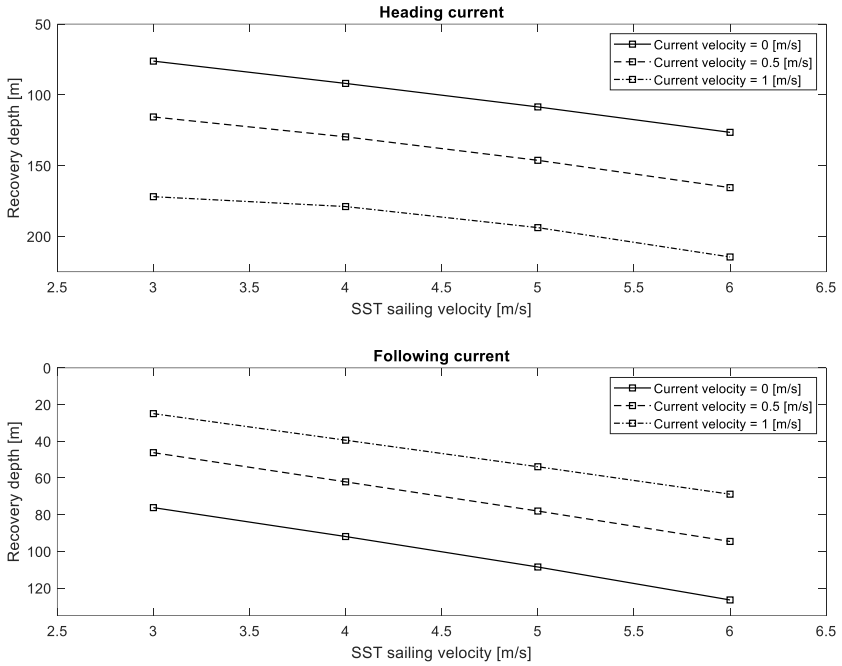

Figure 40 - Jam-to-rise curve for different steady current cases

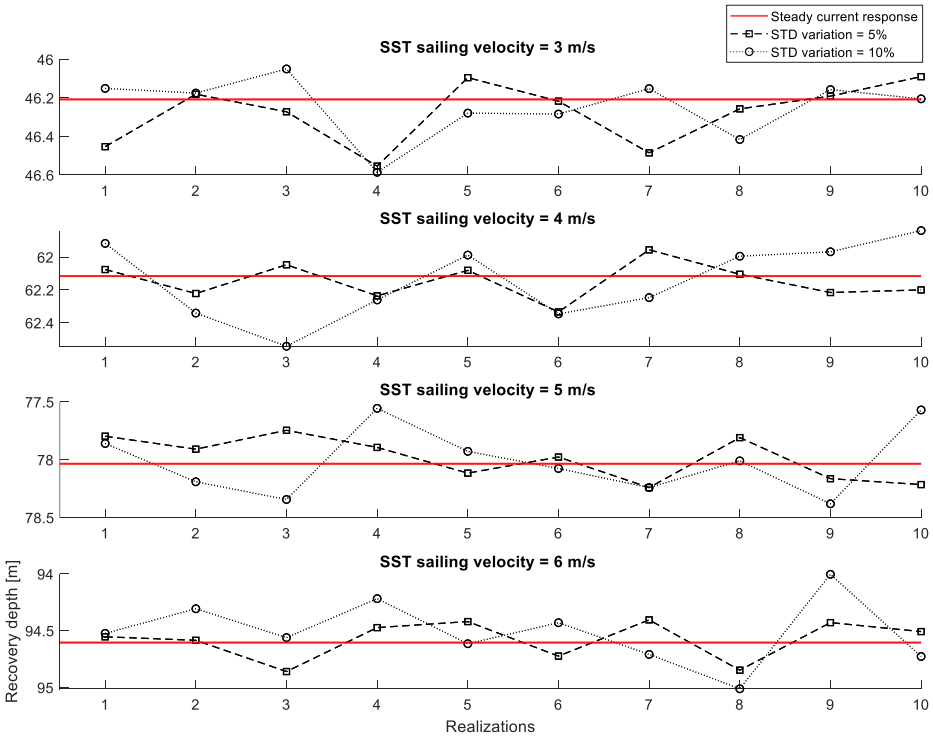

Figure 41 - Simulated SST responses during emergency recovery from jam-to-rise at different sailing velocities and following current velocity = 0.5 [m/s]

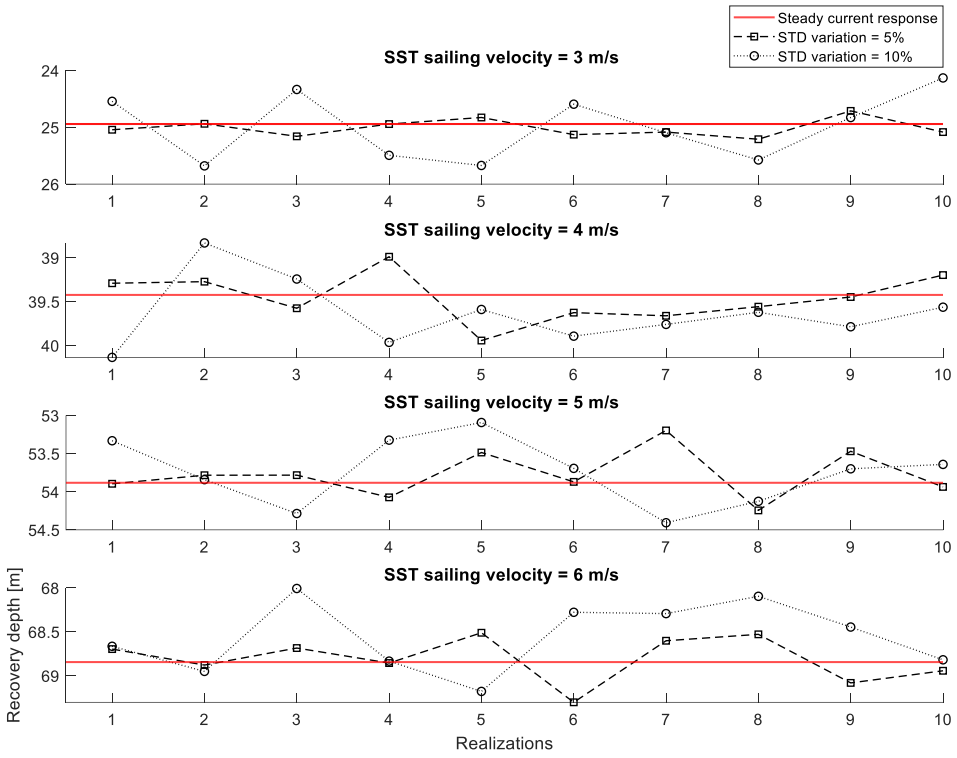

Figure 42 - Simulated SST responses during emergency recovery from jam-to-rise at different sailing velocities and following current velocity = 1 [m/s]

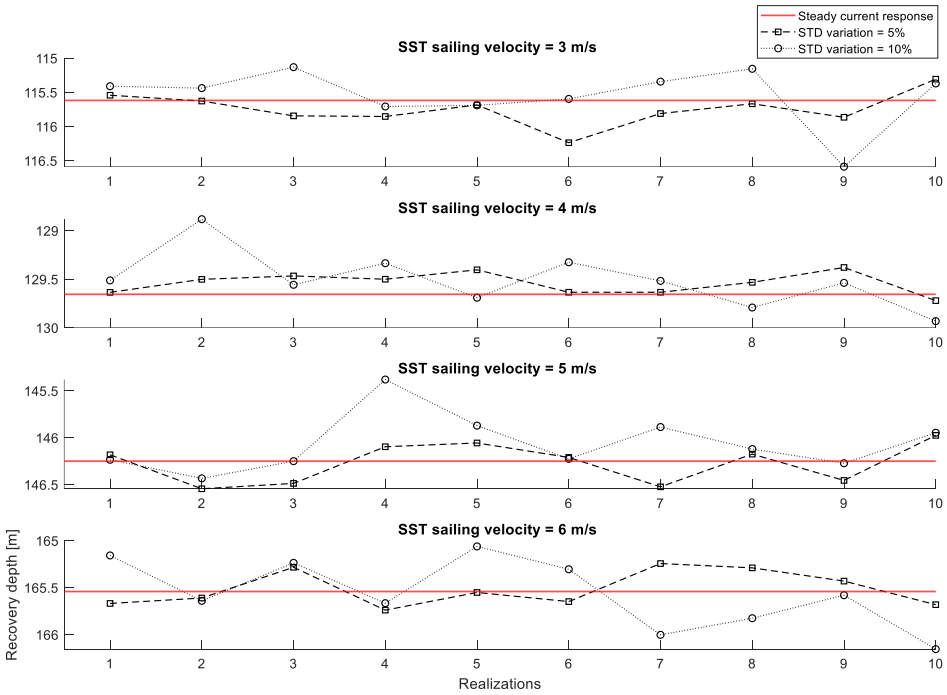

Figure 43 - Simulated SST responses during emergency recovery from jam-to-rise at different sailing velocities and heading current velocity = 0.5 [m/s]

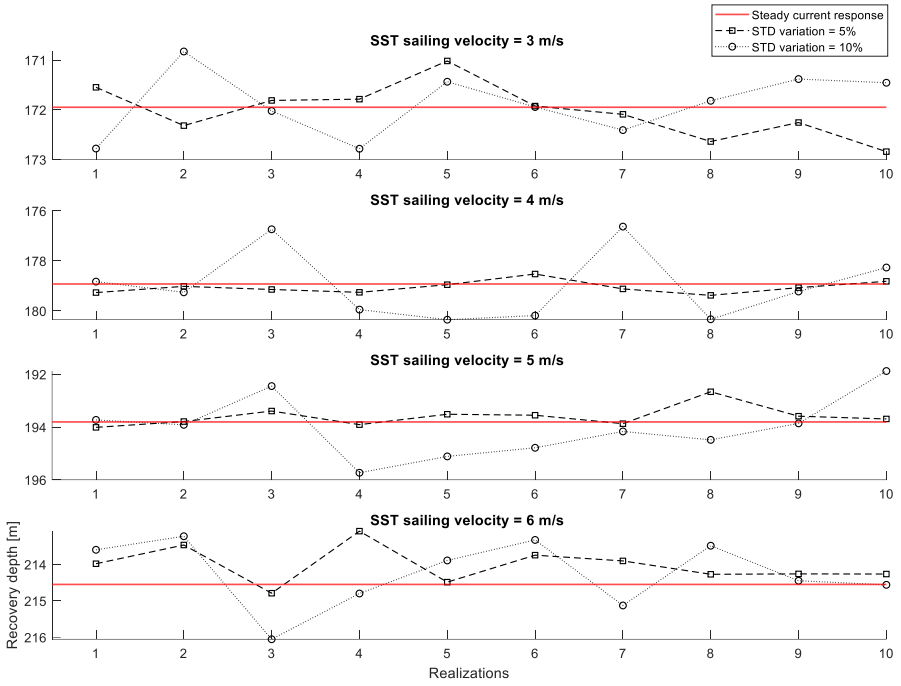

Figure 44 - Simulated SST responses during emergency recovery from jam-to-rise at different sailing velocities and heading current velocity = 1 [m/s]

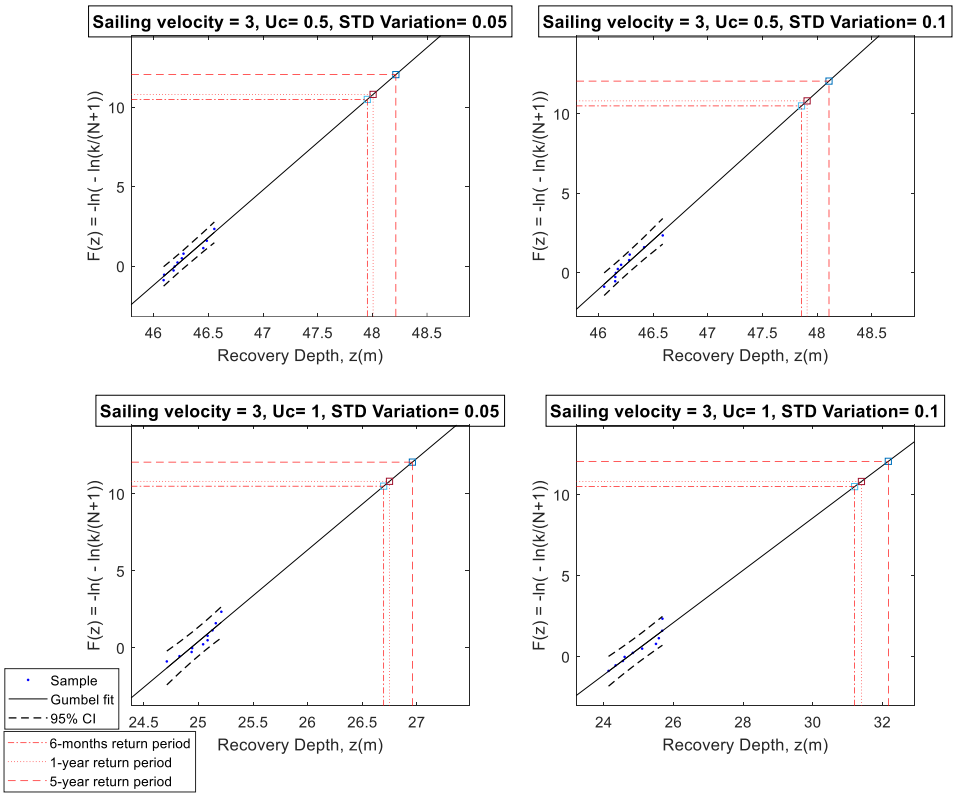

Figure 45 - Probability paper for Gumbel distribution for recovery depth corresponding to SST's velocity of 3 m/s, following current direction

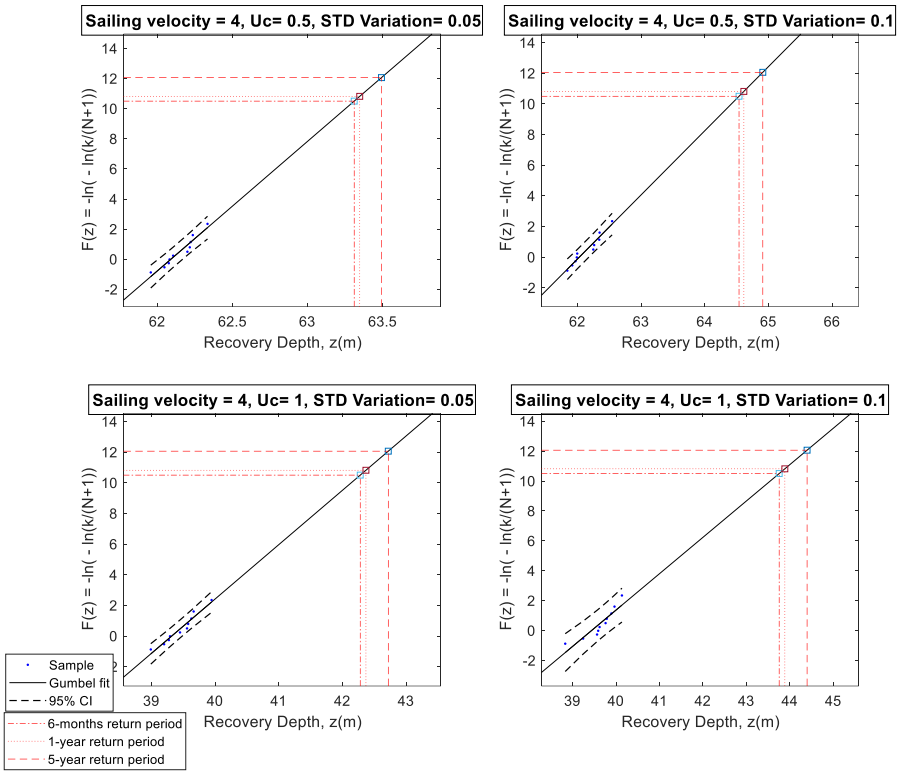

Figure 46 - Probability paper for Gumbel distribution for recovery depth corresponding to SST's velocity of 4 m/s, following current direction

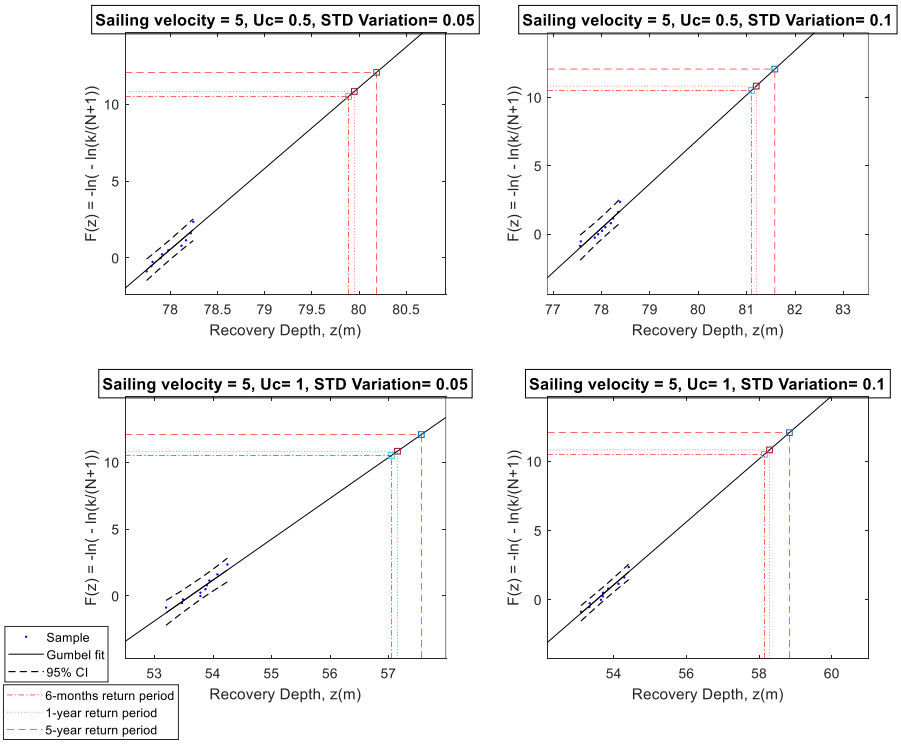

Figure 47 - Probability paper for Gumbel distribution for recovery depth corresponding to SST's velocity of 5 m/s, following current direction

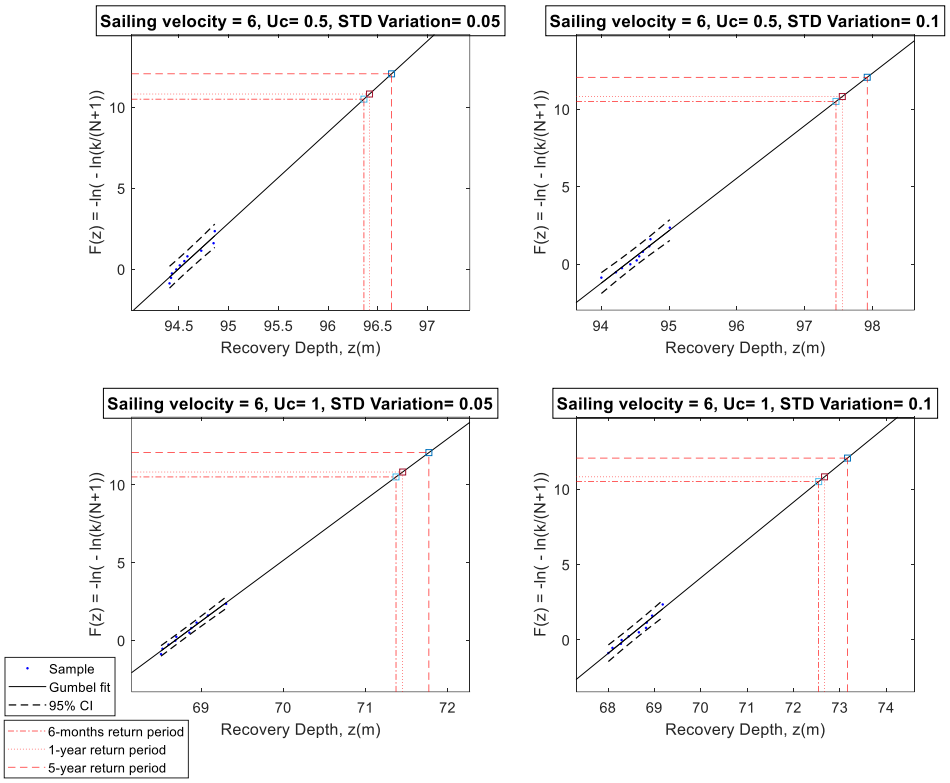

Figure 48 - Probability paper for Gumbel distribution for recovery depth corresponding to SST's velocity of 6 m/s, following current direction

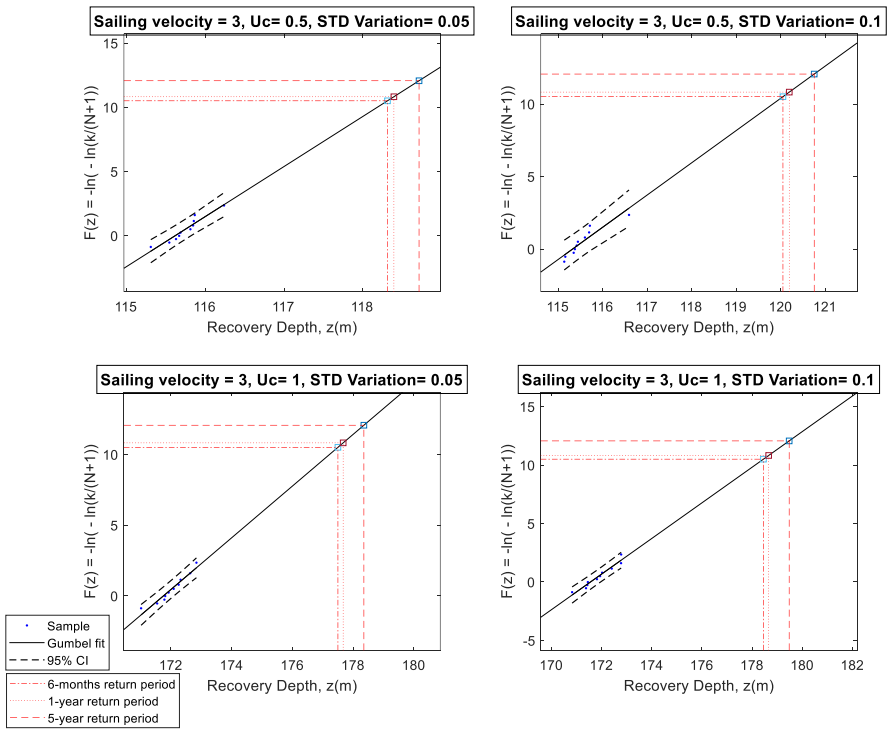

Figure 49 - Probability paper for Gumbel distribution for recovery depth corresponding to SST's velocity of 3 m/s, heading current direction

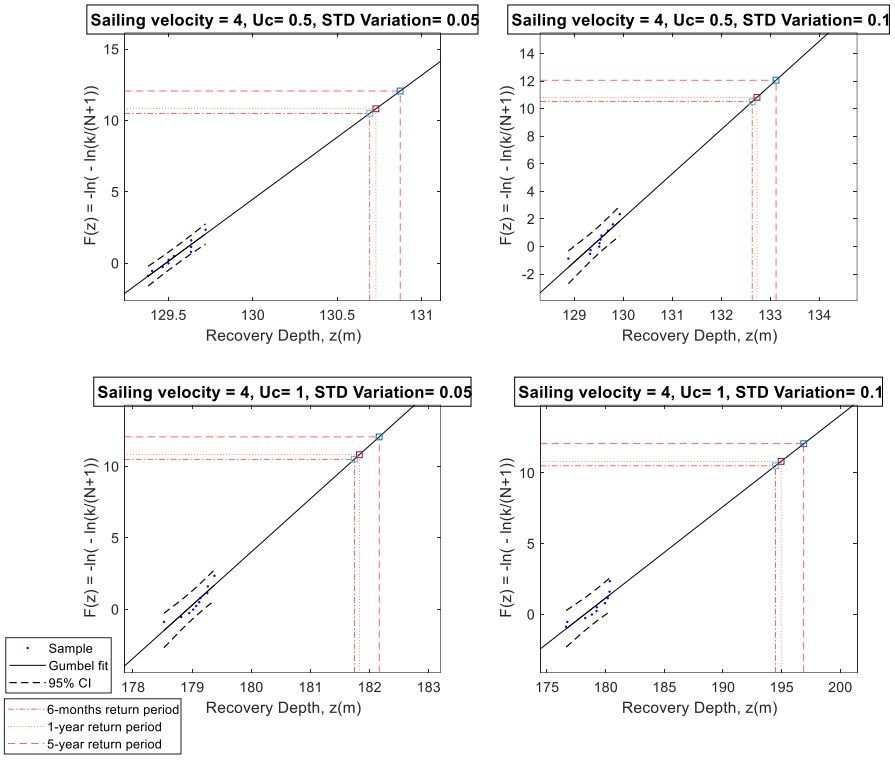

Figure 50 - Probability paper for Gumbel distribution for recovery depth corresponding to SST's velocity of 4 m/s, heading current direction

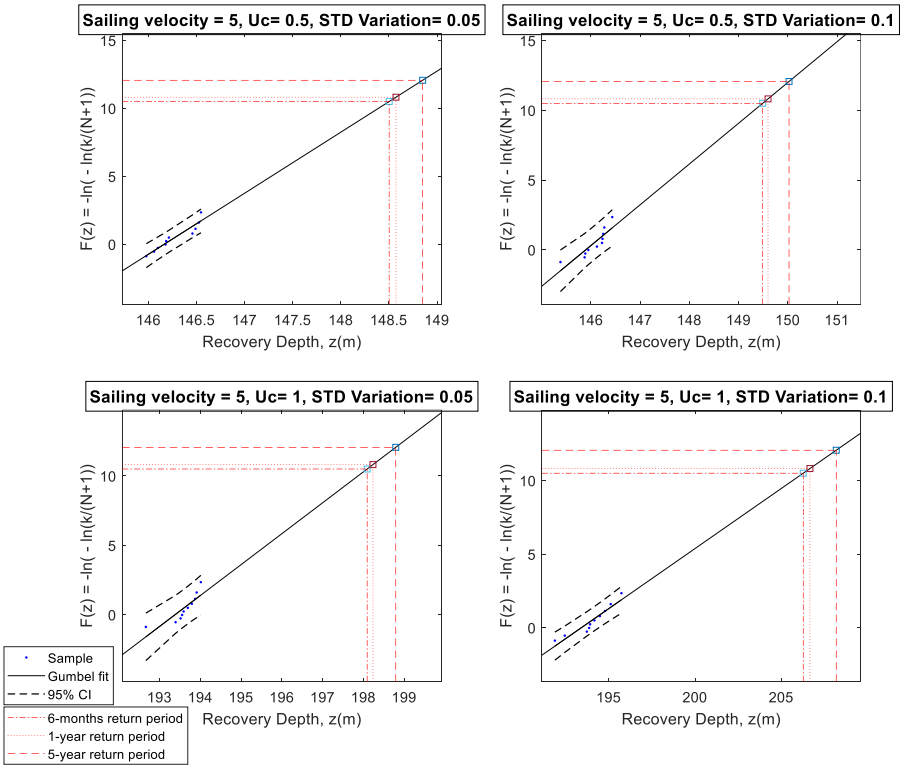

Figure 51 - Probability paper for Gumbel distribution for recovery depth corresponding to SST's velocity of 5 m/s, heading current direction

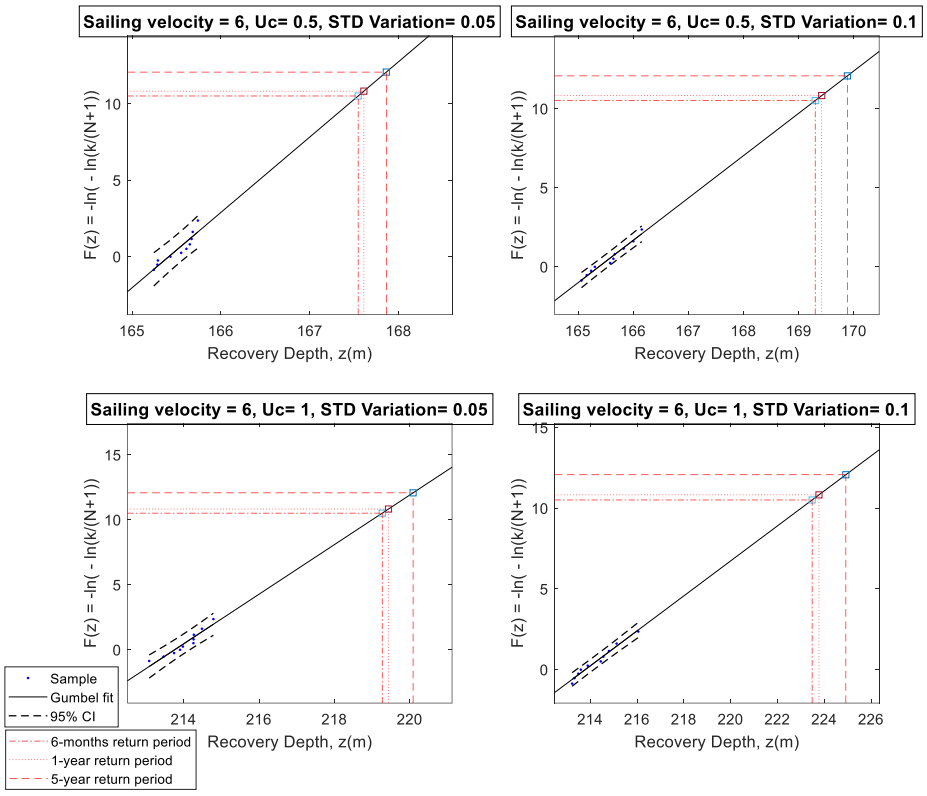

Figure 52 - Probability paper for Gumbel distribution for recovery depth corresponding to SST's velocity of 6 m/s, heading current direction

Table 19 - Recovery depth predictions for several return periods for following current

SST sailing velocity [m/s]	$V_c = 0.5\ m/s$ $CV = 0\%$	$V_c = 0.5\ m/s$ $CV = 5\%$	$V_c = 0.5\ m/s$ $CV = 10\%$	$V_c = 1\ m/s$ $CV = 0\%$	$V_c = 1\ m/s$ $CV = 5\%$	$V_c = 1\ m/s$ $CV = 10\%$
			6 months return period			
3	46.208	(47.954)	(47.856)	24.942	(26.695)	(31.197)
		(47.832. 48.079)	(47.700. 48.022)		(26.576. 26.808)	(30.675. 31.716)
4	62.116	(63.311)	(64.537)	39.424	(42.279)	(43.753)
		(63.232. 63.390)	(64.366. 64.710)		(42.106. 42.452)	(43.474. 44.008)
5	78.035	(79.889)	(81.100)	53.883	(57.048)	(58.142)
		(79.753. 80.027)	(80.881. 81.312)		(56.821. 57.267)	(57.899. 58.386)
6	94.605	(96.360)	(97.459)	68.845	(71.371)	(72.541)
		(96.209. 96.517)	(97.286. 97.631)		(71.266. 71.477)	(72.326. 72.757)
			1-year return period			
3	46.208	(48.007)	(47.907)	24.942	(26.748)	(31.393)
		(47.884. 48.133)	(47.749. 48.074)		(26.631. 26.860)	(30.872. 31.911)
4	62.116	(63.348)	(64.612)	39.424	(42.368)	(43.883)
		(63.269. 63.390)	(64.441. 64.710)		(42.195. 42.452)	(43.610. 44.008)
5	78.035	(79.950)	(81.197)	53.883	(57.151)	(58.281)
		(79.813. 80.088)	(80.980. 81.408)		(56.926. 57.369)	(58.038. 58.526)
6	94.605	(96.417)	(97.552)	68.845	(71.452)	(72.667)
		(94.264. 94.575)	(97.379. 97.724)		(71.347. 71.559)	(72.452. 72.884)
			5-year return period			
3	46.208	(48.215)	(48.107)	24.942	(26.958)	(32.165)
		(48.089. 48.344)	(47.944. 48.281)		(26.846. 27.063)	(31.646. 32.681)
4	62.116	(63.493)	(64.910)	39.424	(42.720)	(44.395)
		(63.414. 63.572)	(64.737. 65.086)		(42.547. 42.893)	(44.145. 44.623)

5	78.035	(80.186)	(81.581)	53.883	(57.559)	(58.828)
		(80.048. 80.326)	(81.370. 81.786)		(57.340. 57.770)	(58.584. 59.074)
6	94.605	(96.638)	(97.919)	68.845	(71.771)	(73.163)
		(96.482. 96.801)	(97.747. 98.090)		(71.663. 71.880)	(72.947. 73.380)

Table 20 - Recovery depth predictions for several return periods for heading current

SST sailing velocity [m/s]	$V_c = 0.5\ m/s$ $CV = 0\%$	$V_c = 0.5\ m/s$ $CV = 5\%$	$V_c = 0.5\ m/s$ $CV = 10\%$	$V_c = 1\ m/s$ $CV = 0\%$	$V_c = 1\ m/s$ $CV = 5\%$	$V_c = 1\ m/s$ $CV = 10\%$
			6 months return period			
3	115.619	(118.314)	(120.052)	171.948	(177.501)	(178.454)
		(118.085. 118.547)	(119.322. 120.895)		(177.177. 177.820)	(178.025. 178.884)
4	129.656	(130.694)	(132.634)	178.924	(181.744)	(194.477)
		(130.616. 130.772)	(132.634. 132.845)		(181.563. 181.912)	(193.220. 195.636)
5	146.251	(148.502)	(149.490)	193.806	(198.091)	(206.271)
		(148.304. 148.702)	(149.157. 149.696)		(197.873. 198.270)	(205.432. 207.080)
6	165.542	(167.544)	(169.298)	214.549	(219.269)	(223.481)
		(167.368. 167.712)	(169.115. 169.482)		(218.922. 219.608)	(223.006. 223.967)
			1-year return period			
3	115.619	(118.395)	(120.195)	171.948	(177.674)	(178.662)
		(118.165. 118.629)	(119.455. 121.048)		(177.352. 177.992)	(178.232. 179.092)
4	129.656	(130.731)	(132.733)	178.924	(181.830)	(194.968)
		(130.653. 130.809)	(132.511. 132.940)		(181.652. 181.994)	(193.731. 196.107)
5	146.251	(148.573)	(149.599)	193.806	(198.233)	(206.659)
		(148.374. 148.773)	(149.373. 149.798)		(198.030. 198.400)	(205.827. 207.461)
6	165.542	(167.608)	(169.416)	214.549	(219.435)	(223.773)
		(167.434. 167.775)	(169.233. 169.600)		(219.090. 219.771)	(223.294. 224.262)
			5-year return period			
3	115.619	(118.715)	(120.756)	171.948	(178.356)	(179.479)
		(118.483. 118.951)	(119.979. 121.652)		(178.038. 178.669)	(179.048. 179.911)
4	129.656	(130.874)	(133.122)	178.924	(182.164)	(196.897)
		(130.796. 130.953)	(132.913. 133.317)		(182.000. 182.316)	(195.743. 197.960)
5	146.251	(148.850)	(150.025)	193.806	(198.792)	(208.185)
		(148.651. 149.052)	(149.828. 150.200)		(198.649. 198.910)	(207.382. 208.959)
6	165.542	(167.860)	(169.881)	214.549	(220.088)	(224.922)
		(167.691. 168.023)	(169.696. 170.067)		(219.752. 220.415)	(224.431. 225.424)

Table 21 – Percentage change in recovery depth compared to the deterministic current case

	Following current				Heading current			
SST sailing velocity [m/s]	$V_c = 0.5$ $CV = 5\%$	$V_c = 0.5$ $CV = 10\%$	$V_c = 1$ $CV = 5\%$	$V_c = 1$ $CV = 10\%$	$V_c = 0.5$ $CV = 5\%$	$V_c = 0.5$ $CV = 10\%$	$V_c = 1$ $CV = 5\%$	$V_c = 1$ $CV = 10\%$
	6-months return period							
3	3.78	3.57	7.03	25.08	2.33	3.83	3.23	3.78
4	1.92	3.90	7.24	10.98	0.80	2.30	1.58	8.69
5	2.38	3.93	5.87	7.90	1.54	2.21	2.21	6.43
6	1.86	3.02	3.67	5.37	1.21	2.27	2.20	4.16
	1-year return period							
3	3.89	3.68	7.24	25.86	2.40	3.96	3.33	3.90
4	1.98	4.02	7.47	11.31	0.83	2.37	1.62	8.97
5	2.45	4.05	6.06	8.16	1.59	2.29	2.28	6.63
6	1.92	3.12	3.79	5.55	1.25	2.34	2.28	4.30
	5-year return period							
3	4.34	4.11	8.08	28.96	2.68	4.44	3.73	4.38
4	2.22	4.50	8.36	12.61	0.94	2.67	1.81	10.05
5	2.76	4.54	6.82	9.18	1.78	2.58	2.57	7.42
6	2.15	3.50	4.25	6.27	1.40	2.62	2.58	4.83

8.4 Appendix D – Jam-to-dive with 10-degree pitch angle

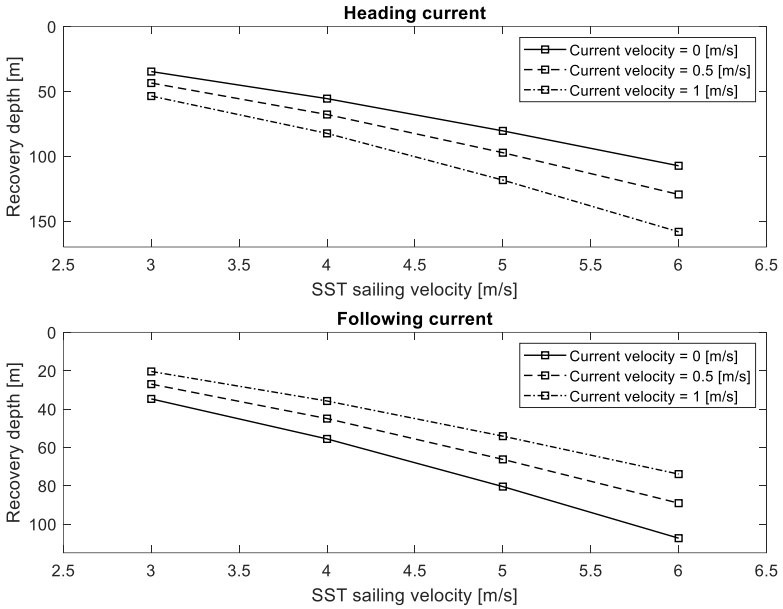

Figure 53 - Jam-to-dive curve for different steady current cases

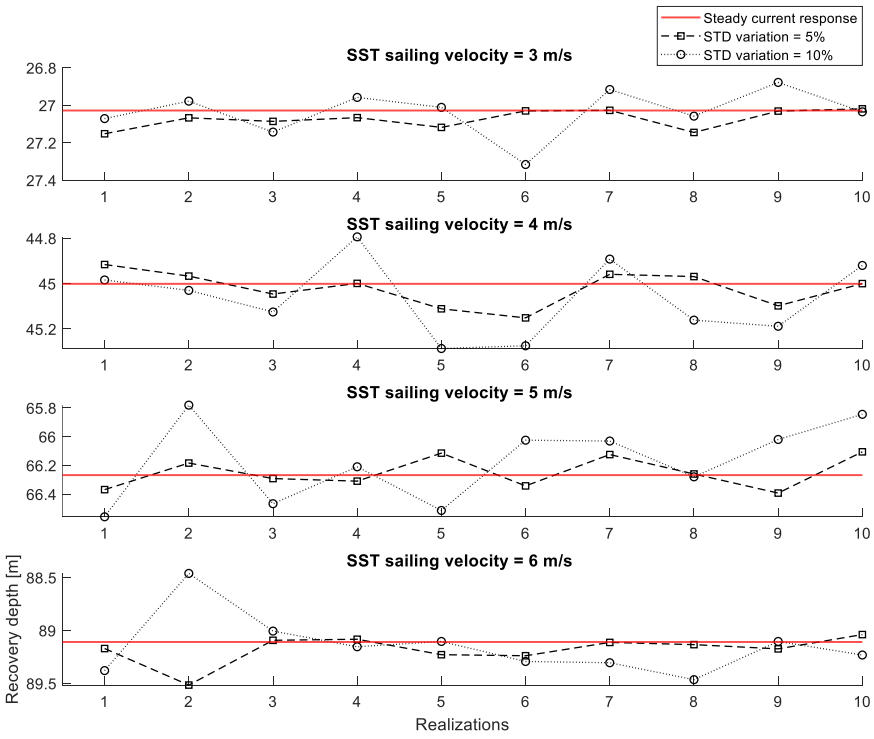

Figure 54 - Simulated SST responses during emergency recovery from jam-to-dive at different sailing velocities and following current velocity = 0.5 [m/s]

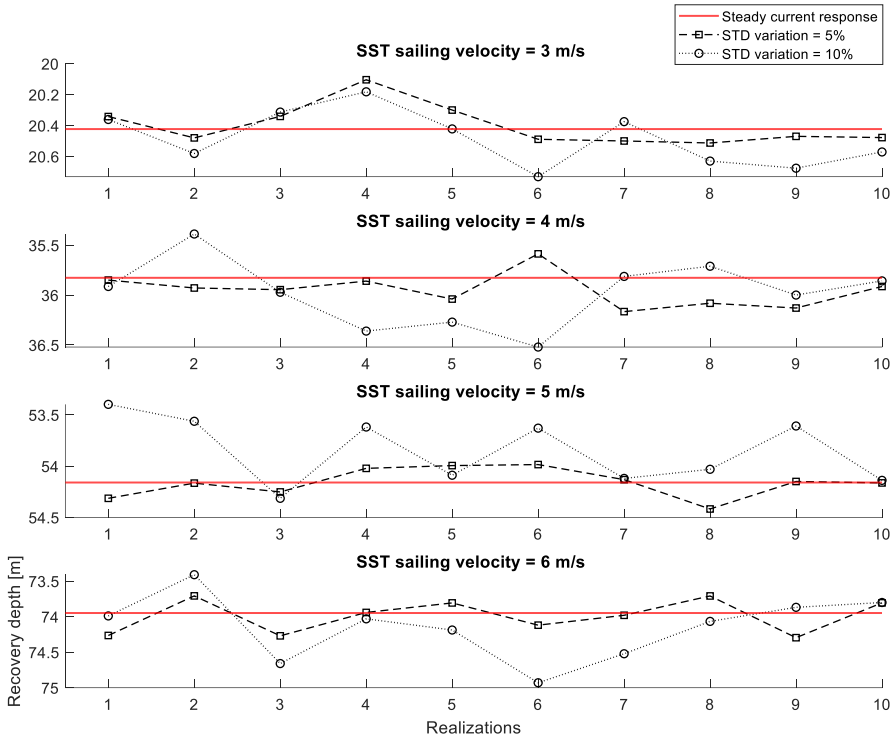

Figure 55 - Simulated SST responses during emergency recovery from jam-to-dive at different sailing velocities and following current velocity = 1 [m/s]

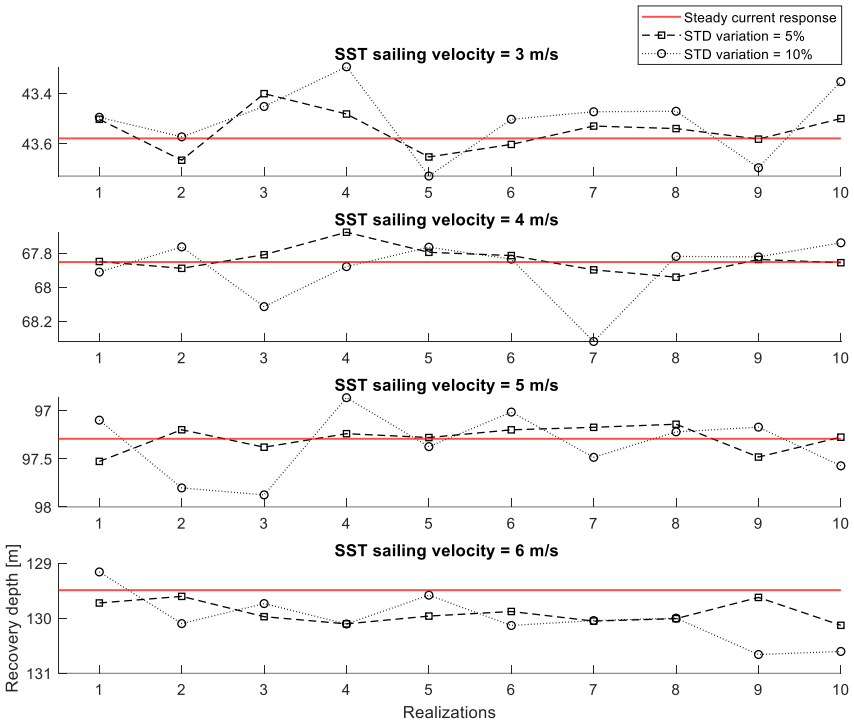

Figure 56 - Simulated SST responses during emergency recovery from jam-to-dive at different sailing velocities and heading current velocity = 0.5 [m/s]

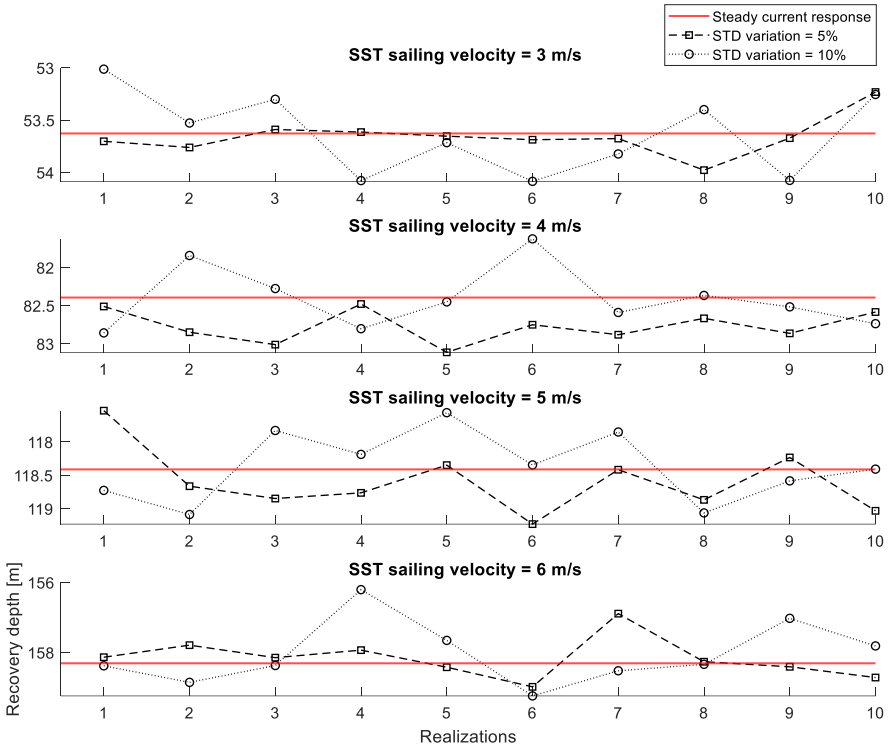

Figure 57 - Simulated SST responses during emergency recovery from jam-to-dive at different sailing velocities and heading current velocity = 1 [m/s]

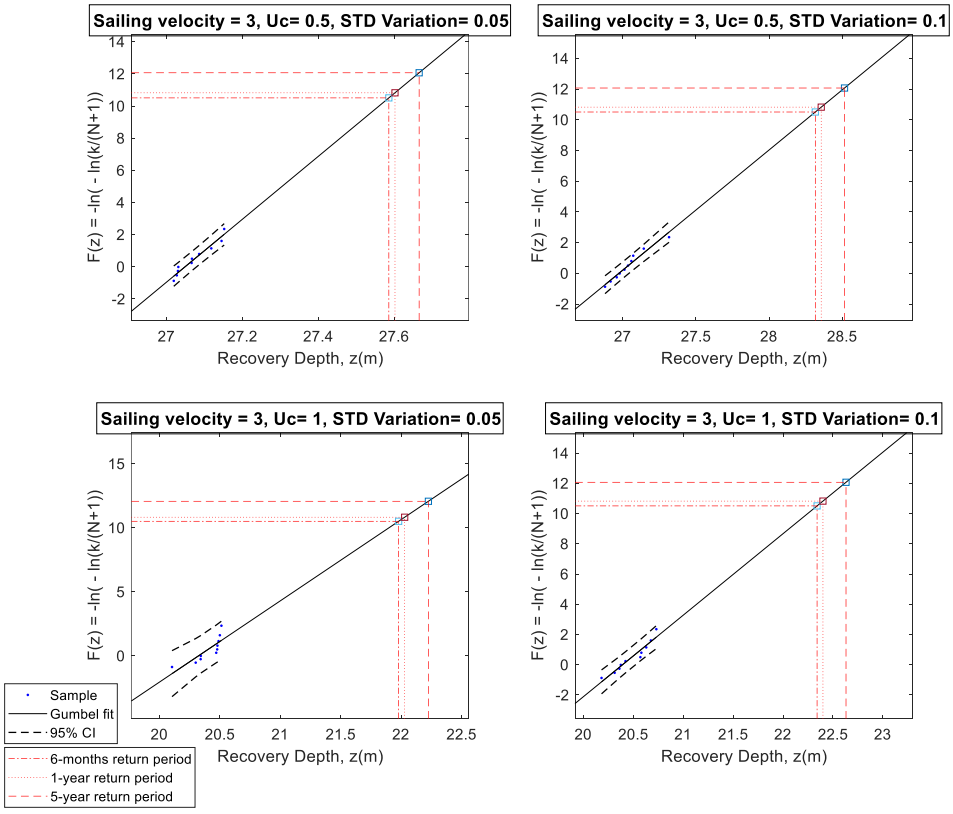

Figure 58 - Probability paper for Gumbel distribution for recovery depth corresponding to SST's velocity of 3 m/s, following current direction

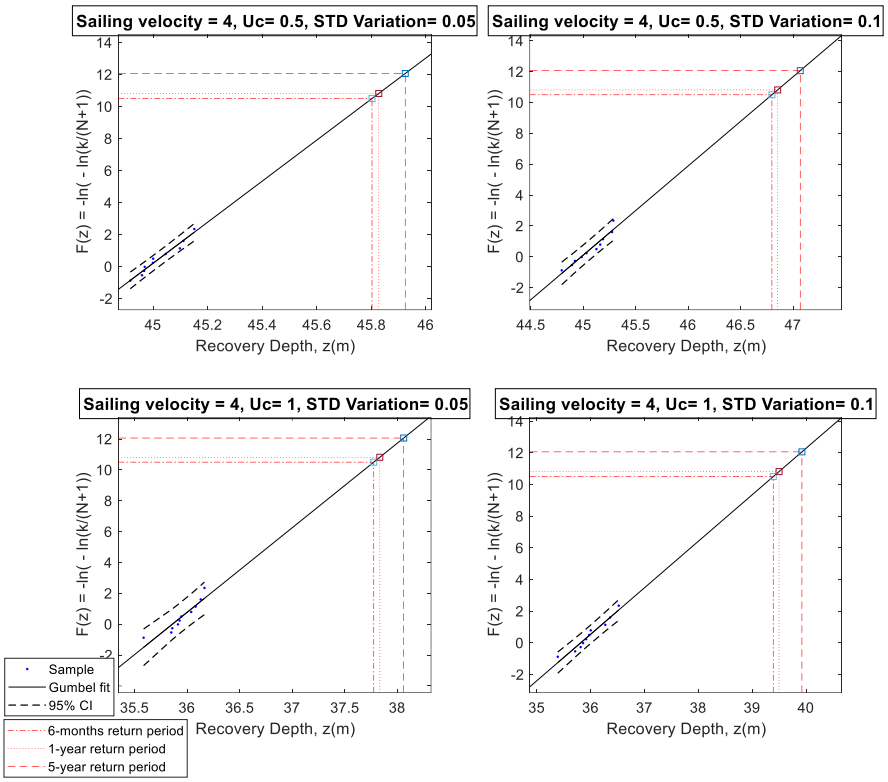

Figure 59 – Probability paper for Gumbel distribution for recovery depth corresponding to SST's velocity of 4 m/s, following current direction

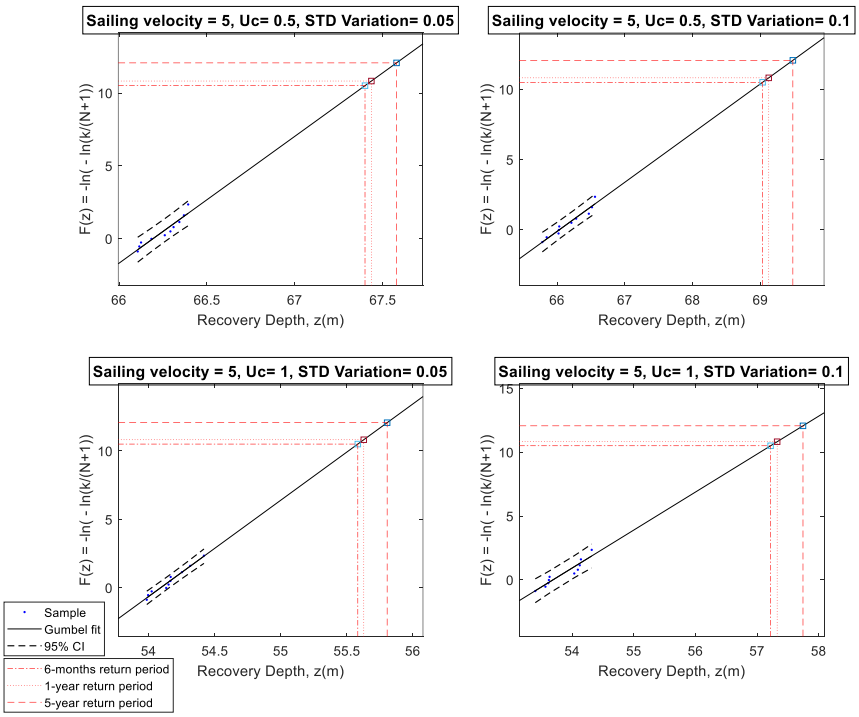

Figure 60 – Probability paper for Gumbel distribution for recovery depth corresponding to SST's velocity of 4 m/s, following current direction

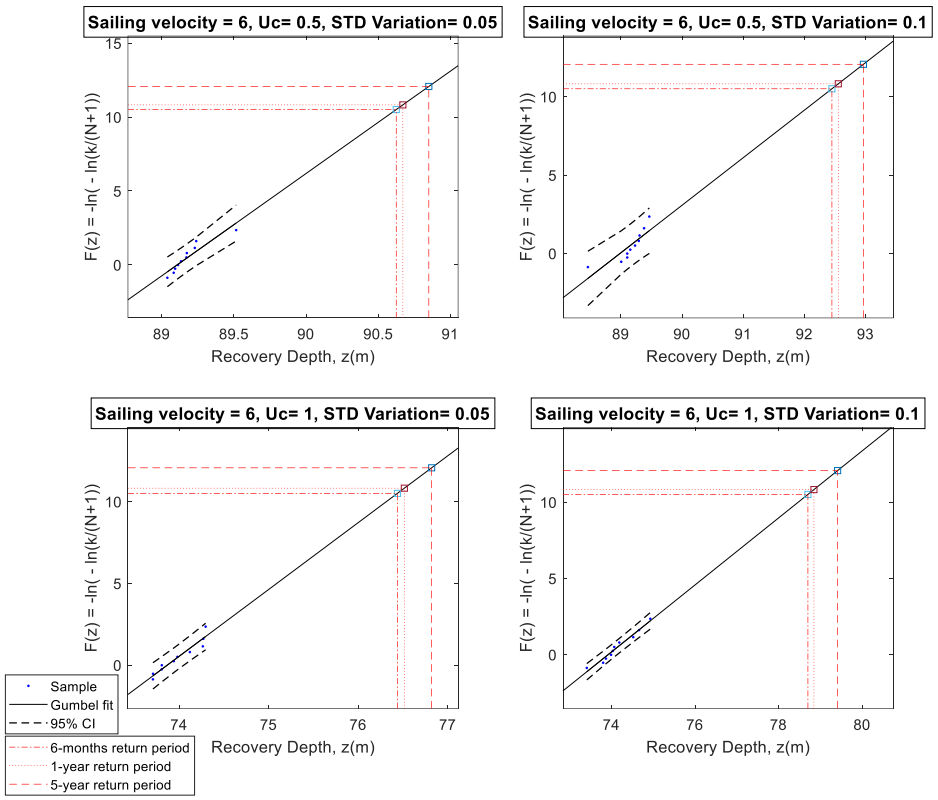

Figure 61 - Probability paper for Gumbel distribution for recovery depth corresponding to SST's velocity of 6 m/s, following current direction

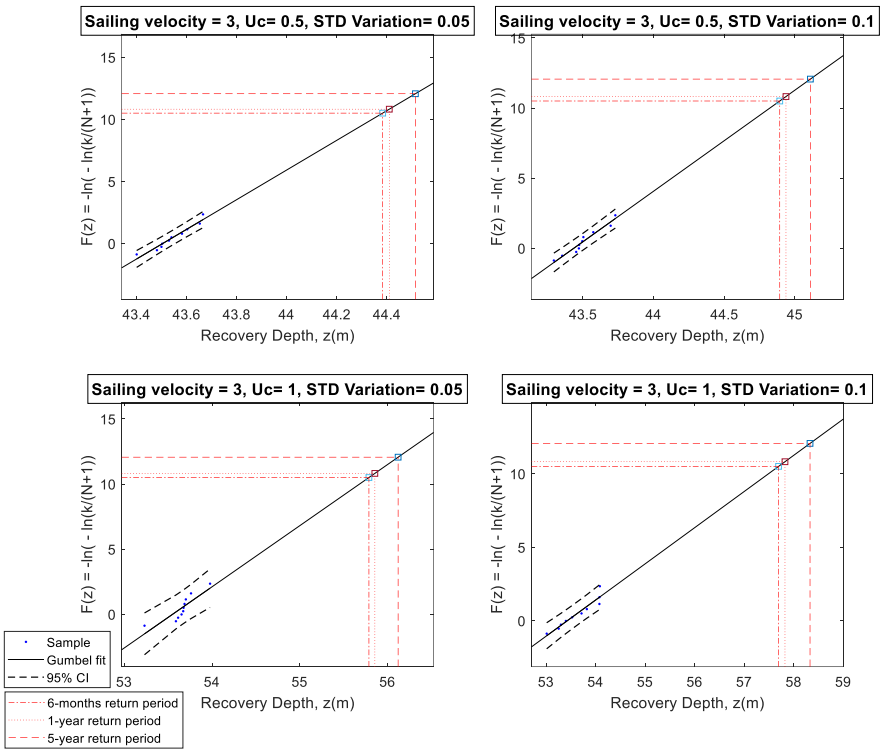

Figure 62 – Probability paper for Gumbel distribution for recovery depth corresponding to SST's velocity of 3 m/s, heading current direction

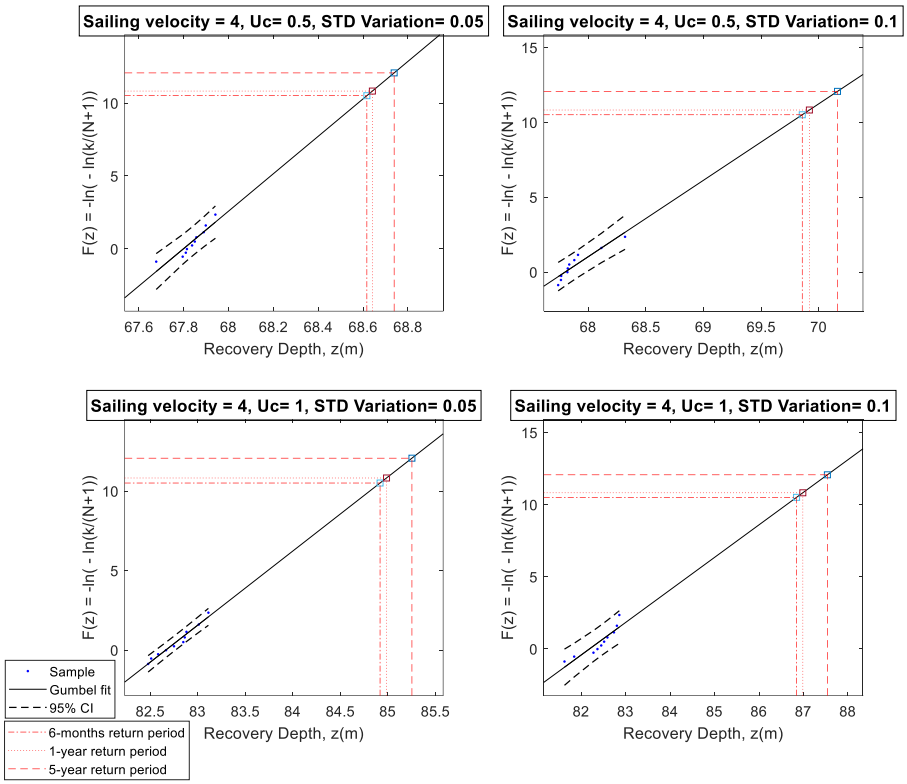

Figure 63 – Probability paper for Gumbel distribution for recovery depth corresponding to SST's velocity of 4 m/s, heading current direction

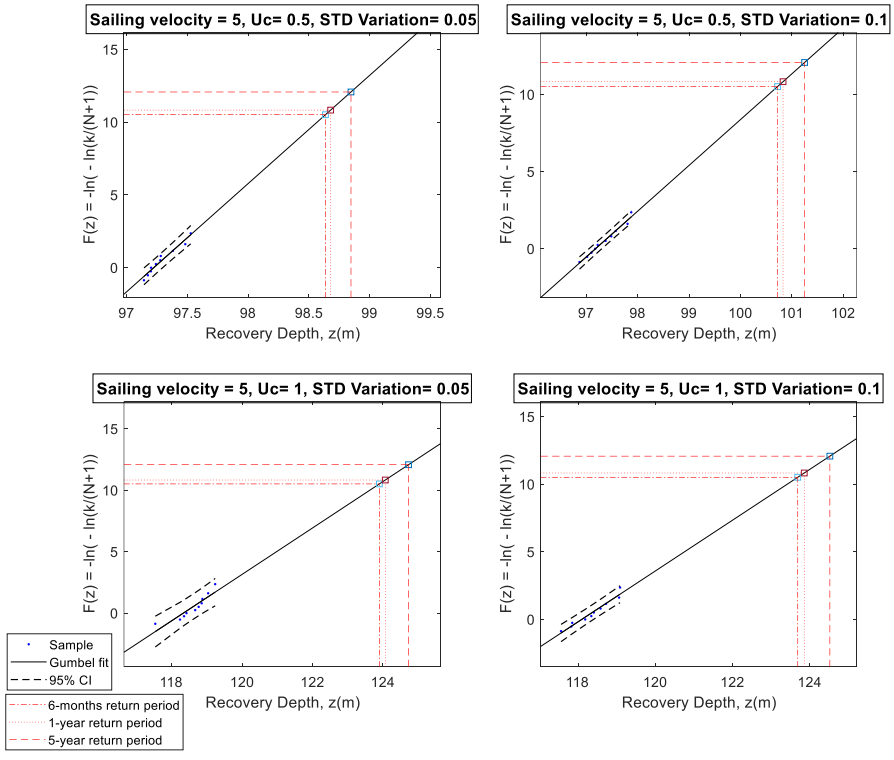

Figure 64 – Probability paper for Gumbel distribution for recovery depth corresponding to SST's velocity of 5 m/s, heading current direction

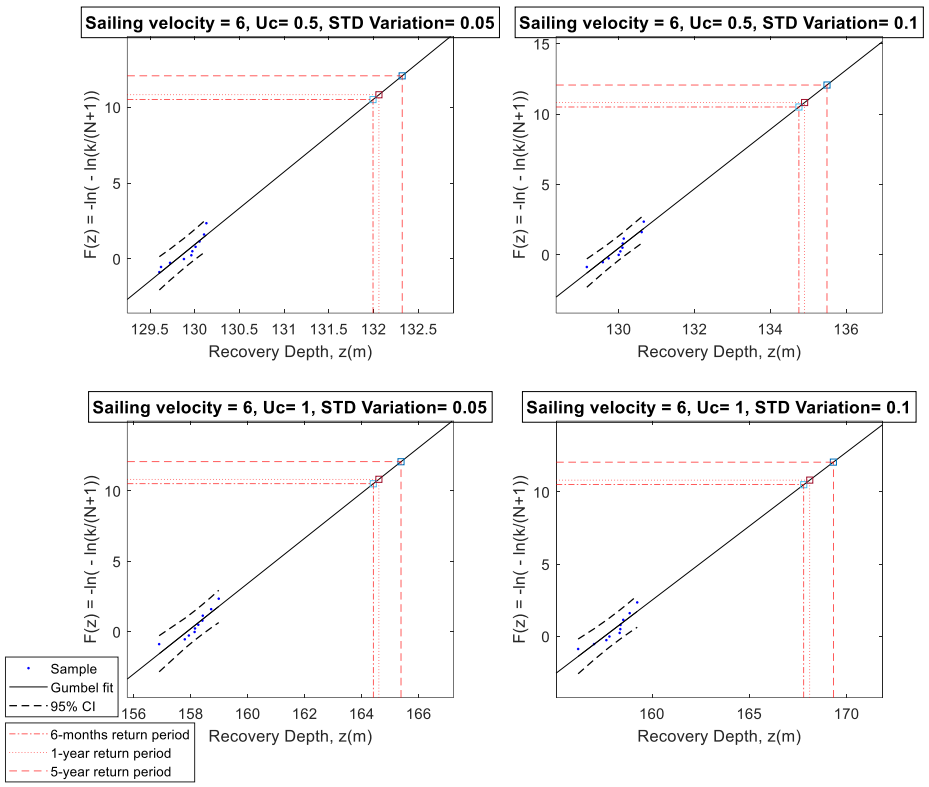

Figure 65 - Probability paper for Gumbel distribution for recovery depth corresponding to SST's velocity of 6 m/s, heading current direction

Table 22 - Recovery depth predictions for several return periods for following current

SST sailing velocity [m/s]	$V_c = 0.5\ m/s$ $CV = 0\%$	$V_c = 0.5\ m/s$ $CV = 5\%$	$V_c = 0.5\ m/s$ $CV = 10\%$	$V_c = 1\ m/s$ $CV = 0\%$	$V_c = 1\ m/s$ $CV = 5\%$	$V_c = 1\ m/s$ $CV = 10\%$
			6 months return period			
3	27.028	(27.586)	(28.317)	20.423	(21.980)	(22.341)
		(27.549, 27.625)	(28.217, 28.421)		(21.880, 22.063)	(22.216, 22.464)
4	45.001	(45.802)	(46.797)	35.827	(37.775)	(39.391)
		(45.757, 45.849)	(46.687, 46.907)		(37.646, 37.897)	(39.183, 39.599)
5	66.268	(67.399)	(69.031)	54.160	(55.583)	(57.217)
		(67.311, 67.486)	(68.834, 69.230)		(55.505, 55.662)	(56.916, 57.520)
6	89.109	(90.626)	(92.449)	73.949	(76.437)	(78.701)
		(90.397, 90.888)	(92.297, 92.574)		(76.234, 76.643)	(78.452, 78.953)
			1-year return period			
3	27.028	(27.602)	(28.357)	20.423	(22.030)	(22.400)
		(27.565, 27.641)	(28.257, 28.462)		(21.934, 22.109)	(22.275, 22.522)
4	45.001	(45.827)	(46.852)	35.827	(37.833)	(39.499)
		(45.781, 45.874)	(46.742, 46.961)		(37.705, 37.953)	(39.290, 39.707)
5	66.268	(67.435)	(69.122)	54.160	(55.628)	(57.324)
		(67.348, 67.522)	(68.924, 69.321)		(55.550, 55.707)	(57.022, 57.626)
6	89.109	(90.671)	(92.554)	73.949	(76.515)	(78.845)
		(90.440, 90.937)	(92.413, 92.669)		(76.311, 76.721)	(78.595, 79.098)
			5-year return period			
3	27.028	(27.666)	(28.516)	20.423	(22.226)	(22.631)
		(27.628, 27.706)	(28.413, 28.625)		(22.151, 22.289)	(22.508, 22.752)
4	45.001	(45.924)	(47.068)	35.827	(38.060)	(39.923)
		(45.878, 45.982)	(46.959, 47.176)		(37.940, 38.172)	(39.715, 40.131)
5	66.268	(67.578)	(69.478)	54.160	(55.805)	(57.743)
		(67.492, 67.664)	(69.279, 69.677)		(55.725, 55.886)	(57.441, 58.046)
6	89.109	(90.851)	(92.974)	73.949	(76.819)	(79.412)
		(90.608, 91.131)	(92.869, 93.042)		(76.614, 77.027)	(79.158, 79.668)

Table 23 - Recovery depth predictions for several return periods for heading current

SST sailing velocity [m/s]	$V_c = 0.5\ m/s$ $CV = 0\%$	$V_c = 0.5\ m/s$ $CV = 5\%$	$V_c = 0.5\ m/s$ $CV = 10\%$	$V_c = 1\ m/s$ $CV = 0\%$	$V_c = 1\ m/s$ $CV = 5\%$	$V_c = 1\ m/s$ $CV = 10\%$
			6 months return period			
3	43.579	(44.383)	(44.892)	53.627	(55.788)	(57.693)
		(44.383, 44.4234)	(44.795, 44.991)		(55.597, 55.961)	(57.370, 58.014)
4	67.852	(68.617)	(69.856)	82.393	(84.918)	(86.845)
		(68.653, 68.667)	(69.568, 70.182)		(84.809, 85.028)	(86.524, 87.140)
5	97.294	(98.637)	(100.721)	118.411	(123.898)	(123.689)
		(98.537, 98.740)	(100.580, 100.863)		(123.540, 124.227)	(123.375, 124.003)
6	129.491	(131.993)	(134.750)	158.308	(164.401)	(167.793)
		(131.827, 132.150)	(134.377, 135.115)		(163.973, 164.795)	(167.101, 168.435)
			1-year return period			
3	43.579	(44.410)	(44.936)	53.627	(55.856)	(57.499)
		(44.359, 44.460)	(44.839, 45.035)		(55.668, 56.026)	(57.499, 58.143)
4	67.852	(68.642)	(69.918)	82.393	(84.986)	(86.986)
		(68.588, 68.691)	(69.626, 70.248)		(84.877, 85.096)	(86.671, 87.275)
5	97.294	(98.679)	(100.687)	118.411	(124.066)	(123.858)
		(98.579, 98.784)	(100.687, 100.971)		(123.715, 124.388)	(123.543, 124.171)
6	129.491	(132.059)	(134.900)	158.308	(164.599)	(168.101)
		(131.895, 132.214)	(134.529, 135.263)		(164.179, 164.984)	(167.422, 168.732)

			5-year return period			
3	43.579	(44.514)	(45.109)	53.627	(56.121)	(58.328)
		(44.464, 44.564)	(45.010, 45.209)		(55.947, 56.278)	(58.006, 58.647)
4	67.852	(68.739)	(70.162)	82.393	(85.253)	(87.538)
		(68.689, 68.784)	(69.856, 70.508)		(85.144, 85.363)	(87.248, 87.805)
5	97.294	(98.947)	(101.248)	118.411	(124.726)	(124.520)
		(98.743, 98.954)	(101.105, 101.392)		(124.405, 125.022)	(124.206, 124.834)
6	129.491	(132.318)	(135.490)	158.308	(165.375)	(169.315)
		(132.162, 132.467)	(135.126, 135.846)		(164.990, 165.728)	(168.682, 169.903)

Table 24 - Percentage change in recovery depth compared to the deterministic current case

D10

SST sailing velocity [m/s]	**Following current**				**Heading current**			
	$V_c = 0.5$ $CV = 5\%$	$V_c = 0.5$ $CV = 10\%$	$V_c = 1$ $CV = 5\%$	$V_c = 1$ $CV = 10\%$	$V_c = 0.5$ $CV = 5\%$	$V_c = 0.5$ $CV = 10\%$	$V_c = 1$ $CV = 5\%$	$V_c = 1$ $CV = 10\%$
	6-months return period							
3	2.06	4.77	7.62	9.39	1.84	3.01	4.03	7.58
4	1.78	3.99	5.44	9.95	1.13	2.95	3.06	5.40
5	1.71	4.17	2.63	5.64	1.38	3.52	4.63	4.46
6	1.70	3.75	3.36	6.43	1.93	4.06	3.85	5.99
	1-year return period							
3	2.12	4.92	7.87	9.68	1.91	3.11	4.16	7.22
4	1.84	4.11	5.60	10.25	1.16	3.04	3.15	5.57
5	1.76	4.31	2.71	5.84	1.42	3.49	4.78	4.60
6	1.75	3.87	3.47	6.62	1.98	4.18	3.97	6.19
	5-year return period							
3	2.36	5.51	8.83	10.81	2.15	3.51	4.65	8.77
4	2.05	4.59	6.23	11.43	1.31	3.40	3.47	6.24
5	1.98	4.84	3.04	6.62	1.70	4.06	5.33	5.16
6	1.95	4.34	3.88	7.39	2.18	4.63	4.46	6.95

8.5 Appendix E – Jam-to-dive with 15-degree pitch angle

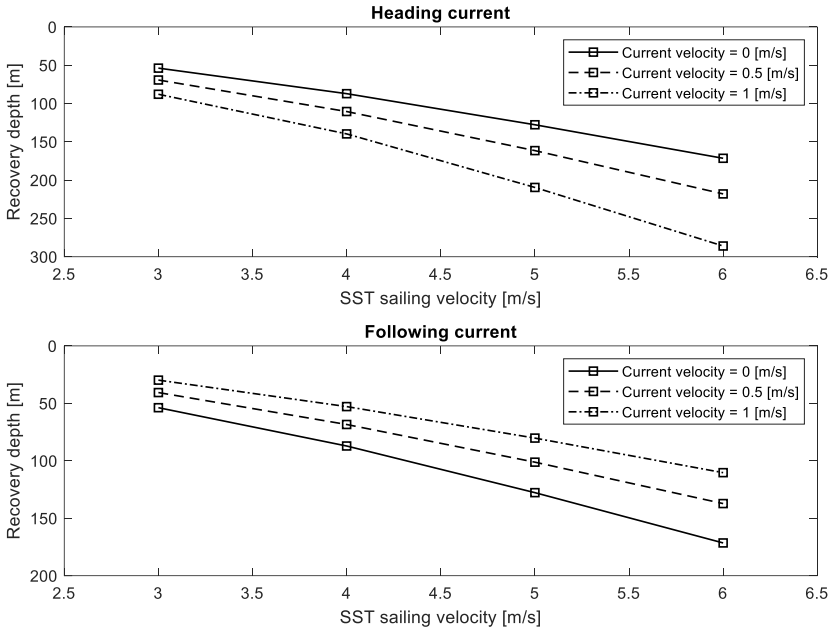

Figure 66 - Jam-to-dive curve for different steady current cases

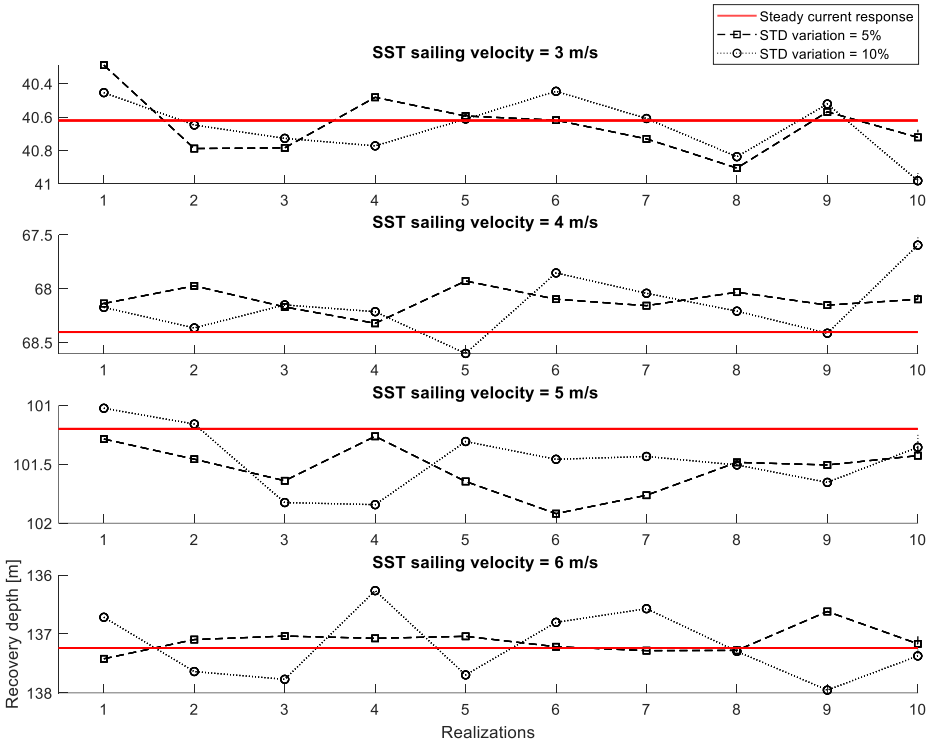

Figure 67 - Simulated SST responses during emergency recovery from jam-to-dive at different sailing velocities and following current velocity = 0.5 [m/s]

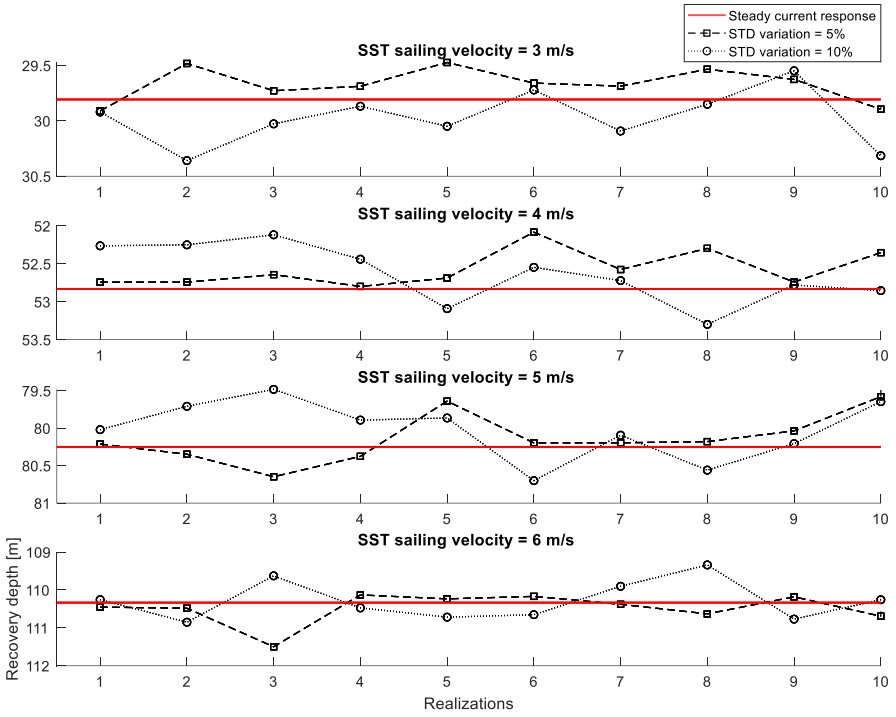

Figure 68 - Simulated SST responses during emergency recovery from jam-to-dive at different sailing velocities and following current velocity = 1 [m/s]

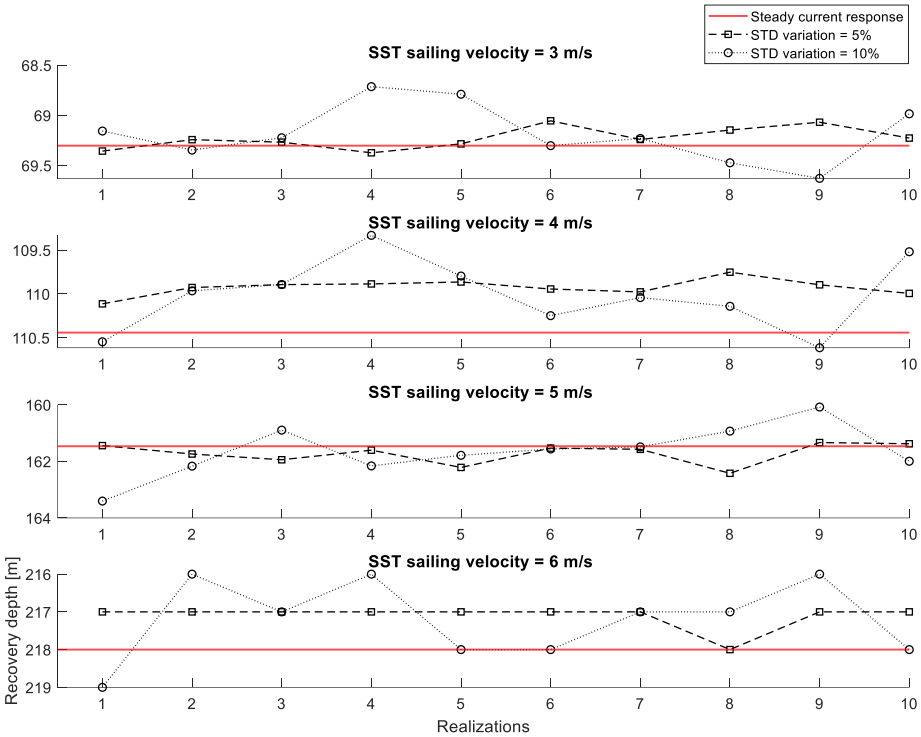

Figure 69 - Simulated SST responses during emergency recovery from jam-to-dive at different sailing velocities and heading current velocity = 0.5 [m/s]

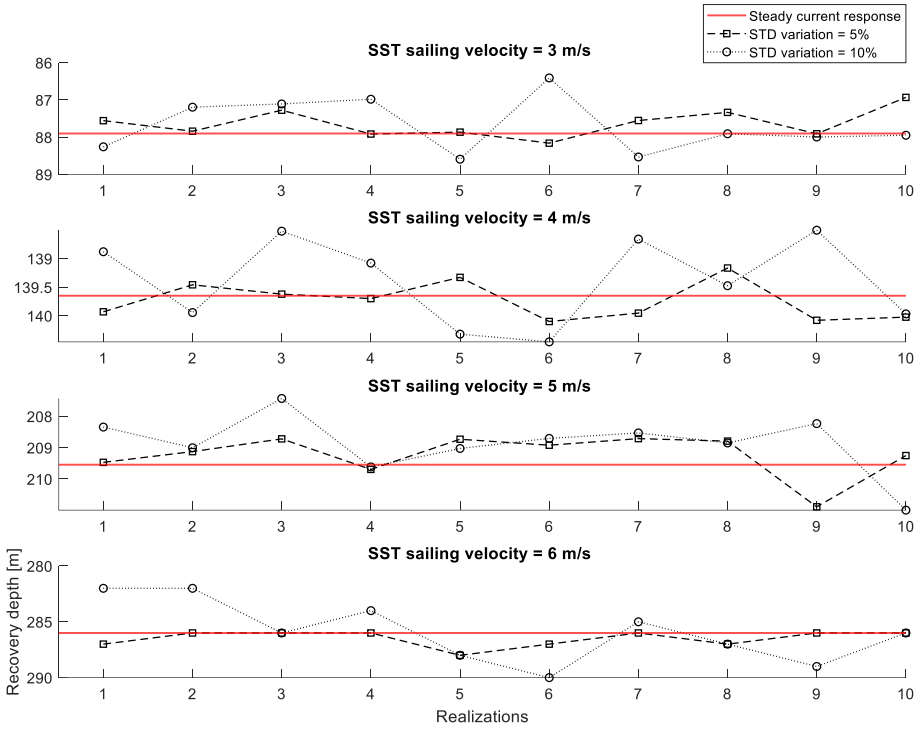

Figure 70 - Simulated SST responses during emergency recovery from jam-to-dive at different sailing velocities and heading current velocity = 1 [m/s]

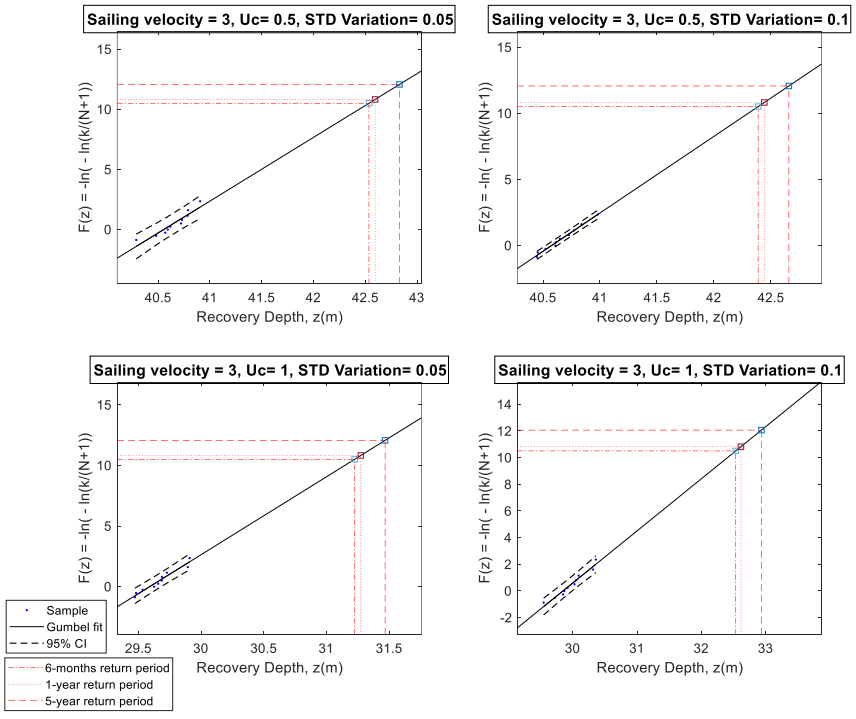

Figure 71 – Probability paper for Gumbel distribution for recovery depth corresponding to SST's velocity of 3 m/s, following current direction

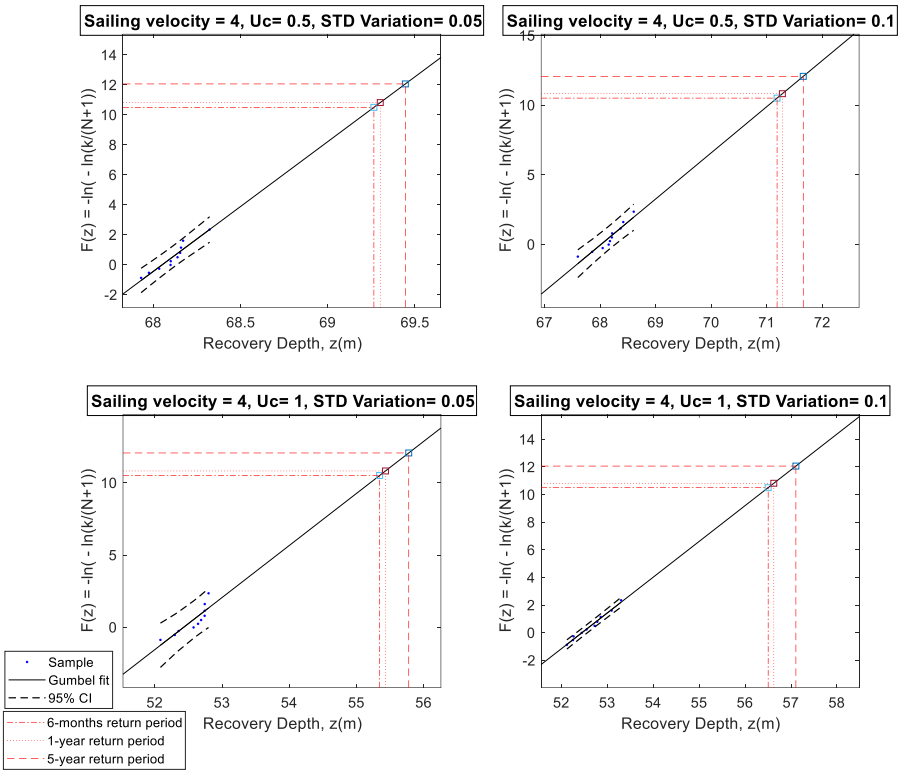

Figure 72 - Probability paper for Gumbel distribution for recovery depth corresponding to SST's velocity of 4 m/s, following current direction

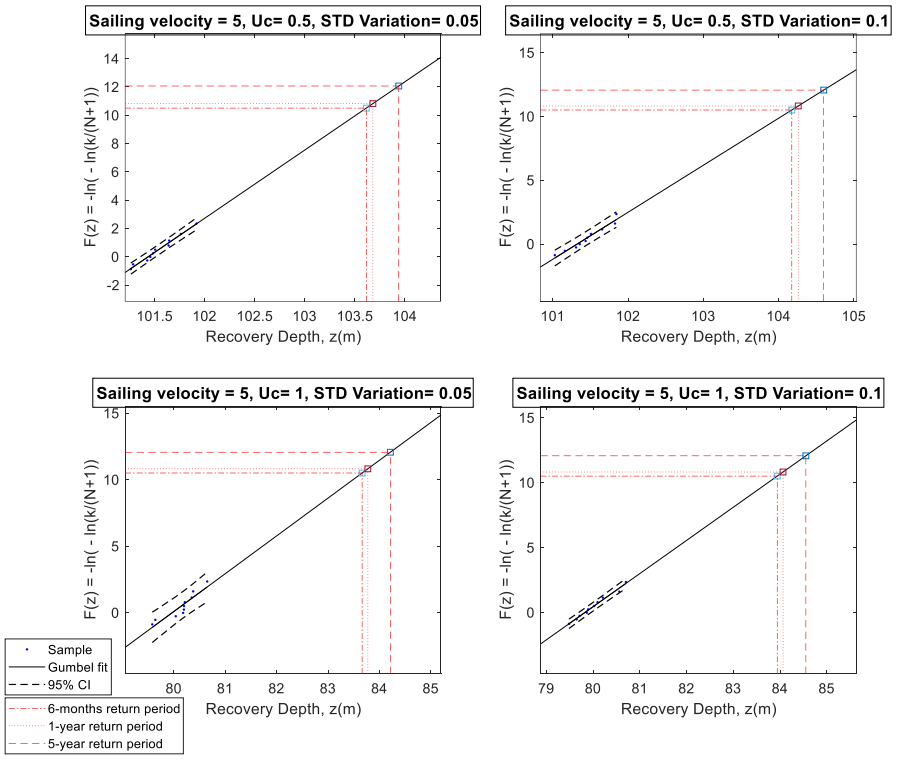

Figure 73 – Probability paper for Gumbel distribution for recovery depth corresponding to SST's velocity of 5 m/s, following current direction

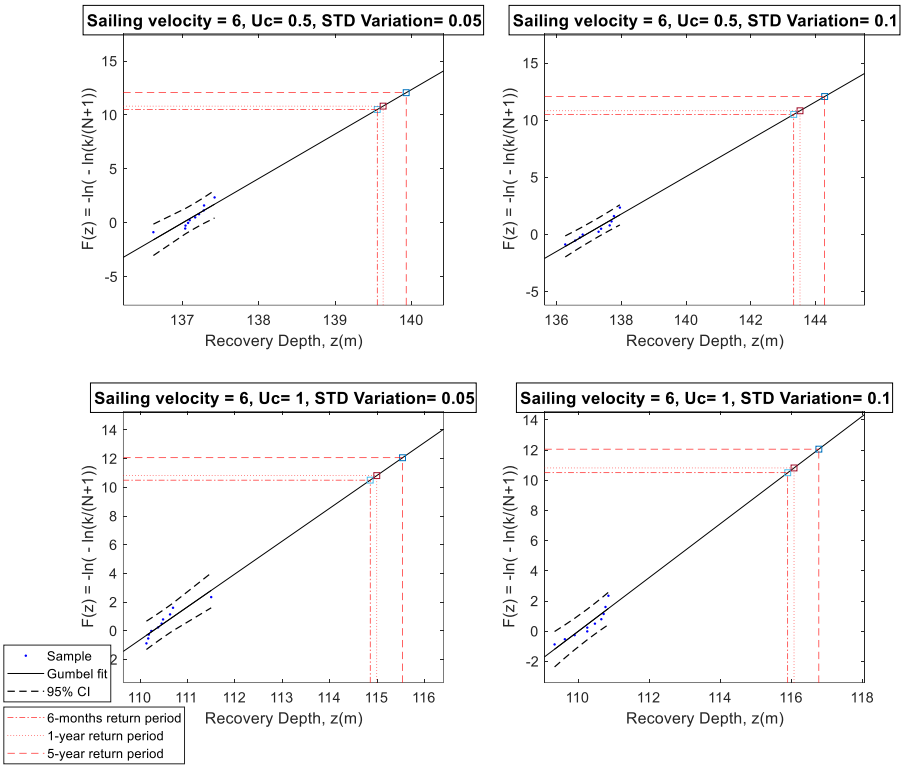

Figure 74 – Probability paper for Gumbel distribution for recovery depth corresponding to SST's velocity of 6 m/s, following current direction

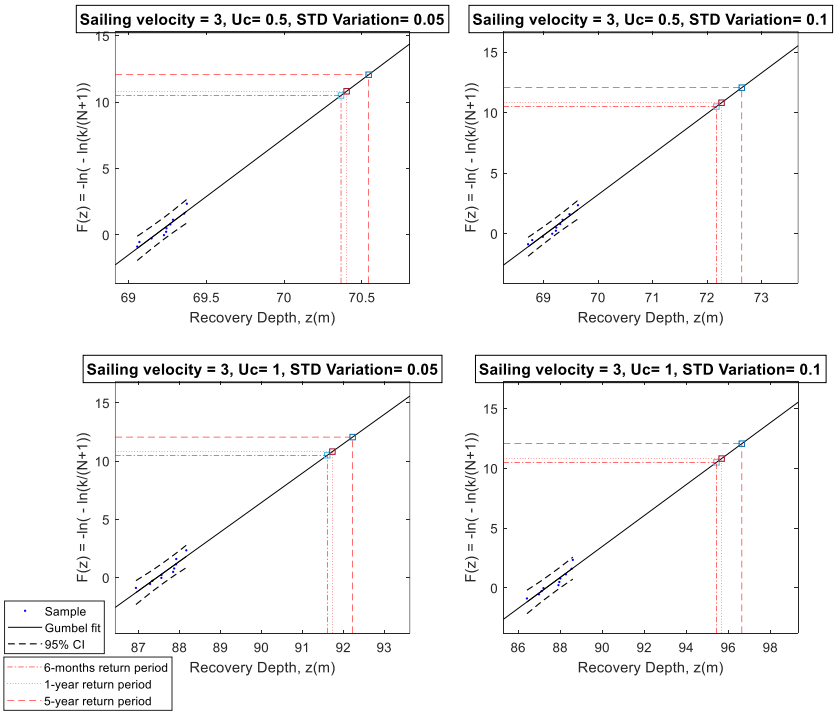

Figure 75 – Probability paper for Gumbel distribution for recovery depth corresponding to SST's velocity of 3 m/s, heading current direction

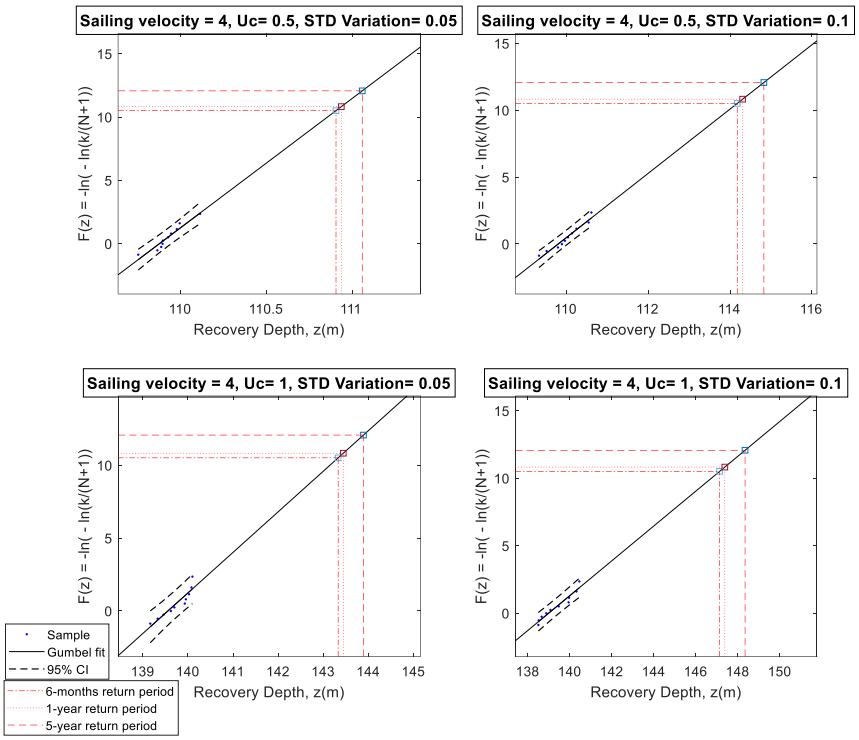

Figure 76 – Probability paper for Gumbel distribution for recovery depth corresponding to SST's velocity of 4 m/s, heading current direction

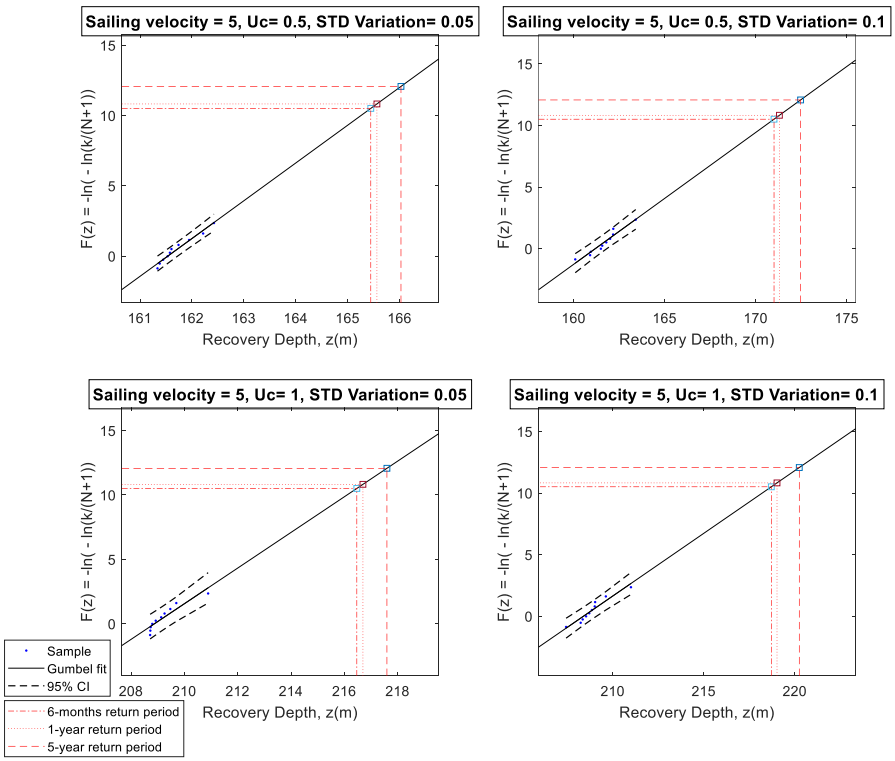

Figure 77 – Probability paper for Gumbel distribution for recovery depth corresponding to SST's velocity of 5 m/s, heading current direction

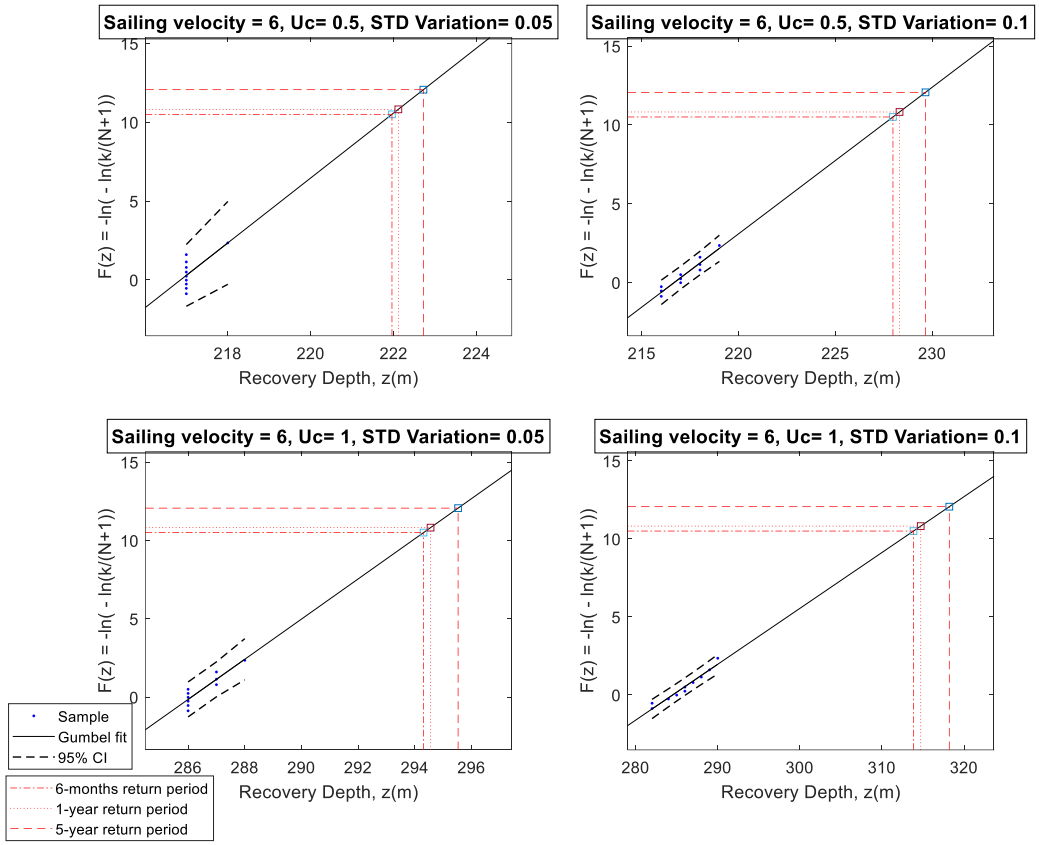

Figure 78 – Probability paper for Gumbel distribution for recovery depth corresponding to SST's velocity of 6 m/s, heading current direction

Table 25 - Recovery depth predictions for several return periods for following current

SST sailing velocity [m/s]	$V_c = 0.5\ m/s$ $CV = 0\%$	$V_c = 0.5\ m/s$ $CV = 5\%$	$V_c = 0.5\ m/s$ $CV = 10\%$	$V_c = 1\ m/s$ $CV = 0\%$	$V_c = 1\ m/s$ $CV = 5\%$	$V_c = 1\ m/s$ $CV = 10\%$
			6 months return period			
3	40.621	(42.535)	(42.388)	29.807	(31.225)	(32.534)
		(42.406, 42.659)	(42.328, 42.449)		(31.118, 31.335)	(32.385, 32.683)
4	68.403	(69.264)	(71.183)	52.831	(55.343)	(56.501)
		(69.172, 69.358)	(70.973, 71.384)		(55.126, 55.534)	(56.363, 56.641)
5	101.200	(103.614)	(104.174)	80.250	(83.662)	(83.939)
		(103.523, 103.706)	(104.017, 104.332)		(83.376, 83.934)	(83.776, 84.105)
6	137.238	(139.553)	(143.326)	110.334	(114.854)	(115.888)
		(139.392, 139.696)	(142.868, 143.774)		(114.167, 115.644)	(115.457, 116.293)
			1-year return period			
3	40.621	(42.595)	(42.443)	29.807	(31.275)	(32.615)
		(42.467, 42.717)	(42.382, 42.504)		(31.167, 31.385)	(32.764)
4	68.403	(69.301)	(71.278)	52.831	(55.431)	(56.624)
		(69.208, 69.394)	(71.071, 71.478)		(55.220, 55.617)	(56.484, 56.764)
5	101.200	(103.680)	(104.260)	80.250	(83.774)	(84.063)
		(103.589, 103.772)	(104.102, 104.418)		(83.490, 84.043)	(83.899, 84.230)
6	137.238	(139.630)	(143.520)	110.334	(114.993)	(116.065)
		(139.473, 139.769)	(143.064, 143.965)		(114.297, 115.792)	(115.640, 116.465)
			5-year return period			
3	40.621	(42.830)	(42.596)	29.807	(31.469)	(32.933)

		(42.708, 42.947)	(42.596, 42.720)		(31.359, 31.580)	(32.784, 33.082)
4	68.403	(69.445)	(71.654)	52.831	(55.776)	(57.105)
		(69.352, 69.539)	(71.454, 71.846)		(55.588, 55.943)	(56.964, 57.247)
5	101.200	(103.938)	(104.598)	80.250	(84.212)	(84.551)
		(103.845, 104.031)	(104.440, 104.031)		(83.940, 84.470)	(84.384, 84.721)
6	137.238	(139.932)	(144.281)	110.334	(115.536)	(116.763)
		(139.795, 140.054)	(143.834, 144.718)		(114.805, 116.376)	(116.360, 117.141)

Table 26 - Recovery depth predictions for several return periods for heading current

SST sailing velocity [m/s]	$V_c = 0.5\ m/s$ $CV = 0\%$	$V_c = 0.5\ m/s$ $CV = 5\%$	$V_c = 0.5\ m/s$ $CV = 10\%$	$V_c = 1\ m/s$ $CV = 0\%$	$V_c = 1\ m/s$ $CV = 5\%$	$V_c = 1\ m/s$ $CV = 10\%$
			6 months return period			
3	69.303	(70.366)	(72.169)	87.902	(91.604)	(95.429)
		(70.283, 70.446)	(71.979, 72.356)		(91.311, 91.887)	(94.845, 95.996)
4	110.441	(110.906)	(114.177)	139.650	(143.330)	(147.137)
		(110.827, 110.986)	(113.942, 114.411)		(143.040, 143.608)	(146.579, 147.700)
5	161.466	(165.443)	(170.999)	209.544	(216.467)	(218.706)
		(165.178, 165.717)	(170.297, 171.710)		(215.363, 217.726)	(217.708, 219.762)
6	218,000	(221.955)	(227.966)	286.000	(294.307)	(313.840)
		(220.024, 225.742)	(227.079, 228.867)		(293.084, 295.661)	(312.269, 315.404)
			1-year return period			
3	69.303	(70.402)	(72.264)	87.902	(91.730)	(95.674)
		(70.319, 70.482)	(72.075, 72.450)		(91.439, 92.010)	(95.093, 96.237)
4	110.441	(110.937)	(114.309)	139.650	(143.444)	(147.382)
		(110.858, 111.017)	(114.074, 114.543)		(143.156, 143.720)	(146.824, 147.947)
5	161.466	(165.560)	(171.296)	209.544	(216.696)	(219.017)
		(165.294, 165.837)	(170.591, 172.007)		(215.578, 217.971)	(218.011, 220.082)
6	218,000	(222.109)	(228.307)	286.000	(294.553)	(314.724)
		(220.140, 225.970)	(227.417, 229.230)		(293.319, 295.923)	(313.155, 316.285)
			5-year return period			
3	69.303	(70.544)	(72.635)	87.902	(92.224)	(96.636)
		(70.463, 70.623)	(72.449, 72.818)		(91.943, 92.495)	(96.071, 97.186)
4	110.441	(111.059)	(114.828)	139.650	(143.891)	(148.348)
		(110.980, 111.140)	(114.594, 115.060)		(143.613, 144.158)	(147.784, 148.917)
5	161.466	(166.024)	(172.460)	209.544	(217.596)	(220.240)
		(165.749, 166.310)	(171.750, 173.177)		(216.423, 218.935)	(219.200, 221.342)
6	218,000	(222.713)	(229.646)	286.000	(295.525)	(318.201)
		(220.596, 226.864)	(228.747, 230.560)		(294.243, 296.946)	(316.641, 319.754)

Table 27 - Percentage change in recovery depth compared to the deterministic current case

D15	Following current				Heading current			
SST sailing velocity [m/s]	$V_c = 0.5$ $CV = 5\%$	$V_c = 0.5$ $CV = 10\%$	$V_c = 1$ $CV = 5\%$	$V_c = 1$ $CV = 10\%$	$V_c = 0.5$ $CV = 5\%$	$V_c = 0.5$ $CV = 10\%$	$V_c = 1$ $CV = 5\%$	$V_c = 1$ $CV = 10\%$
	6-months return period							
3	4.71	4.35	4.76	9.15	1.53	4.14	4.21	8.56
4	1.26	4.06	4.75	6.95	0.42	3.38	2.64	5.36
5	2.39	2.94	4.25	4.60	2.46	5.90	3.30	4.37
6	1.69	4.44	4.10	5.03	1.81	4.57	2.90	9.73
	1-year return period							
3	4.86	4.49	4.93	9.42	1.59	4.27	4.35	8.84
4	1.31	4.20	4.92	7.18	0.45	3.50	2.72	5.54
5	2.45	3.02	4.39	4.75	2.54	6.09	3.41	4.52
6	1.74	4.58	4.22	5.19	1.88	4.73	2.99	10.04
	5-year return period							
3	5.44	4.86	5.58	10.49	1.79	4.81	4.92	9.94
4	1.52	4.75	5.57	8.09	0.56	3.97	3.04	6.23
5	2.71	3.36	4.94	5.36	2.82	6.81	3.84	5.10
6	1.96	5.13	4.71	5.83	2.16	5.34	3.33	11.26

8.6 Appendix F – Jam-to-dive with 20-degree pitch angle

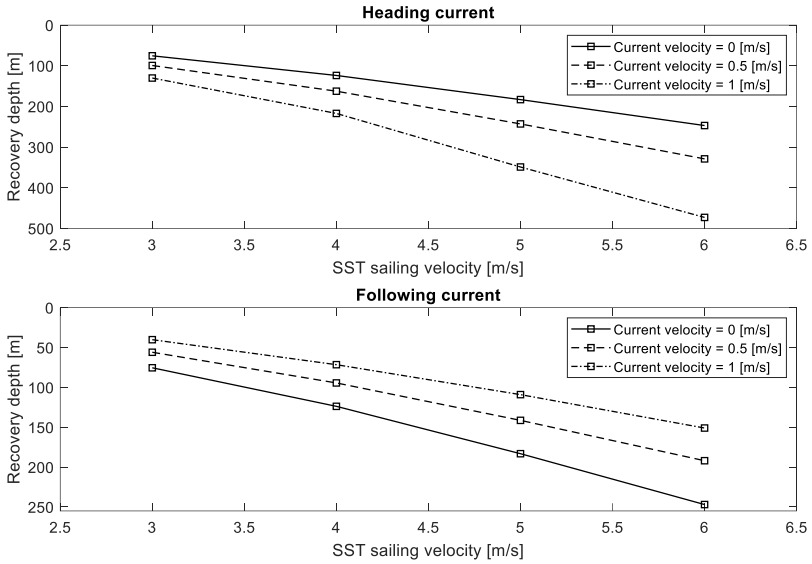

Figure 79 - Jam-to-dive curve for different steady current cases

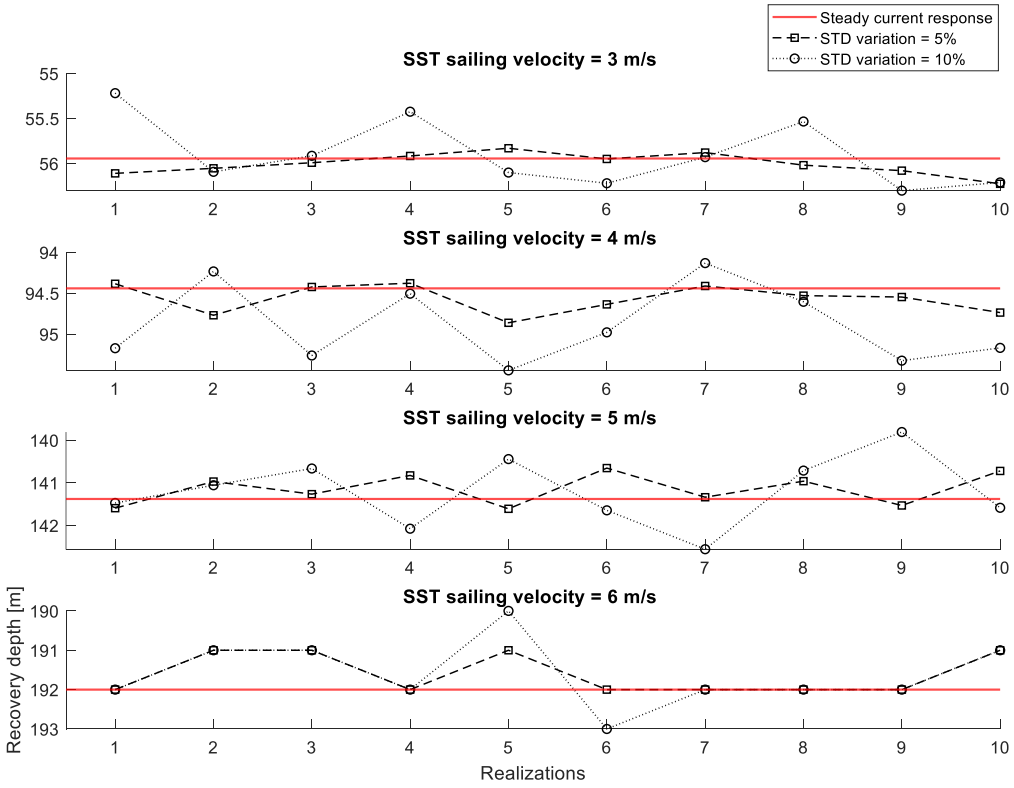

Figure 80 – Simulated SST responses during emergency recovery from jam-to-dive at different sailing velocities and following current velocity = 0.5 [m/s]

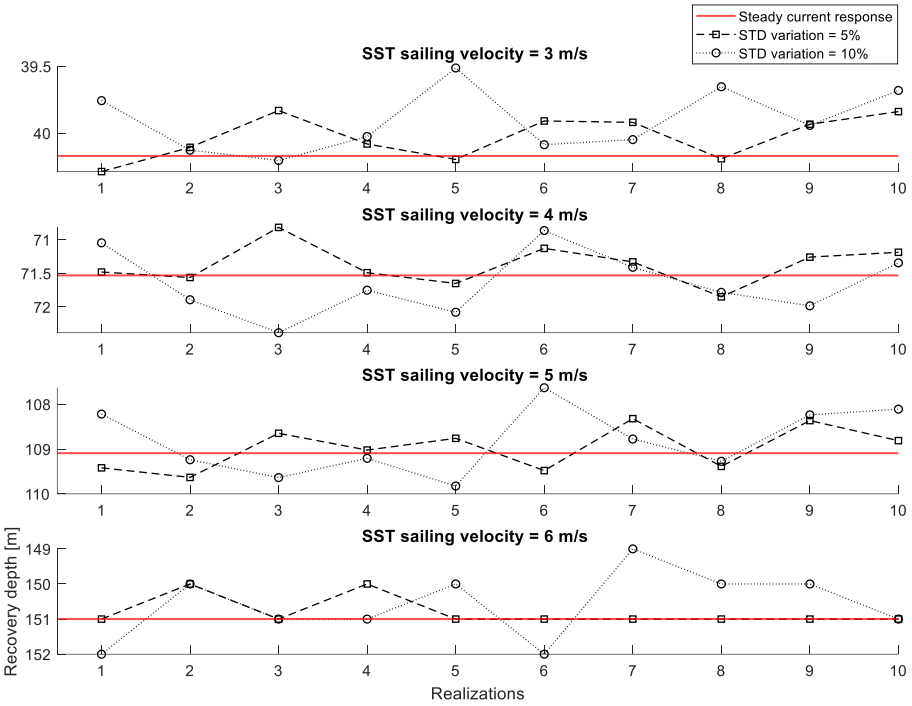

Figure 81 – Simulated SST responses during emergency recovery from jam-to-dive at different sailing velocities and following current velocity = 1 [m/s]

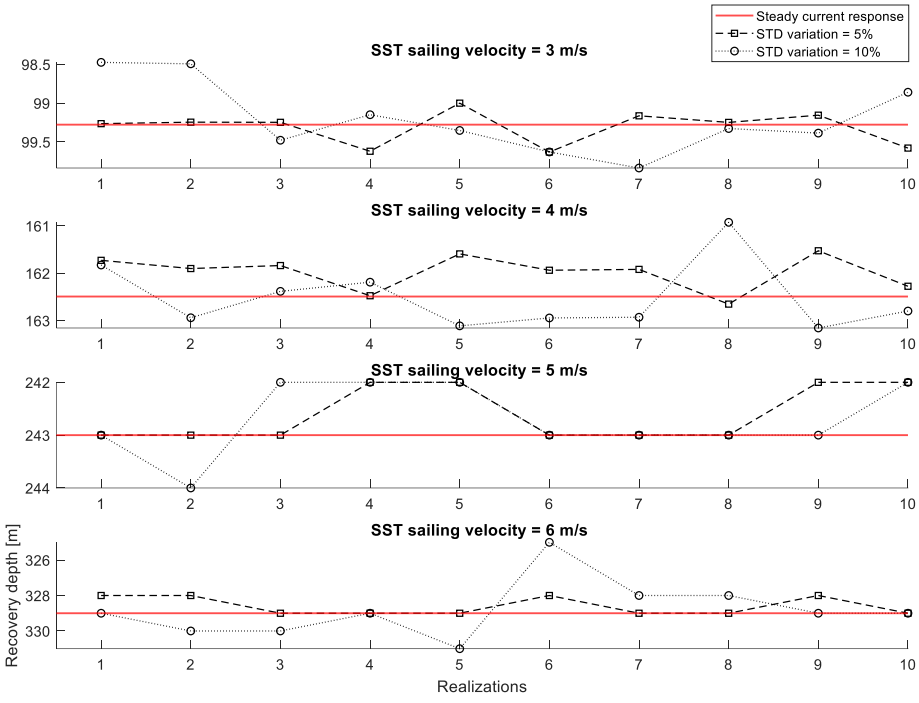

Figure 82 – Simulated SST responses during emergency recovery from jam-to-dive at different sailing velocities and heading current velocity = 0.5 [m/s]

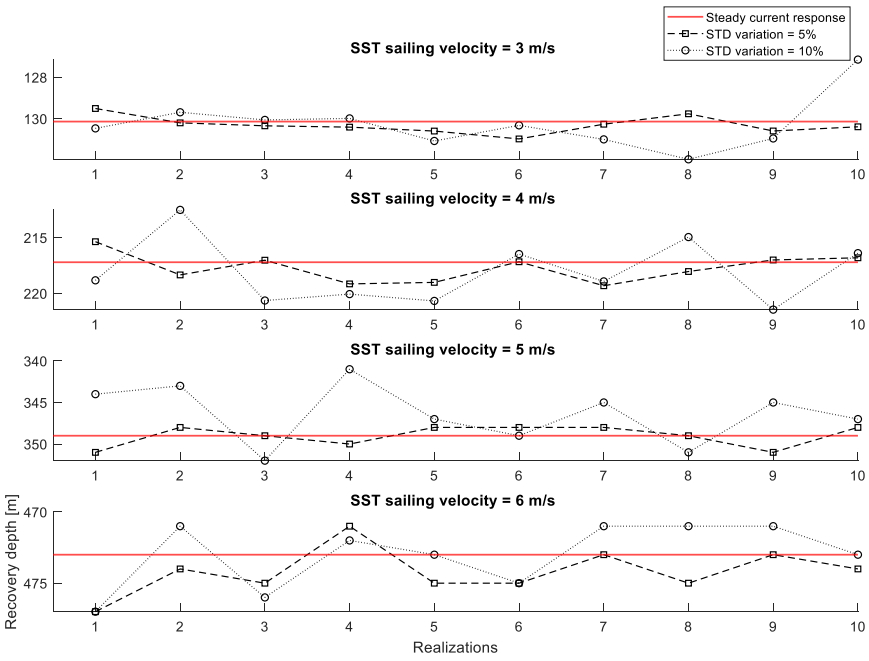

Figure 83 – Simulated SST responses during emergency recovery from jam-to-dive at different sailing velocities and heading current velocity = 1 [m/s]

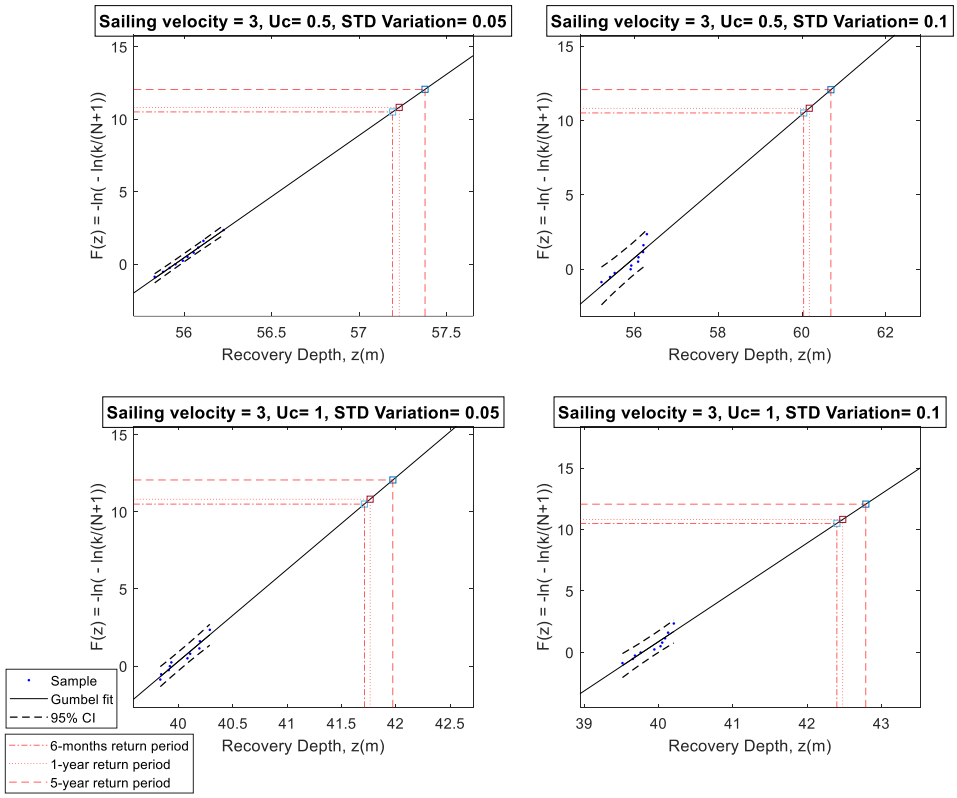

Figure 84 - Probability paper for Gumbel distribution for recovery depth corresponding to SST's velocity of 3 m/s, following current direction

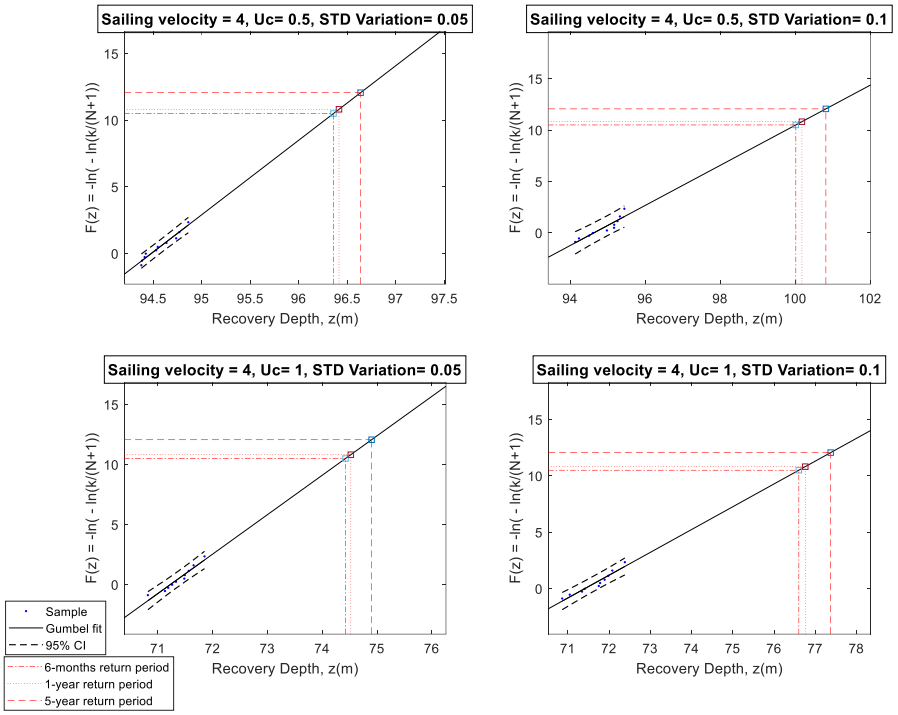

Figure 85 – Probability paper for Gumbel distribution for recovery depth corresponding to SST's velocity of 4 m/s, following current direction

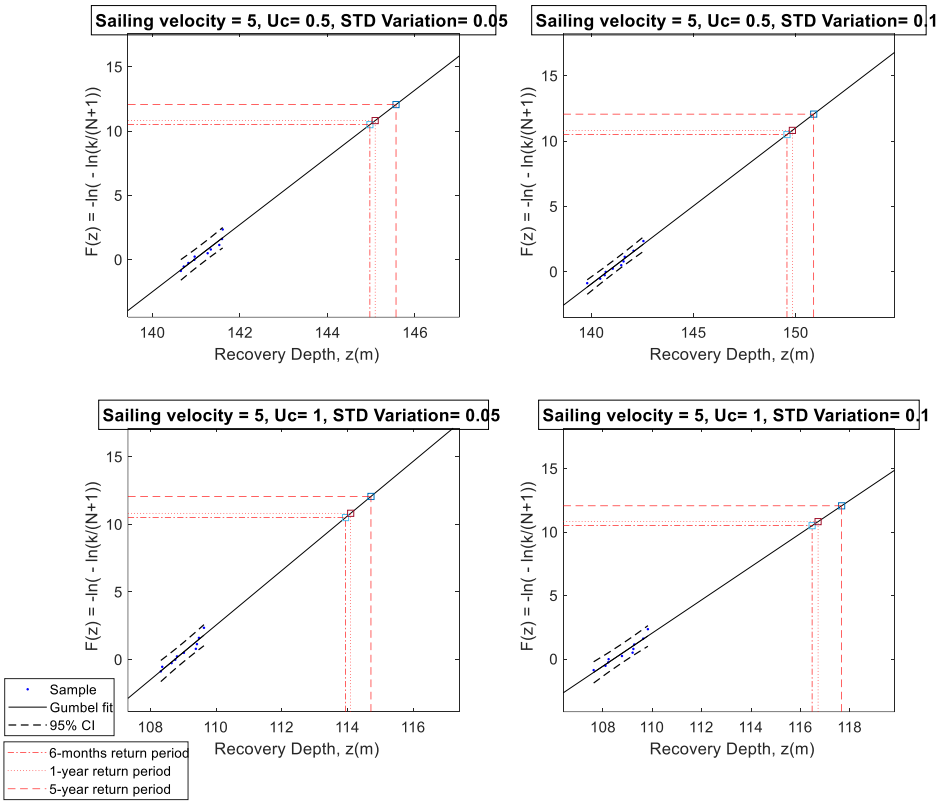

Figure 86 – Probability paper for Gumbel distribution for recovery depth corresponding to SST's velocity of 5 m/s, following current direction

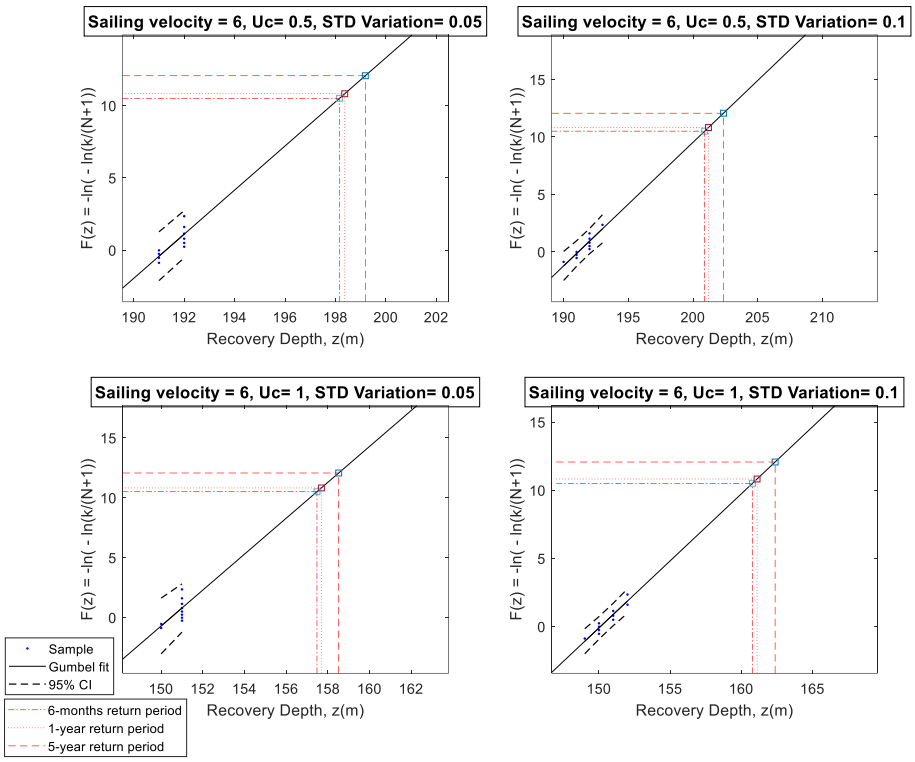

Figure 87 – Probability paper for Gumbel distribution for recovery depth corresponding to SST's velocity of 6 m/s, following current direction

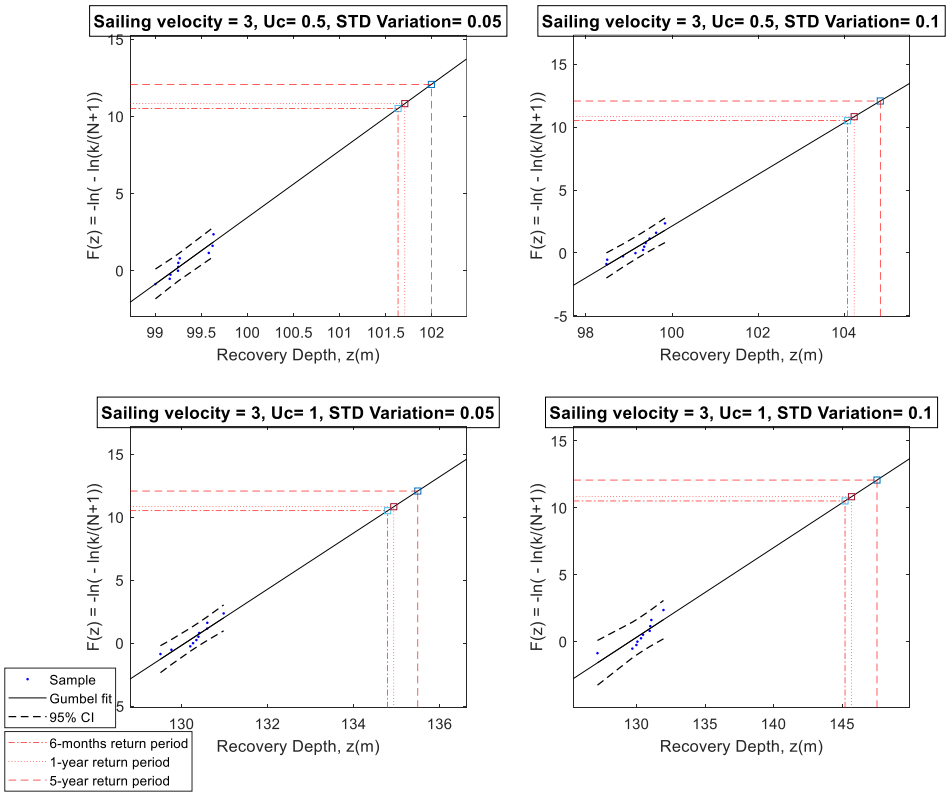

Figure 88 – Probability paper for Gumbel distribution for recovery depth corresponding to SST's velocity of 3 m/s, heading current direction

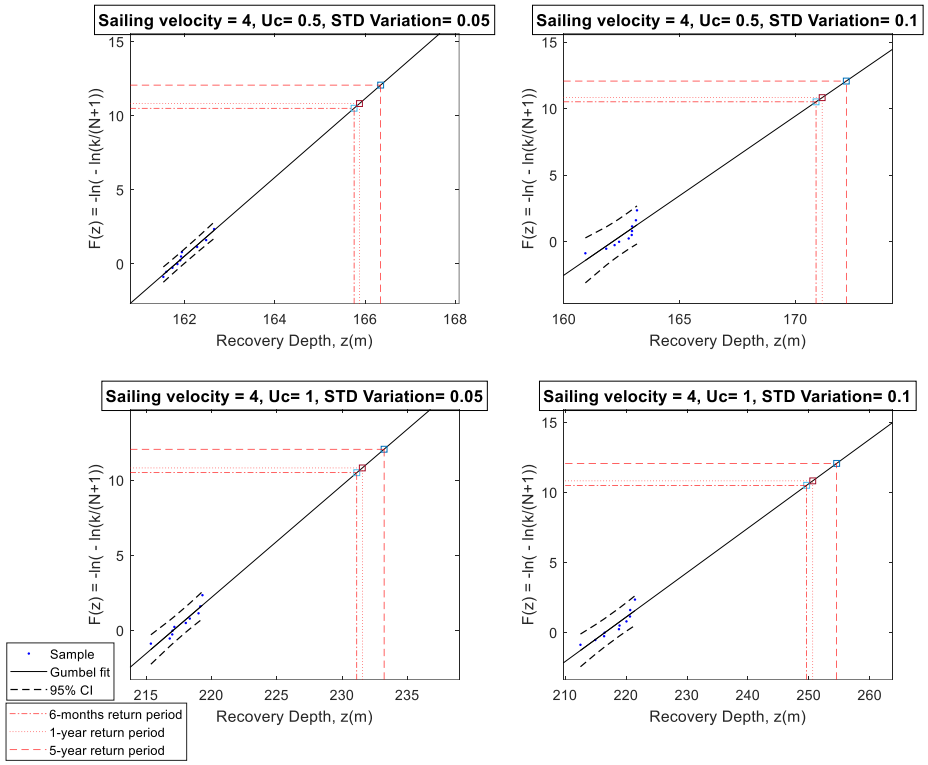

Figure 89 – Probability paper for Gumbel distribution for recovery depth corresponding to SST's velocity of 4 m/s, heading current direction

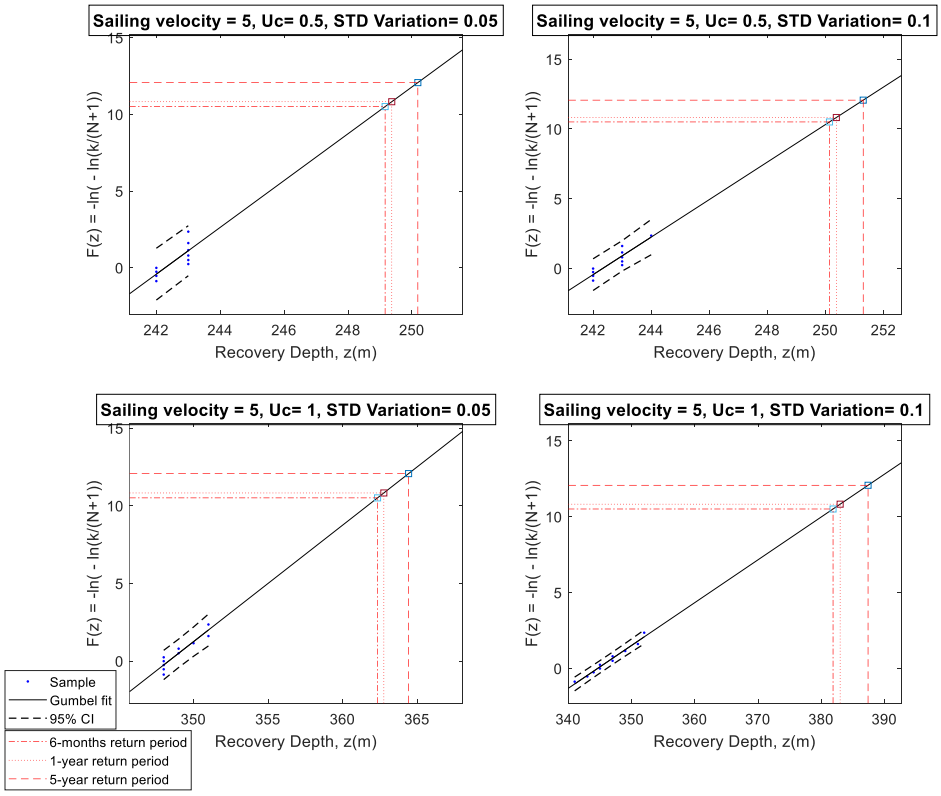

Figure 90 – Probability paper for Gumbel distribution for recovery depth corresponding to SST's velocity of 5 m/s, heading current direction

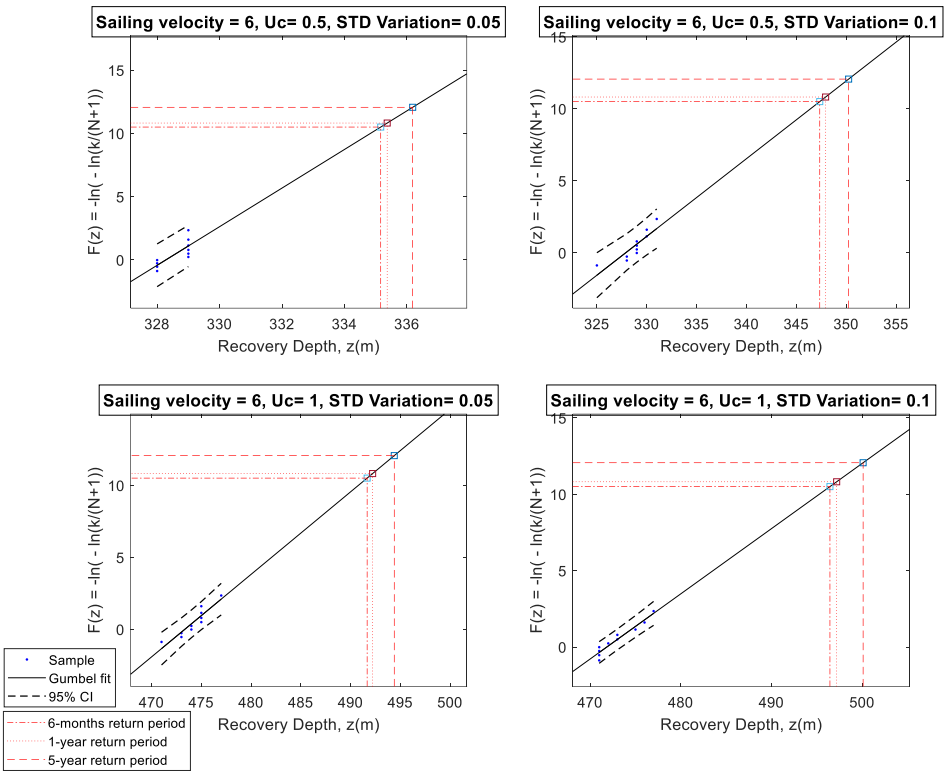

Figure 91 - Probability paper for Gumbel distribution for recovery depth corresponding to SST's velocity of 6 m/s, heading current direction

Table 28 - Recovery depth predictions for several return periods for following current

SST sailing velocity [m/s]	$V_c = 0.5\ m/s$ $CV = 0\%$	$V_c = 0.5\ m/s$ $CV = 5\%$	$V_c = 0.5\ m/s$ $CV = 10\%$	$V_c = 1\ m/s$ $CV = 0\%$	$V_c = 1\ m/s$ $CV = 5\%$	$V_c = 1\ m/s$ $CV = 10\%$
			6 months return period			
3	55.945	(57.192)	(60.042)	40.170	(41.711)	(42.399)
		(57.153, 57.232)	(59.707, 60.352)		(41.595, 41.828)	(41.595, 41.928)
4	94.441	(96.358)	(100.017)	71.531	(74.424)	(76.601)
		(96.248, 96.471)	(99.595, 100.423)		(74.243, 74.603)	(76.291, 76.906)
5	141.380	(144.972)	(149.587)	109.093	(113.936)	(116.469)
		(144.674, 145.270)	(149.161, 150.011)		(113.574, 114.297)	(115.918, 117.012)
6	192.000	(198.159)	(200.901)	151.000	(157.477)	(160.784)
		(197.289, 198.967)	(199.994, 201.778)		(157.481, 157.475)	(159.886, 161.689)
			1-year return period			
3	55.945	(57.230)	(60.173)	40.170	(41.764)	(42.477)
		(57.191, 57.270)	(59.844, 60.479)		(41.648, 41.881)	(42.288, 42.661)
4	94.441	(96.415)	(100.180)	71.531	(74.521)	(76.758)
		(96.304, 96.528)	(99.761, 100.582)		(74.340, 74.700)	(76.449, 77.062)
5	141.380	(145.093)	(149.852)	109.093	(114.092)	(116.711)
		(144.795, 145.391)	(149.427, 150.277)		(113.730, 114.453)	(116.162, 117.253)
6	192.000	(198.367)	(201.195)	151.000	(157.688)	(161.106)
		(197.505, 199.167)	(200.293, 202.067)		(157.747, 157.650)	(160.206, 162.013)
			5-year return period			
3	55.945	(57.378)	(60.689)	40.170	(41.973)	(42.788)
		(57.338, 57.418)	(60.380, 60.976)		(41.856, 42.092)	(42.603, 42.967)
4	94.441	(96.638)	(100.819)	71.531	(74.900)	(77.373)
		(96.524, 96.753)	(100.413, 101,208)		(74.722, 75.075)	(77.070, 77.672)
5	141.380	(145.569)	(150.895)	109.093	(114.709)	(117.663)

6	192.000	(142.270, 145.868) (199.183) (198.353, 199.954)	(150.470, 151.319) (202.353) (201.471, 203.205)	151.000	(114.348, 115.069) (158.519) (158.796, 158.338)	(117.120, 118.200) (162.374) (161.469, 163.285)

Table 29 - Recovery depth predictions for several return periods for heading current

SST sailing velocity [m/s]	$V_c = 0.5\ m/s$ $CV = 0\%$	$V_c = 0.5\ m/s$ $CV = 5\%$	$V_c = 0.5\ m/s$ $CV = 10\%$	$V_c = 1\ m/s$ $CV = 0\%$	$V_c = 1\ m/s$ $CV = 5\%$	$V_c = 1\ m/s$ $CV = 10\%$
			6 months return period			
3	99.278	(101.632) (101.382, 101.891)	(104.080) (103.719, 104.427)	130.138	(134.789) (134.449, 135.115)	(145.206) (144.377, 145.902)
4	162.492	(165.756) (165.521, 165.997)	(170.893) (170.363, 171.340)	217.207	(231.126) (230.090, 232.138)	(249.630) (247.222, 251.899)
5	243.000	(249.159) (248.289, 249.967)	(250.138) (249.186, 251.124)	349.000	(362.344) (360.705, 364.089)	(381.872) (380.234, 383.522)
6	329.000	(335.159) (334.289, 335.967)	(347.348) (346.117, 348.420)	473.000	(491.664) (490.153, 493.131)	(496.450) (494.334, 498.656)
			1-year return period			
3	99.278	(101.705) (101.454, 101.966)	(104.235) (103.877, 104.578)	130.138	(134.931) (134.594, 135.254)	(145.678) (144.894, 146.337)
4	162.492	(165.875) (165.639, 166.118)	(171.158) (170.652, 171.584)	217.207	(231.550) (230.519, 232.557)	(250.627) (248.250, 252.868)
5	243.000	(249.367) (248.505, 250.167)	(250.373) (249.417, 251.364)	349.000	(362.766) (361.114, 354.525)	(382.994) (381.352, 384.648)
6	329.000	(335.367) (334.505, 336.167)	(347.934) (346.747, 348.969)	473.000	(492.217) (490.714, 493.969)	(497.191) (495.060, 499.414)
			5-year return period			
3	99.278	(101.994) (101.737, 102.260)	(104.842) (104.497, 105.173)	130.138	(135.489) (135.165, 135.801)	(147.538) (146.930, 148.048)
4	162.492	(166.345) (166.102, 166.594)	(172.200) (171.791, 172.544)	217.207	(233.218) (232.207, 234.206)	(254.553) (252.295, 256.680)
5	243.000	(250.183) (249.353, 250.954)	(251.299) (250.326, 252.306)	349.000	(364.427) (362.724, 366.240)	(387.409) (385.750, 389.080)
6	329.000	(336.183) (335.353, 336.954)	(350.243) (349.226, 351.129)	473.000	(494.390) (492.920, 495.817)	(500.110) (497.919, 502.395)

Table 30 - Percentage change in recovery depth compared to the deterministic current case

D20	Following current				Heading current			
SST sailing velocity [m/s]	$V_c = 0.5$ $CV = 5\%$	$V_c = 0.5$ $CV = 10\%$	$V_c = 1$ $CV = 5\%$	$V_c = 1$ $CV = 10\%$	$V_c = 0.5$ $CV = 5\%$	$V_c = 0.5$ $CV = 10\%$	$V_c = 1$ $CV = 5\%$	$V_c = 1$ $CV = 10\%$
	6-months return period							
3	2.23	7.32	3.84	5.55	2.37	4.84	3.57	11.58
4	2.03	5.90	4.04	7.09	2.01	5.17	6.41	14.93
5	2.54	5.80	4.44	6.76	2.53	2.94	3.82	9.42
6	3.21	4.64	4.29	6.48	1.87	5.58	3.95	4.96
	1-year return period							
3	2.30	7.56	3.97	5.74	2.44	4.99	3.68	11.94
4	2.09	6.08	4.18	7.31	2.08	5.33	6.60	15.39
5	2.63	5.99	4.58	6.98	2.62	3.03	3.94	9.74
6	3.32	4.79	4.43	6.69	1.94	5.76	4.06	5.11
	5-year return period							
3	2.56	8.48	4.49	6.52	2.74	5.60	4.11	13.37
4	2.33	6.75	4.71	8.17	2.37	5.97	7.37	17.19
5	2.96	6.73	5.15	7.86	2.96	3.42	4.42	11.01
6	3.74	5.39	4.98	7.53	2.18	6.46	4.52	5.73